It's about time: novel drug discovery concepts for the molecular pharmacological characterization fo the cannabinoid CB2 receptor

Bouma, J.

Chapter 3

Kinetic multiplex assay to assess biased signaling of clinical agonists at the cannabinoid CB_2 receptor

Jara Bouma, Sanjay Sunil Kumar, Barry J.W. van den Berg, Cas van der Horst, Samuel R.J. Hoare, Matthias Wittwer, Wolfgang Guba, Uwe Grether, Mario van der Stelt, Laura H. Heitman

Manuscript in preparation.

Abstract

Studying biased signaling of G protein-coupled receptors (GPCRs) holds promise for the identification of ligands with a better therapeutic window. However, proper examination of biased signaling remains challenging by risking introduction of system or observation bias. Therefore, we developed a novel multiplex assay that simultaneously and kinetically detects cAMP production and ß-arrestin-2 recruitment in the same well. To investigate the applicability of the kinetic multiplex assay, we investigated seventeen clinically tested agonists for the cannabinoid CB_2 receptor (CB_2R), a promising GPCR for treating tissue injury and inflammation. Additionally, we included four widely used preclinical agonists and the endocannabinoids. Kinetic binding parameters were determined to extensively profile each agonist. Time-dependent activation was investigated by applying endpoint, semi-kinetic and kinetic analyses. Agonist-mediated CB_2R activation and signaling was time sensitive for several agonists, including Nabilone and LY-2828360, whereas this did not apply to the endocannabinoids. Similar potency and efficacy parameters were obtained from semi-kinetic and kinetic methods of analysis, while the latter provided additional signaling rate constants k_1 and k_2. Fast CB_2R engagement (k_{on}) of agonists resulted in increased affinity and potency, while slowly dissociating agonists extended the interaction between CB_2R and ß-arrestin-2. Moreover, superagonists Tedalinab, Olorinab, PRS-211375 and ART-27.13 were characterized by fast k_1 values. No significant biased signaling was observed in our system. Altogether, this chapter accentuates the potential of multiplexing functional responses and performing kinetic analyses to provide an extensive preclinical profile for agonists that may better predict their *in vivo* pharmacological effects. Ultimately, providing a full kinetic context for binding and activation of GPCR ligands could advance drug discovery efforts.

3.1 Introduction

Biased signaling, also known as ligand bias, biased agonism or functional selectivity, describes the ability of a ligand to preferentially activate one pathway over another by stabilizing distinct conformations of the receptor[1–4]. Bias on G protein-coupled receptors (GPCRs) is most frequently observed between G proteins and ß-arrestins but may also occur amongst the G protein or ß-arrestin family subtypes[5,6]. Consequently, activation of distinct pathways by an agonist may lead to different biological effects. Therefore, studying biased signaling may provide the potential to increase the therapeutic window if a specific signaling pathway is associated with efficacy, while another with side effects[1–4,7]. Recently, this was exemplified by the FDA approval of the first GPCR biased agonist, oliceridine, for the μ-opioid receptor to treat moderate to severe acute pain in adults[8]. G protein signaling after μ-opioid receptor activation improved antinociception, while ß-arrestin recruitment was related to adverse effects such as respiratory repression[9].

The *in vitro* study of biased signaling, however, is challenging and influenced by many factors[1,10,11]. Different receptor, transducer or effector levels, or stoichiometry between these components in various cellular backgrounds may introduce system bias[1,12]. Furthermore, interpretation of bias is dependent on the choice of reference ligand, such as a tool compound to report 'ligand benchmark-bias' or the endogenous ligand for quantification of 'ligand physiology-bias'. A tool compound with a balanced profile across studied pathways allows for the identification of 'ligand pathway-bias'[1]. Moreover, most commonly used functional assays are employed as endpoint assays, i.e., measured at one specific time point. However, agonist-mediated receptor activation may change over time and could be influenced by the dynamics and kinetics of the ligand-receptor interaction[1,10]. The importance of kinetic context for biased signaling was first highlighted in a study on the dopamine D_2 receptor, which demonstrated that the direction of ligand bias changed over time and conclusions on bias were therefore highly dependent on the selected time point[13]. In addition, biased agonists displayed a longer residence time (RT) at the receptor compared to the endogenous agonist [13]. Functional parameters have previously been correlated to the target-binding kinetics of agonists at several GPCRs[14–16]. Important developments in the field such as the TRUPATH platform, which allows for screening of biased G protein signaling in separate assays, are made to include the kinetic context of signaling[17,18]. Nevertheless, the majority of studies that report on biased signaling are performed with separate cellular assays for the different signaling pathways, use endpoint assays and/or do not quantify the kinetic signaling traces with fit-for-purpose mathematical analyses. Thus, a novel design of *in vitro* assays and methods of data analysis to report functional parameters in conjunction with kinetic parameters, such as binding kinetics and signaling constants, is warranted to study the *in vitro* pharmacology profile of candidate drugs[19,20].

Targeting of cannabinoid CB_2 receptor (CB_2R) has demonstrated great potential in preclinical studies for the treatment of autoimmune conditions, pain and diseases with an inflammatory component. This receptor is predominantly expressed on immune cells and plays a key role in the regulation of several inflammatory processes via activation by the endocannabinoids (eCBs) anandamide (AEA) and 2-arachidonoylglycerol (2-AG)[21–25]. To date, the focus has been on activation of CB_2R to enhance immunosuppressive effects[25,26]. A recent review by

Brennecke *et al.* analyzed all granted patents for CB_2R ligands since 2010 and described at least twenty CB_2R agonists that have progressed to clinical development[25]. Of these, only three are currently on the market that are described to non-selectively activate CB_2R, i.e., Dronabinol; a synthetic Δ^9-tetrahydrocannabinol (Δ^9-THC), Nabilone; a synthetic Δ^9-THC analogue and cannabidiol (CBD) (**Figure 3.1**, **Table 3.1**)[21,25]. Additionally, combinations of THC and CBD have been approved for the treatment of multiple sclerosis-associated spasticity[27]. Of note, we recently demonstrated that CBD does not bind or activate CB_2R, and the therapeutic effect might be due to polypharmacology at other proteins[28,29]. Five CB_2R agonists are currently still in clinical trials, whereas the development of the remaining agonists has been discontinued due to a variety of reasons[25]. Several issues have been hypothesized to explain the poor preclinical to clinical translation, including, but not limited to, a lack of translational animal models or differential signaling bias at the receptor level[25,30].

In various studies, biased signaling of diverse agonists and inverse agonists at CB_2R has been investigated[31–38]. A large consensus study combined the results from several independent academic and industry laboratories for a well-defined set of commonly used CBR ligands[35]. All ligands were screened on activation in five separate *in vitro* endpoint assays, i.e., GTPγS binding, cAMP production, ß-arrestin-2 recruitment, pERK stimulation and GIRK

Table 3.1 **Clinical CB_2R agonists, developmental status and indications.**

Agonist	Highest phase of development	Status	Indication(s)
Dronabinol	Launched	Active	Appetite loss, anorexia, chemotherapy-induced nausea and vomiting
Nabilone	Launched	Active	Chemotherapy-induced nausea and vomiting
Cannabidiol	Launched	Active	Dravet syndrome, Lennox-Gastaut syndrome
Lenabasum	Phase 3	Active	Dermatomyositis, cystic fibrosis, diffuse cutaneous systemic sclerosis, systemic lupus erythematosus
Olorinab	Phase 2	Active	Inflammatory bowel disease-related pain
CMX-020	Phase 2	Active	Osteoarthritis, knee osteoarthritis, pain, chronic pain
Cannabinol	Phase 2	Active	Chronic insomnia disorder, epidermolysis bullosa
KN 387271	Phase 2	Discontinued	Traumatic brain injury, stroke
GW-842166X	Phase 2	Discontinued	Dental and musculoskeletal pain
S-777469	Phase 2	Discontinued	Atopic dermatitis, pruritis
LY-2828360	Phase 2	Discontinued	Osteoarthritic knee pain
PRS-211375	Phase 2	Discontinued	Dental pain, coronary artery bypass graft
ART-27.13	Phase 1	Active	Anorexia, pain, cachexia, chemotherapy-induced nausea and vomiting
NTRX-07	Phase 1	Active	Alzheimer's disease, neuropathic pain
EHP-101	Phase 1	Discontinued	Multiple sclerosis, scleroderma, cutaneous systemic sclerosis
Tedalinab	Phase 1	Discontinued	Neuropathic pain, osteoarthritis, inflammatory pain disorders
TAK-937	Phase 1	Discontinued	Stroke

Information obtained from Brennecke *et al.* (2021)[25] and clinicaltrails.gov (accessed in January 2024).

activation. The most prominent bias at CB_2R was found between inhibition of cAMP production and ß-arrestin-2 recruitment, although bias factors remained low compared to other GPCRs. Furthermore, agonists HU308, HU910 and JWH133 were most balanced between all pathways and were thus recommended by the authors for use in further bias studies. To the best of our knowledge, bias at CB_2R has not been studied with a focus on the kinetic context and in general little is known about the binding kinetics of CB_2R agonists.

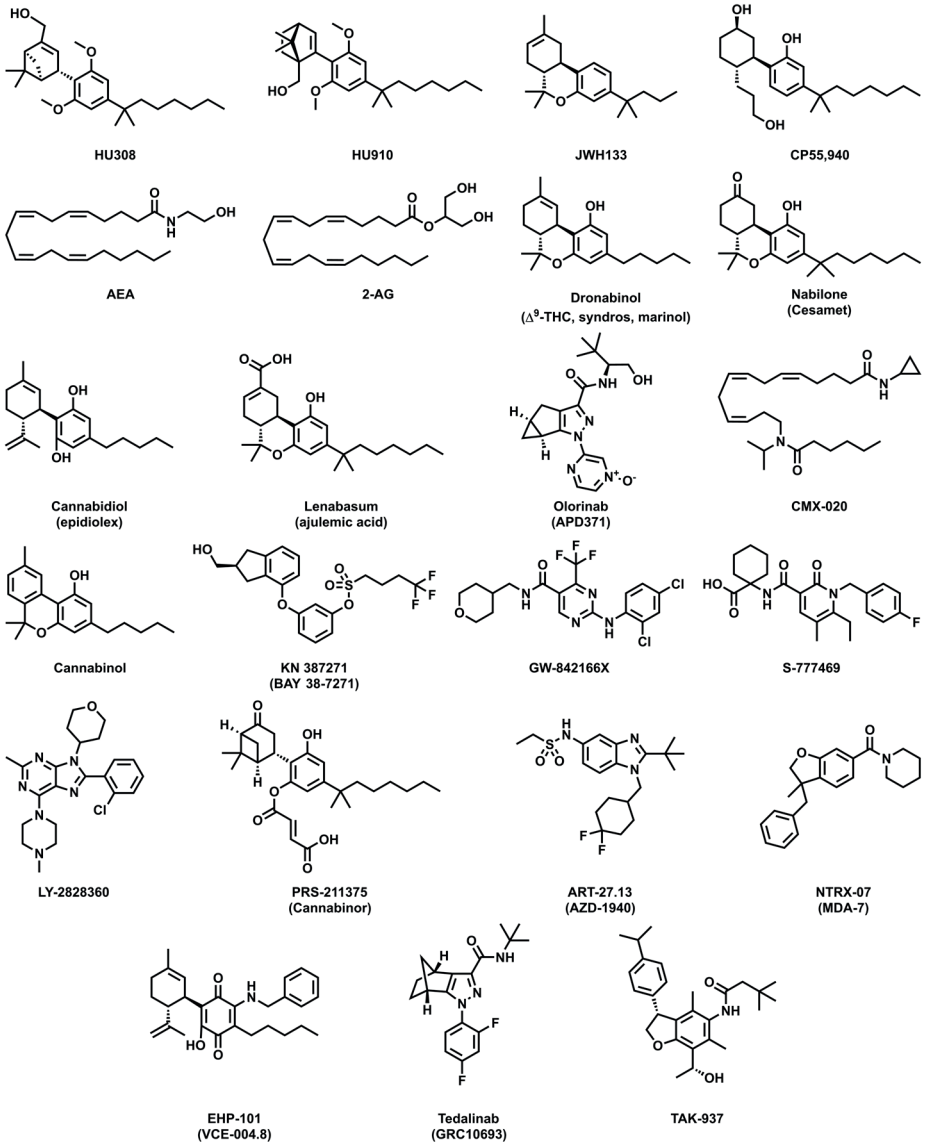

Figure 3.1 Chemical structures of cannabinoid CB_2 receptor agonists used in this study.
Benchmark agonists (HU308, HU910, JWH133 and CP55,940) and endocannabinoids (AEA, 2-AG). Clinical agonists ordered on highest phase of clinical development reached (in January 2024): launched (Dronabinol, Nabilone, Cannabidiol), phase 3 (Lenabasum), phase 2 (Olorinab, CMX-020, Cannabinol, KN 387271, GW-842166X, S-777469, LY-282360, PRS-211375), phase 1 (ART-27.13, NTRX-07, EHP-101, Tedalinab, TAK-937) with alternative names in between brackets.

Here, we aimed to develop a novel multiplex assay that simultaneously detects cAMP production and ß-arrestin-2 recruitment after receptor activation in a time-dependent manner in a single well. Seventeen CB_2R agonists that were examined in clinical trials were screened to investigate the applicability of this novel multiplex assay (**Figure 3.1**, **Table 3.1**). These agonists encompassed various chemotypes, clinical development phases and indications (**Figure 3.1**, **Table 3.1**), which are further specified in a review by Brennecke *et al.*[25]. This highlights the broad spectrum of CB_2R drug discovery and the adaptability of CB_2R to accommodate distinct agonists in the orthosteric binding pocket that can all activate the receptor. Furthermore, we included four widely used preclinical agonists and the endocannabinoids as benchmarks. Affinity and binding kinetics of the agonists were determined to ensure interaction with CB_2R and to obtain a more complete preclinical profile of the agonists. We explored the time-dependency of receptor activation by use of various methods of data analysis for the multiplex assay, i.e., endpoint, semi-kinetic and kinetic. We found that there were different time-dependent effects in inhibition of cAMP production and ß-arrestin-2 recruitment and that time-dependency varied per agonist used. Moreover, results from the semi-kinetic and kinetic analyses were well correlated, while the kinetic analysis additionally provided signaling rate constants k_1 and k_2. Superagonists in ß-arrestin-2 recruitment, i.e., agonists with higher efficacy compared to full agonist CP55,940, were characterized by fast k_1 values, whereas not all agonists with fast k_1 values behaved as superagonists. Moreover, a quick engagement of agonists with the receptor, i.e., fast association rate constant k_{on}, resulted in high affinity and kinetic potency (pIR_{50}). In our novel multiplex system, we did not detect statistically significant bias for any of the agonists relative to HU308. However, small differences were observed in trends for bias signaling, which were in some cases dependent on the method of analysis. Altogether, this study highlights and provides the potential of multiplexing functional readouts and including a kinetic view to CB_2R drug discovery programs, which can be extended to other GPCRs for an improved screening of biased signaling.

3.2 Results

3.2.1 Detection of binding affinity and kinetics of agonists at CB_2R

The investigated agonist set including benchmark agonists, endocannabinoids and clinical agonists displayed a high variety in chemotypes (**Figure 3.1**). Moreover, the agonists were highly diverse in terms of lipophilicity (LogD, K_{ow}LogP), solubility, brain lipid binding, membrane permeation and protein binding (**Table S3.1**), providing a structurally and chemically diverse set of agonists to demonstrate the applicability of the new signaling assay.

Prior to the development of the new signaling assay, all agonists were screened for their binding affinity and binding kinetics at CB_2R in [^{3}H]RO6957022 binding assays to ensure interaction with CB_2R (**Figure 3.2**, **Table 3.2**). From [^{3}H]RO6957022 displacement assays, it was observed that most agonists displayed affinity for CB_2R, which ranged from a moderate pK_i value of 6.30 ± 0.07 for AEA to high affinities below 10 nM for CP55,940, Dronabinol, ART-27.13, Tedalinab and TAK-937 (**Table 3.2**). In contrast, cannabidiol

(CBD), GW-842166X and EHP-101 were not able to displace [^{3}H]RO6957022 even at high concentrations, indicative of no affinity for CB_2R.

All agonists for which affinity could be determined were subjected to competition association assays to determine their binding kinetics at CB_2R (**Figure 3.2**, **Table 3.2**). The association of [^{3}H]RO6957022 to CB_2R was followed for 2 h in the absence (control) or presence of an IC_{50} concentration of competing agonist. Agonists with similar residence times (RT) to the radioligand used, such as CP55,940, displayed an association curve with a similar shape to the control curve (**Figure 3.2a**). Agonists with a longer RT compared to [^{3}H]RO6957022, such as HU308 presented a characteristic overshoot (**Figure 3.2b**). On the other hand, a slowly ascending curve was characteristic for agonists with a shorter RT compared to the radioligand, such as 2-AG and Tedalinab (**Figure 3.2c**,**d**). Using the Motulsky-Mahan equation, the kinetic binding parameters k_{on} and k_{off} were determined and subsequently these parameters were converted into engagement time (ET) for 1 μM of agonist and RT, respectively. ETs differed by 260-fold, with the fastest engagement to CB_2R for CP55,940 of below 1 s, and the slowest ETs for HU308 and AEA of 144 ± 48 s and 152 ± 10 s, respectively (**Table 3.2**). On the other hand, RTs only differed 44-fold. Dronabinol had the shortest interaction with CB_2R as represented by a RT of 2.1 ± 1.0 min, while TAK-937 displayed the longest RT of 93.2 ± 13.9 min (**Table 3.2**). Of note, due to the fast binding kinetics of CMX-020, CBN and KN 387271, their binding kinetics could not be quantified as these fell outside the assay's resolution.

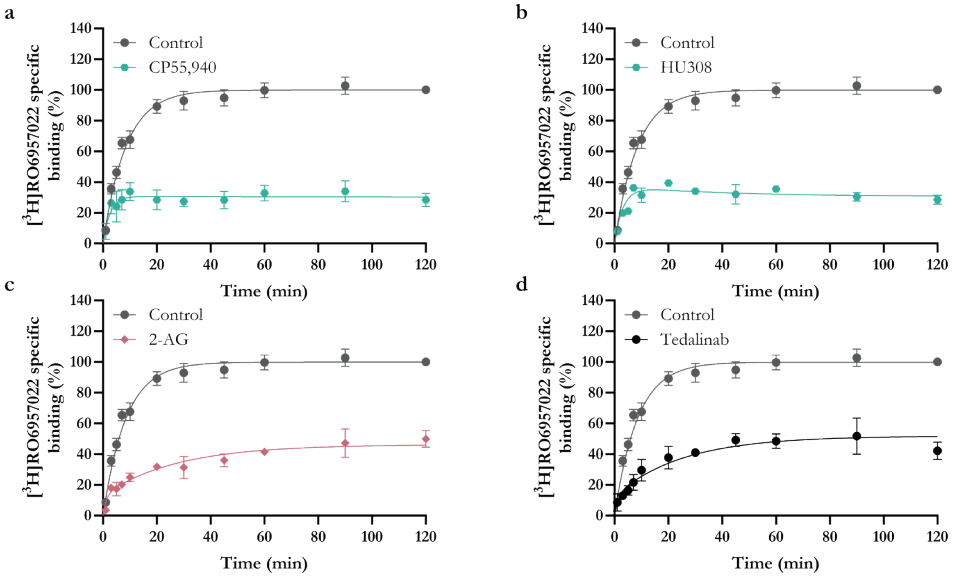

Figure 3.2 Evaluation of CB_2R target binding kinetics of representative benchmark agonists CP55,940 and HU308, endocannabinoid 2-AG, and clinical agonist Tedalinab.
Competition association assay with [^{3}H]RO6957022 on CB_2R in the absence (control) or presence of an IC_{50} concentration of representative competing agonists with (a) similar, (b) longer or (c, d) shorter receptor residence time (RT) compared to control, i.e., the radioligand used. Benchmark agonists are turquoise hexagons (⬢), 2-AG coral diamonds (◆) and clinical agonist Tedalinab black circles (●). Data are shown as mean ± SEM from three independent experiments performed in duplicate.

Table 3.2 Binding affinity and kinetic binding parameters of benchmark agonists, endocannabinoids (eCB) and clinical agonists on CB_2R.

	Agonist	CB_2R pK_i (K_i in nM) or displacement at 10 µM (%)[a]	k_{on} (M^{-1} s^{-1})[b]	ET (s)[c]	k_{off} (s^{-1})[d]	RT (min)[e]	K_D (nM)[f]	CB_1R pK_i (K_i in nM) or displacement at 10 µM (%)[g]	CB_2R selectivity[h]
Benchmark	**HU308**†	7.03 ± 0.10 (92.4)	(7.0 ± 2.3) × 10^3	143.5 ± 47.9	(2.3 ± 0.4) × 10^{-4}	71.0 ± 11.3	33.7	21 ± 9	>100
	HU910	7.18 ± 0.09 (65.7)	(1.4 ± 0.2) × 10^4	72.4 ± 11.9	(4.5 ± 1.0) × 10^{-4}	37.0 ± 7.9	32.6	5.62 ± 0.13 (2384)	36.3
	JWH133	7.40 ± 0.07 (39.7)	(7.6 ± 3.6) × 10^4	13.1 ± 6.2	(2.5 ± 1.1) × 10^{-3}	6.7 ± 3.0	32.6	48 ± 2	>250
	CP55,940†	8.85 ± 0.08 (1.4)	(1.8 ± 0.4) × 10^6	0.6 ± 0.1	(5.2 ± 0.9) × 10^{-4}	32.3 ± 5.5	0.3	8.91 ± 0.16 (1.2)	0.9
eCB	**AEA**†	6.31 ± 0.07 (484.5)	(6.6 ± 0.5) × 10^3	152.3 ± 10.4	(2.4 ± 0.1) × 10^{-3}	6.8 ± 0.4	371.7	6.60 ± 0.07 (254.1)	0.5
	2-AG†	7.01 ± 0.06 (97.3)	(5.3 ± 1.0) × 10^4	18.8 ± 3.6	(2.3 ± 0.3) × 10^{-3}	7.4 ± 1.0	42.7	6.60 ± 0.15 (251.8)	2.6
Clinical	**Dronabinol**	8.07 ± 0.26 (8.6)	(3.5 ± 1.5) × 10^5	2.9 ± 1.2	(7.8 ± 3.7) × 10^{-3}	2.1 ± 1.0	22.5	7.70 ± 0.09 (20.0)	2.3
	Nabilone	7.85 ± 0.07 (14.1)	(1.0 ± 0.2) × 10^5	9.9 ± 1.6	(6.3 ± 0.3) × 10^{-4}	26.6 ± 1.3	6.2	8.17 ± 0.06 (6.8)	0.5
	Cannabidiol	53 ± 2	N.A.	N.A.	N.A.	N.A.	N.A.	10 ± 7	N.A.
	Lenabasum	6.51 ± 0.11 (310.0)	(1.8 ± 0.9) × 10^4	55.8 ± 29.1	(2.6 ± 0.4) × 10^{-3}	6.4 ± 1.0	144.9	6.49 ± 0.08 (321.9)	1.0
	Olorinab†	7.45 ± 0.09 (35.3)	(2.5 ± 0.4) × 10^4	40.1 ± 5.9	(3.7 ± 0.6) × 10^{-4}	44.9 ± 6.6	14.9	-15 ± 8	>280
	CMX-020	6.37 ± 0.15 (428.9)	N.D.	N.D.	N.D.	N.D.	N.D.	7.05 ± 0.01 (88.2)	0.2
	Cannabinol	7.44 ± 0.16 (36.3)	N.D.	N.D.	N.D.	N.D.	N.D.	6.91 ± 0.07 (122.3)	3.4
	KN 387271	7.40 ± 0.08 (39.6)	N.D.	N.D.	N.D.	N.D.	N.D.	7.84 ± 0.05 (14.5)	0.4
	GW-842166X	27 ± 1	N.A.	N.A.	N.A.	N.A.	N.A.	2 ± 1	N.A.
	S-777469	6.37 ± 0.02 (423.3)	(1.0 ± 0.1) × 10^4	96.2 ± 10.5	(2.5 ± 0.7) × 10^{-3}	6.7 ± 2.0	239.1	-11 ± 3	>20
	LY-2828360	7.43 ± 0.14 (36.9)	(5.5 ± 0.7) × 10^4	18.1 ± 2.3	(1.8 ± 0.5) × 10^{-3}	9.2 ± 2.3	32.9	5.69 ± 0.06 (2040)	55.3
	PRS-211375	7.45 ± 0.11 (35.4)	(2.7 ± 0.7) × 10^4	36.8 ± 10.1	(5.3 ± 0.6) × 10^{-4}	31.6 ± 3.8	19.4	6.13 ± 0.06 (743.6)	21.0
	ART-27.13	8.93 ± 0.05 (1.2)	(4.1 ± 0.3) × 10^5	2.4 ± 0.2	(2.9 ± 0.4) × 10^{-4}	57.4 ± 8.4	0.7	7.71 ± 0.01 (19.7)	16.7
	NTRX-07	6.47 ± 0.09 (337.5)	(4.0 ± 1.1) × 10^4	25.3 ± 6.9	(6.5 ± 0.9) × 10^{-3}	2.6 ± 0.4	163.6	31 ± 3	>29
	EHP-101	24 ± 22	N.A.	N.A.	N.A.	N.A.	N.A.	-25 ± 11	N.A.
	Tedalinab	8.23 ± 0.08 (5.9)	(8.3 ± 1.5) × 10^5	1.2 ± 0.2	(2.4 ± 0.4) × 10^{-3}	7.0 ± 1.0	2.9	6.05 ± 0.05 (885.1)	149.9
	TAK-937	8.89 ± 0.05 (1.3)	(6.1 ± 1.6) × 10^5	1.6 ± 0.4	(1.8 ± 0.3) × 10^{-4}	93.2 ± 13.9	0.3	8.12 ± 0.11 (7.6)	5.8

To obtain a better understanding of the relationship between the affinity and kinetic binding parameters several correlation plots were constructed (**Figure S3.1**). The equilibrium pK_i and kinetic pK_D values were significantly correlated, validating the competition association assay (R^2 0.93, p <0.0001) (**Figure S3.1a**). Furthermore, association rate constant k_{on} significantly correlated with affinity (R^2 0.78, p <0.0001), while dissociation rate constant k_{off} did not correlate to affinity (**Figure S3.1b**,**c**). This indicated that fast association is the driving factor for high affinity on CB_2R. The kinetic map, which presents the connection between k_{on} (x-axis), k_{off} (y-axis) and kinetic affinity K_D (diagonals lines), highlighted the diversity of combinations between k_{on} and k_{off} to reach similar affinities. Furthermore, it indicated no clear clustering of groups of agonists based on one of the binding parameters, underlining the chemical diversity of the agonists (**Figure S3.1d**).

To get insight in selectivity over CB_1R, binding affinities of all agonists were determined in [^{3}H]CP55,940 displacement assays at this receptor (**Table 3.2**). Agonists CBD, GW-842166X and EHP-101 were devoid of CB_1R affinity, as was the case for CB_2R. As expected, no pronounced selectivity for either CBR was found for the endocannabinoids or CMX-020, a 2-AG derivative. Similarly, no selectivity was observed for CP55,940, Dronabinol, Nabilone, Lenabasum, Cannabinol, KN 387271 and TAK-937. A maximum 150-fold selectivity for CB_2R was found for Tedalinab and more than 15-fold CB_2R selectivity was detected for HU910, LY-2828360, PRS-211375 and ART-27.13. Furthermore, exclusive CB_2R affinity was observed for HU308, JWH133, Olorinab, S-777469 and NTRX-07.

To draw connections between molecular descriptors of CB_2R agonists and their binding, various correlation plots were constructed (**Figure S3.2**). None of the physicochemical parameters PSA, LogD or LogP of the agonists were correlated with either affinity (pK_i) or association and dissociation rate constants k_{on} and k_{off} (**Figure S3.2**). This suggested that the overall lipophilicity of the molecules, represented by different parameters, is not predictive for equilibrium or kinetic binding parameters at CB_2R. Altogether, structurally and chemically diverse CB_2R agonists varied greatly in affinity for CB_2R and selectivity over CB_1R. Affinity was predominantly driven by association rate constants of the agonists, but a general kinetic profile was not observed for the structurally diverse agonists investigated in this study.

← **Table 3.2** *(continued legend)*

[a, b, d] Binding parameters of agonists on CB_2R were determined in [^{3}H]RO6957022 displacement (affinity pK_i) and competition association (association, k_{on}, and dissociation, k_{off}, rate constants) assays on CHOK1_hCB_2bgal membranes at 10 °C. [c] Engagement time (ET) of the agonist to the receptor was determined for 1 μM agonist by employing equation 2 and is expressed in seconds (s), whereas k_{on} is expressed in M^{-1} s^{-1}. [e] Residence time (RT) was determined following equation 3 and is expressed in min, whereas k_{off} is expressed in s^{-1}. [f] Kinetic K_D values were determined using equation 4. [g] Binding affinity (pK_i) of agonists on CB_1R was determined in [^{3}H]CP55,940 displacement assays on CHOK1_hCB_1bgal membranes at 25 °C and [h] CB_2R selectivity was calculated using equation 1 or in the absence of CB_1R affinity defined as at least fold over highest concentration tested (10 μM). Values represent the mean ± SEM of at least three independent experiments performed in duplicate (*n* indicates the number of biological replicates). N.A is not applicable, N.D. is not detectable. [†] CB_2R data previously published[39].

3.2.2 Development and validation of a kinetic multiplex assay for CB_2R

To investigate biased signaling in one cellular system and in a kinetic context, we developed a novel multiplex assay. The new signaling assay incorporated two luminescent technologies for detection of inhibition of cAMP production, via $G\alpha_i$ activation, and ß-arrestin-2 recruitment after CB_2R activation to improve the detection of potential biased signaling of clinically relevant agonists. The inhibition of cAMP production was measured via the GloSensor technology, which was visualized by addition of GloSensor cAMP reagent. The NanoBiT technology was used to detect ß-arrestin-2 recruitment to CB_2R for which Vivazine was used as substrate (**Table S3.2**). The two technologies were combined in a multiplex assay to simultaneously measure both signaling events under the same assay conditions and in the same cellular background, and as such improve the validity of any observed signaling bias.

The multiplex assay was validated using full agonist CP55,940 as a reference (**Figure 3.3**). The pGloSensor plasmid was transfected into HEK293T cells already stably expressing CB_2R-SmBiT and LgBiT-ß-arrestin-2 (**Table S3.2**). After transfection, the cells were equilibrated with either cAMP reagent, Vivazine or a combination of cAMP reagent and Vivazine (i.e., termed "multiplex reagent") for 2 hours. Subsequently, cells were stimulated with 1 µM FSK to increase cAMP levels prior to inhibition due to CB_2R activation, which did not induce any detectable ß-arrestin-2 recruitment (**Figure S3.3**). After 1 hour, cells were stimulated with increasing concentrations of CP55,940 and the responses for the three different reagents were monitored on the cAMP channel (595 nm filter) and ß-arrestin channel (460 nm filter). Specific luminescent signals were only detected on the cAMP channel, but not the ß-arrestin channel, for cells that were pre-equilibrated with cAMP reagent (**Figure 3.3a**,**b**). *Vice versa*, in the presence of Vivazine, luminescent signals were only evident on the ß-arrestin channel and not the cAMP channel (**Figure 3.3c**,**d**). Pre-equilibration with the multiplex reagent resulted in the detection of CB_2R activation on both channels, and the traces were similar to the individually observed cAMP and ß-arrestin responses (**Figure 3.3a-f**). To quantify the results, the area under the curve (AUC) was determined from all time traces and presented in dose-response curves (**Figure 3.3g**,**h**). This confirmed the lack of agonist-mediated responses measured on the cAMP channel for Vivazine only, whereas the pEC_{50} values of CP55,940 obtained with cAMP reagent or multiplex reagent were similar, 8.86 and 8.55, respectively (**Table S3.3**). Similarly, CP55,940-induced ß-arrestin-2 recruitment was only measured in the presence of Vivazine or multiplex reagent, which resulted in similar pEC_{50} values, i.e., 8.20 and 8.16, respectively.

As this protocol clearly distinguished between the responses obtained for inhibition of cAMP production and ß-arrestin-2 recruitment of full agonist CP55,940, we continued screening the remaining benchmark agonists, endocannabinoids and clinical agonists with the FSK-induced multiplex assay.

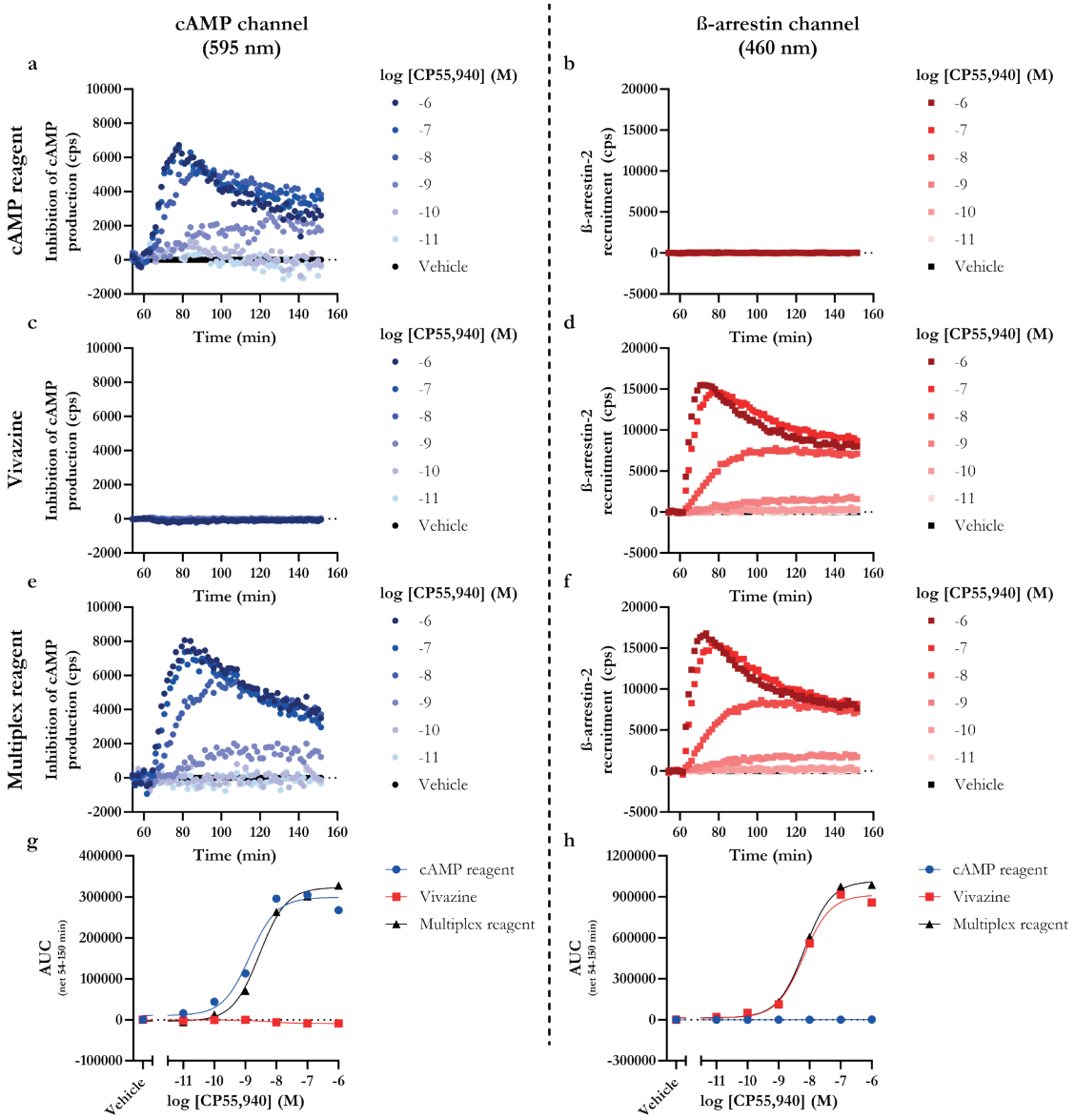

Figure 3.3 Validation and characterization of the multiplexed cAMP production and ß-arrestin-2 recruitment assay on HEK293T CB_2R-SmBiT LgBiT-ß-arrestin-2 cells with full agonist CP55,940.
Representative forskolin- and vehicle-corrected time traces of CP55,940 stimulation on HEK293T CB_2R-SmBiT LgBiT-ß-arrestin-2 cells pre-equilibrated with (a, b) only cAMP reagent, (c, d) only Vivazine, or (e, f) multiplex reagent (cAMP reagent and Vivazine) for 2 h at 25 °C. The signals were simultaneously recorded at the (a, c, e) cAMP channel (595 nm) and (b, d, f) ß-arrestin channel (460 nm). Area Under the Curve (AUC) was determined from the time traces after detection on the (g) cAMP channel or (h) ß-arrestin channel. Data are shown as mean from a (a-f) representative experiment or (g-h) mean of two independent experiments all performed in duplicate.

3.2.3 Characterization of time traces by benchmark agonists, endocannabinoids and clinical agonists in the multiplex assay

All benchmark agonists, endocannabinoids and clinical agonists were screened in the multiplex assay and the signaling time traces at different concentrations of agonist were recorded in the two specific readouts (**Figure 3.4**, **S3.4-S3.7**, **Table 3.3**, **3.4**). Typically, at high concentrations of agonist the inhibition of cAMP production increased for the first 20 minutes after which the signals decreased with a tendency to return to baseline levels, although a complete return was not observed within the selected assay time (**Figure 3.4**, **S3.4**, **S3.5**). At lower concentrations of agonist, the inhibition of cAMP production increased, although at a lower rate than with high agonist concentrations, to reach a steady plateau within our assay time.

Strikingly, for several clinical agonists (AEA, Dronabinol, CBD, Lenabasum, CMX-020, CBN, KN 387271, GW-842166X, NTRX-07 and EHP-101), the cAMP production by 10 μM of agonist did not return to basal levels, whereas by 1 μM agonist it did (**Figure S3.4**, **S3.5**). Of note, CBD and EHP-101 only modified cAMP levels at 10 μM. Intriguingly, 10 μM Olorinab induced a small inhibition of cAMP levels, which quickly returned to forskolin baseline levels and even further increased cAMP levels (**Figure S3.5a**). To this end, the cAMP production of saturating concentrations (>100x K_i value) or 10 μM of all agonists was investigated in parental HEK293T cells devoid of CB_2R expression (**Figure S3.8**). For multiple agonists (Dronabinol, CBD, Lenabasum, Olorinab, CMX-020, CBN, KN 387271, GW-842166X, LY-2828360, ART-27.13, NTRX-07 and TAK-937), we observed CB_2R-independent cAMP responses. Consequently, for these agonists 10 μM was removed from the dose-response curves in the semi-kinetic and kinetic analysis, i.e., the methods of analysis using the full time traces.

In almost all cases, a high concentration of agonist induced a quick increase in ß-arrestin-2 recruitment, which fell back to a steady state above baseline (**Figure 3.4**, **S3.6**, **S3.7**). On the other hand, lower concentrations of agonist caused recruitment of ß-arrestin-2, which increased towards a steady plateau above baseline. No increase in luminescence, as a consequence of ß-arrestin-2 recruitment to CB_2R, was observed for any concentration of CBD or EHP-101, while a small increase in luminescence was observed by 10 and 1 μM GW-842166X (**Figure S3.6i**, **S3.7k**).

An advantage of the multiplex assay is the possibility of observing the difference in initiation of the two signaling events over time, which was visualized for agonists CP55,940, HU308, HU910, 2-AG, PRS-211375 and Tedalinab at a saturating concentration (**Figure 3.4**, **S3.4-S3.7**). In all cases, the peak response of ß-arrestin-2 recruitment was reached earlier than the peak response of the inhibition of cAMP production. The peak response for both ß-arrestin-2 recruitment and inhibition of cAMP production for PRS-211375 was markedly higher than the peak responses of CP55,940-mediated activation (**Figure 3.4a**,**e**). Similarly, the peak response for ß-arrestin-2 recruitment by Tedalinab was higher than by CP55,940, while the cAMP peak responses were similar (**Figure 3.4a**,**f**). Moreover, agonist-induced differences between the steepness of the decline phase after the peak responses are observed. For instance, a steep decline in ß-arrestin-2 recruitment is observed for CP55,940,

2-AG, PRS-211375 and Tedalinab, while the decline is more moderate for HU308 and HU910. Altogether, the shape of the curves is a first indication towards agonist-mediated differences in functional responses. In particular, differences in maximal effect are observed, but the time traces also accentuate variations in the responses over time.

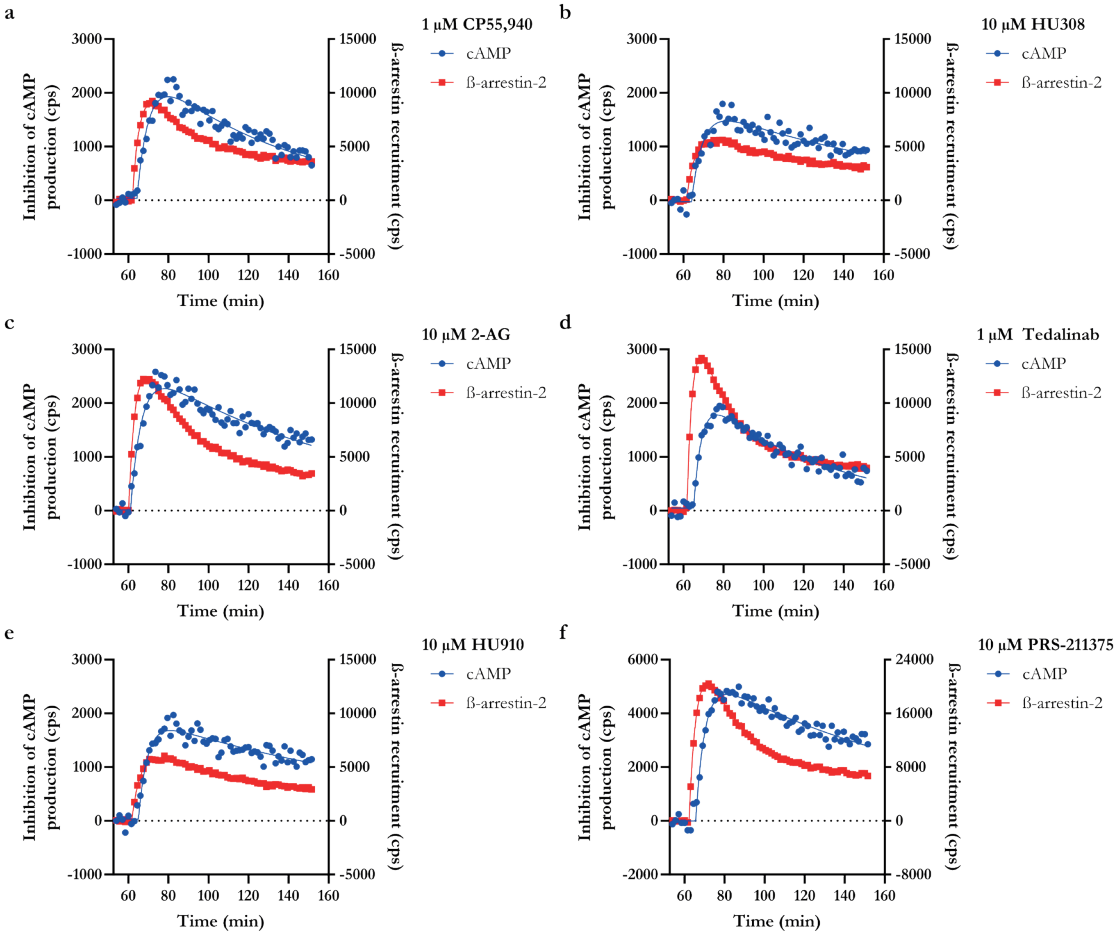

Figure 3.4 Kinetic functional characterization of representative agonists CP55,940, HU308, HU910, 2-AG, PRS-211375 and Tedalinab in the multiplex assay on HEK293T CB_2R-SmBiT LgBiT-ß-arrestin-2 cells. Representative forskolin- and vehicle-corrected time traces for inhibition of cAMP production (left y-axis) and ß-arrestin-2 recruitment (right y-axis) by (a) 1 µM CP55,940, (b) 10 µM HU308, (c) 10 µM HU910, (d) 10 µM 2-AG, (e) 10 µM PRS-211375 or (f) 1 µM Tedalinab in the multiplex assay on CB_2R. Data are shown as mean from a representative experiment all performed in duplicate. Representative dose-dependent time traces of all agonists can be found in Figures 3.S4-3.S7.

3.2.4 Endpoint quantification of CB_2R activation by benchmark agonists, endocannabinoids and clinical agonists in the multiplex assay

To quantify the effects of the benchmark agonists, endocannabinoid and clinical agonists in the multiplex assay, their potency and efficacy values were determined with three different methods of analysis. Initially, all data was analyzed at four different time points to investigate the time-dependency of activation. To this end, dose-response curves of cAMP production and ß-arrestin-2 recruitment were created for 7.5, 15, 30 and 60 min after agonist addition (**Figure S3.9-S3.12**). Note that, no dose-response curves could be generated for 90 min after agonist addition as cAMP production returned to vehicle conditions for all agonist concentrations. No potency values could be determined for the inhibition of cAMP production or ß-arrestin-2 recruitment by CBD, GW-842166X or EHP-101, which is in line with their lack of CB_2R affinity (**Table 3.2**, **S3.4**, **S3.5**). Potency and efficacy values were only quantified for the early (7.5 min) and late (60 min) time point and the differences between those were calculated (**Figure 3.5**, **Table S3.4**, **S3.5**).

Potency and efficacy values of HU910, JWH133, AEA, 2-AG, Dronabinol, Lenabasum, CBN, KN 387271, S-777469 and Tedalinab remained unaffected over time (**Figure 3.5**, **S3.9b**,**c**,**f**,**j**, **S3.10f**,**l**, **Table S3.4**). On the other hand, potency values for CP55,940, Nabilone, Olorinab, PRS-211375, ART-27.13 and TAK-937 were significantly increased over time, whereas there was no time-dependent effect on efficacy (**Figure 3.5**, **S3.9d**,**h**, **S3.10a**,**h**,**i**,**m**, **Table S3.4**). Interestingly, NTRX-07's potency was significantly decreased over time, while a seeming increase in efficacy was not statistically significant (**Table S3.4**). While no pEC_{50} value could be determined for LY-2828360 after 7.5 min (pEC_{50} <10 µM),

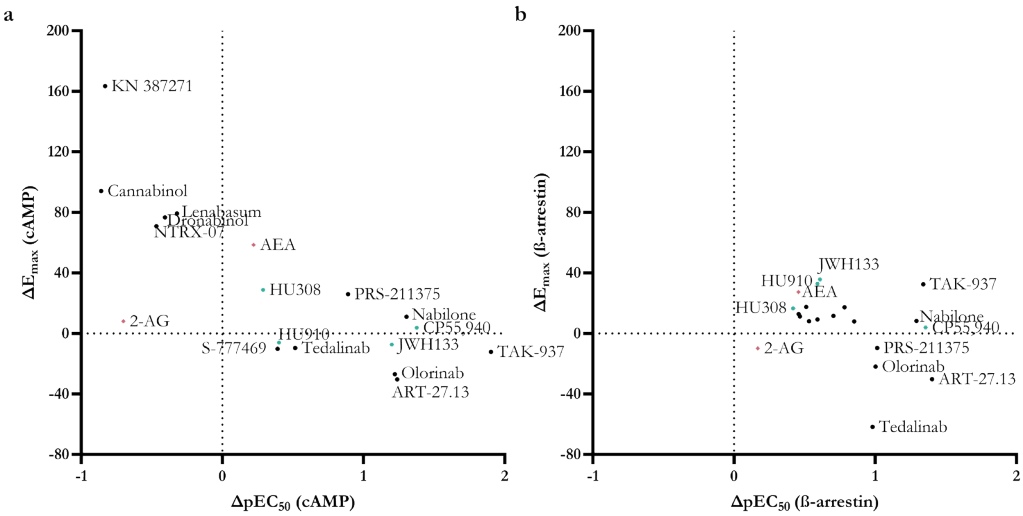

Figure 3.5 Time-dependent effect on potency and efficacy of benchmark agonists, endocannabinoids and clinical agonists in the multiplex assay on HEK293T CB_2R-SmBiT LgBiT-ß-arrestin-2 cells.
Differences in potency (ΔpEC_{50}) and efficacy (ΔE_{max}) from (a) cAMP production and (b) ß-arrestin-2 recruitment assays by benchmark agonists, endocannabinoids and clinical agonists after 60 min of stimulation compared to 7.5 min. Benchmark agonists are turquoise hexagons (⬢), endocannabinoids coral diamonds (◆) and clinical agonists black circles (●). Data are shown as mean from at least three independent experiments performed in duplicate.

its potency increased over time to 7.45 ± 0.38 (**Figure S3.9g**, **Table S3.4**). Alternatively, HU308's potency was not dependent on time, but its efficacy was significantly increased from partial (78 ± 4%) to full agonism (106 ± 7%, **Figure 3.5**, **S3.9a**, **Table S3.4**).

The potency and efficacy of HU308 and 2-AG for ß-arrestin-2 recruitment were not dependent on time (**Figure 3.5**, **S3.11a,f**, **Table S3.5**). Endocannabinoid AEA's potency was unaffected by longer incubation, but AEA's efficacy was significantly increased to 53 ± 3% after 60 min compared to 26 ± 0% at 7.5 min (**Figure 3.5**, **S3.11e**, **Table S3.5**). The potency of the seventeen remaining agonists was significantly increased over time with varying effects on efficacy. Specifically, the efficacy was significantly increased for HU910, JWH133, CP55,940, Dronabinol, CMX-020, KN 387271, LY-2828360 and TAK-937, while the efficacy of Nabilone, Lenabasum, CBN, S-777469, PRS-211375 and NTRX-07 remained unaffected (**Figure 3.5**, **S3.11**, **S3.12**, **Table S3.5**). On the other hand, the efficacy of Tedalinab was significantly decreased over time, and a similar trend was observed for Olorinab and ART-27.13 (**Figure 3.5**, **S3.12a,i,l**, **Table S3.5**).

This method of analysis showed that activation by certain agonists is not time-dependent, whereas for other agonists potency and/or efficacy might be increased or decreased over time, and this may differs depending on functional assay. Furthermore, it suggests that interpretation of results is highly dependent on the selected time point for data analysis, i.e., endpoint analyses (and assays) can influence conclusions on ligand function and bias.

3.2.5 Semi-kinetic quantification of CB_2R activation by benchmark agonists, endocannabinoids and clinical agonists in the multiplex assay

To incorporate the kinetic time traces, a second semi-kinetic method of analysis was pursued, which is commonly used to analyze time traces obtained from functional assays. To this end, the AUC of the full 90 min of activation was plotted against the agonist concentration and potency and efficacy values were determined for cAMP production and ß-arrestin-2 recruitment. For agonists that showed CB_2R-independent cAMP production (Dronabinol, CBD, Lenabasum, Olorinab, CMX-020, CBN, KN 387271, GW-842166X, LY-2828360, ART-27.13, NTRX-07 and TAK-937), the curves were analyzed up to 1 µM in cAMP production (**Figure S3.8-S3.10**). Furthermore, no potency values were determined for CBD, GW-842166X and EHP-101 due to their lack of cAMP production or ß-arrestin-2 recruitment, which is in line with their lack of CB_2R affinity (**Table 3.2- 3.4**).

Potency values determined for inhibition of cAMP production spanned a wide range. Dronabinol and CBN displayed the lowest potencies with pEC_{50} values of 5.66 ± 0.06 and 5.70 ± 0.05, respectively, whereas agonists CP55,940, ART-27.13 and Tedalinab were full agonists and exhibited sub nanomolar potency with pEC_{50} values of 9.15 ± 0.16, 9.5 ± 0.27 and 9.38 ± 0.25, respectively (**Table 3.3**). HU308, HU910, 2-AG, Nabilone, Lenabasum, CMX-020, PRS-211375 and NTRX-07 behaved as full agonists with E_{max} values >90%, but with lower potency values compared to the before mentioned agonists, i.e., pEC_{50} values between 6.15 ± 0.17 and 7.80 ± 0.17.

Table 3.3 **Inhibition of forskolin-induced cAMP production by benchmark agonists, endocannabinoids (eCB) and clinical agonists determined in the multiplex assay on CB_2R.**

	Agonist	pEC_{50}	E_{max} or activation at 1 μM (%)	pIR_{50}	IR_{max} or activation at 10 μM (%)	k_1 (min^{-1})	k_2 (min^{-1})
Benchmark	**HU308**	6.57 ± 0.03	95 ± 3	6.03 ± 0.11	90 ± 4	0.26 ± 0.08	0.012 ± 0.002
	HU910	6.93 ± 0.08	102 ± 5	6.44 ± 0.17	89 ± 9	0.24 ± 0.08	0.012 ± 0.005
	JWH133	6.96 ± 0.07	88 ± 5	6.46 ± 0.12	79 ± 10	0.15 ± 0.01	0.026 ± 0.005
	CP55,940	9.15 ± 0.16	103 ± 5	7.90 ± 0.22	102 ± 1	0.24 ± 0.07[§]	0.015 ± 0.002[§]
eCB	**AEA**	6.41 ± 0.12	73 ± 12	5.73 ± 0.21	65 ± 5	0.15 ± 0.05[§]	N.A.
	2-AG	6.15 ± 0.17	92 ± 16	6.16 ± 0.26	94 ± 7	0.26 ± 0.04	0.011 ± 0.001
Clinical	**Dronabinol**	5.66 ± 0.06	79 ± 19	6.65 ± 0.20	24 ± 1	0.08 ± 0.03	N.A.
	Nabilone	7.80 ± 0.17	99 ± 13	6.85 ± 0.19	81 ± 12	0.23 ± 0.02	0.004 ± 0.001
	Cannabidiol	N.D.	-8 ± 2[§]	N.D.	4 ± 0[#]	N.D.	N.D.
	Lenabasum	6.50 ± 0.07	132 ± 19	6.13 ± 0.15	93 ± 11	0.14 ± 0.01[§]	0.007 ± 0.001[§]
	Olorinab	7.88 ± 0.08	61 ± 14	6.92 ± 0.14	79 ± 10	0.14 ± 0.04[§]	0.042 ± 0.015[§]
	CMX-020	6.47 ± 0.13	109 ± 7	6.70 ± 0.58	53 ± 11	0.14 ± 0.03[§]	N.A.
	Cannabinol	5.70 ± 0.05	81 ± 17	6.53 ± 0.02	10 ± 1	0.04 ± 0.01	N.A.
	KN 387271	7.96 ± 0.20	78 ± 11	7.29 ± 0.08	109 ± 29	0.30 ± 0.11[§]	0.009 ± 0.002[§]
	GW-842166X	N.D.	37 ± 3[§]	N.D.	65 ± 13[#]	0.19 ± 0.01[§]	N.D.
	S-777469	7.04 ± 0.12	86 ± 12	6.71 ± 0.20	88 ± 10	0.22 ± 0.02	0.011 ± 0.002
	LY-2828360	6.89 ± 0.25	26 ± 5	6.33 ± 0.18	43 ± 7	0.24 ± 0.05	0.014 ± 0.003
	PRS-211375	7.18 ± 0.33	94 ± 11	6.41 ± 0.17	105 ± 4	0.24 ± 0.01	0.005 ± 0.002
	ART-27.13	9.15 ± 0.27	96 ± 11	7.93 ± 0.33	113 ± 23	0.24 ± 0.01[§]	0.012 ± 0.000[§]
	NTRX-07	6.70 ± 0.17	110 ± 27	6.59 ± 0.26	79 ± 3	0.20 ± 0.03[§]	0.006 ± 0.002[§]
	EHP-101	N.D.	19 ± 2[§]	N.D.	5 ± 1[#]	N.D.	N.D.
	Tedalinab	9.38 ± 0.25	97 ± 6	8.53 ± 0.14	114 ± 16	0.26 ± 0.03[§]	0.018 ± 0.002[§]
	TAK-937	8.56 ± 0.11	81 ± 3	7.07 ± 0.16	85 ± 3	0.20 ± 0.01[§]	0.008 ± 0.001[§]

Potency (pEC_{50}, pIR_{50}) and efficacy (E_{max}, IR_{max}) values were determined from AUC and initial rate dose-response curves, respectively, derived from the cAMP time traces in the multiplex assay. In the absence of a DRC, maximal activation (%) was determined at 10 (#) or 1 μM (§) of agonist. Signaling rate constants k_1 and k_2 were determined at 10 μM or 1 μM (§) of agonist. Data are mean from at least three independent experiments performed in duplicate. N.A is not applicable, N.D. is not detectable.

Table 3.4 ß-arrestin-2 recruitment by benchmark agonists, endocannabinoids (eCB) and clinical agonists determined in the multiplex assay on CB_2R.

	Agonist	pEC_{50}	E_{max} or activation at 1 µM (%)	pIR_{50}	IR_{max} or activation at 10 µM (%)	k_1 (min^{-1})	k_2 (min^{-1})
Benchmark	**HU308**	6.57 ± 0.03	95 ± 3	6.03 ± 0.11	90 ± 4	0.26 ± 0.08	0.012 ± 0.002
	HU910	6.93 ± 0.08	102 ± 5	6.44 ± 0.17	89 ± 9	0.24 ± 0.08	0.012 ± 0.005
	JWH133	6.96 ± 0.07	88 ± 5	6.46 ± 0.12	79 ± 10	0.15 ± 0.01	0.026 ± 0.005
	CP55,940	9.15 ± 0.16	103 ± 5	7.90 ± 0.22	102 ± 1	0.24 ± 0.07[§]	0.015 ± 0.002[§]
eCB	**AEA**	6.41 ± 0.12	73 ± 12	5.73 ± 0.21	65 ± 5	0.15 ± 0.05[§]	N.A.
	2-AG	6.15 ± 0.17	92 ± 16	6.16 ± 0.26	94 ± 7	0.26 ± 0.04	0.011 ± 0.001
Clinical	**Dronabinol**	5.66 ± 0.06	79 ± 19	6.65 ± 0.20	24 ± 1	0.08 ± 0.03	N.A.
	Nabilone	7.80 ± 0.17	99 ± 13	6.85 ± 0.19	81 ± 12	0.23 ± 0.02	0.004 ± 0.001
	Cannabidiol	N.D.	-8 ± 2[§]	N.D.	4 ± 0[#]	N.D.	N.D.
	Lenabasum	6.50 ± 0.07	132 ± 19	6.13 ± 0.15	93 ± 11	0.14 ± 0.01[§]	0.007 ± 0.001[§]
	Olorinab	7.88 ± 0.08	61 ± 14	6.92 ± 0.14	79 ± 10	0.14 ± 0.04[§]	0.042 ± 0.015[§]
	CMX-020	6.47 ± 0.13	109 ± 7	6.70 ± 0.58	53 ± 11	0.14 ± 0.03[§]	N.A.
	Cannabinol	5.70 ± 0.05	81 ± 17	6.53 ± 0.02	10 ± 1	0.04 ± 0.01	N.A.
	KN 387271	7.96 ± 0.20	78 ± 11	7.29 ± 0.08	109 ± 29	0.30 ± 0.11[§]	0.009 ± 0.002[§]
	GW-842166X	N.D.	37 ± 3[§]	N.D.	65 ± 13[#]	0.19 ± 0.01[§]	N.D.
	S-777469	7.04 ± 0.12	86 ± 12	6.71 ± 0.20	88 ± 10	0.22 ± 0.02	0.011 ± 0.002
	LY-2828360	6.89 ± 0.25	26 ± 5	6.33 ± 0.18	43 ± 7	0.24 ± 0.05	0.014 ± 0.003
	PRS-211375	7.18 ± 0.33	94 ± 11	6.41 ± 0.17	105 ± 4	0.24 ± 0.01	0.005 ± 0.002
	ART-27.13	9.15 ± 0.27	96 ± 11	7.93 ± 0.33	113 ± 23	0.24 ± 0.01[§]	0.012 ± 0.000[§]
	NTRX-07	6.70 ± 0.17	110 ± 27	6.59 ± 0.26	79 ± 3	0.20 ± 0.03[§]	0.006 ± 0.002[§]
	EHP-101	N.D.	19 ± 2[§]	N.D.	5 ± 1[#]	N.D.	N.D.
	Tedalinab	9.38 ± 0.25	97 ± 6	8.53 ± 0.14	114 ± 16	0.26 ± 0.03[§]	0.018 ± 0.002[§]
	TAK-937	8.56 ± 0.11	81 ± 3	7.07 ± 0.16	85 ± 3	0.20 ± 0.01[§]	0.008 ± 0.001[§]

Potency (pEC_{50}, pIR_{50}) and efficacy (E_{max}, IR_{max}) values were determined from AUC and initial rate dose-response curves, respectively, derived from the ß-arrestin-2 recruitment time traces in the multiplex assay. In the absence of a DRC, maximal activation (%) was determined at 10 (#) or 1 µM (§) of agonist. Signaling rate constants k_1 and k_2 were determined at 10 µM or 1 µM (§) of agonist. Data are mean from at least three independent experiments performed in duplicate. N.A is not applicable, N.D. is not detectable.

Secondly, the recruitment of ß-arrestin-2 to CB_2R was determined in the multiplex assay (**Table 3.4**). Potency values, calculated from the AUC-derived dose-response curves, ranged from 5.90 ± 0.14 for 2-AG to 8.54 ± 0.04 for CP55,940. Various degrees of partial agonism were observed in the agonist set. HU910, JWH133 were full agonists with E_{max} values > 90%, while Olorinab, PRS-211375, ART-27.13 and Tedalinab recruited ß-arrestin-2 to CB_2R with a higher efficacy than reference full agonist CP55,940 with E_{max} values of 114 ± 1%, 108 ±2%, 107 ±1% and 137 ± 5%, respectively, and could therefore be described as superagonists in this readout. All remaining fourteen agonists displayed partial agonism in ß-arrestin-2 recruitment with E_{max} values between 10 and 90%.

3.2.6 Kinetic quantification of CB_2R activation by benchmark agonists, endocannabinoids and clinical agonists in the multiplex assay

To use the kinetic data to its fullest potential, kinetic signaling parameters were calculated using the kinetic mathematical model by Hoare *et al.*, i.e., currently the only equations available for such analysis[20]. The initial rate (IR) was determined for each time trace and the kinetic potency (pIR_{50}) and kinetic efficacy (IR_{max}) were obtained from the generated dose-response IR curve. Furthermore, the signaling rate constants k_1 and k_2 were determined at a saturating concentration of agonist, i.e., 10 µM or 1 µM agonist (**Table 3.3**, **3.4**). From the kinetic trace fits, peak responses were obtained and also used to generate dose-response curves for parameter quantification. However, these results were identical to the AUC data and therefore not further analyzed (data not shown). No potency values were determined for CBD, GW-842166X and EHP-101 due to their lack of inhibition of cAMP production or ß-arrestin-2 recruitment to CB_2R, which is in line with their lack of CB_2R affinity (**Table 3.2-3.4**).

Based on the shape of the agonist-induced inhibition of cAMP production time traces, a statistical comparison between two rise-and-fall equations was performed, i.e., the simpler 'rise-and-fall to baseline' which describes a decline of signaling, and more complex 'rise-and-fall to steady state', which describes a decline to levels above baseline. The first fit was statistically preferred for inhibition of cAMP production. The kinetic potencies ranged from pIR_{50} values of 5.73 ± 0.21 for AEA to 8.53 ± 0.14 for Tedalinab (**Table 3.3**). A large variety in kinetic efficacy was observed with full agonists HU308, CP55,940, 2-AG, Lenabasum, KN 387271, PRS-211375, ART-27.13 and Tedalinab displaying IR_{max} values over 90%. All other twelve agonists displayed partial agonism, which ranged from 10 ± 1% for CBN to 89 ± 9 % for HU910. Moreover, two signaling rate constants k_1 and k_2 for the agonist-mediated inhibition of cAMP production were calculated, where the rising phase of the curve is characterized by k_1, and the fall phase by k_2. These constants were determined at saturating concentrations of agonist, i.e., 10 µM for most agonists and 1 µM for potent agonists CP55,940, ART-27.13, Tedalinab and TAK-9337 (**Table 3.3**). Values for k_1 ranged from 0.04 ± 0.01 min^{-1} for slowly activating agonist CBN to 0.30 ± 0.11 min^{-1} for faster agonist KN 387271, a difference of maximally 7.5-fold, while k_2 values differed maximally 10-fold between fastest agonist Olorinab (0.042 ± 0.015 min^{-1}) and slowest detectable agonist Nabilone (0.004 ± 0.001 min^{-1}).

Based on the shape of the ß-arrestin-2 recruitment traces, a statistical comparison between the two available rise-and-fall fits was performed, i.e., 'rise-and-fall to baseline' and 'rise-and-fall to steady state' equations, where in this case the latter was statistically preferred. The kinetic potencies ranged from pIR_{50} values of 5.19 ± 0.02 for AEA to 7.5 ± 0.07 for Tedalinab (**Table 3.4**). Superagonists Olorinab, PRS-211375, ART-27.13 and Tedalinab displayed high IR_{max} values of 157 ± 2%, 133 ± 12%, 148 ± 3% and 234 ±10%, respectively, while 2-AG behaved as a full agonist with a kinetic efficacy of 90 ± 17%. All thirteen remaining agonists displayed partial agonism in ß-arrestin-2 recruitment to CB_2R with IR_{max} values ranging from 4 ± 1% for Dronabinol to 80 ± 10% for HU308. The two signaling rate constants k_1 and k_2 for the agonist-mediated ß-arrestin recruitment were determined at saturating concentrations of agonist, i.e., 10 μM for most agonists and 1 μM for potent agonists (**Table 3.4**). The rising phase of the curve and corresponding parameter k_1 only differed less than 4-fold from slow agonist JWH133 (0.18 ± 0.01 min^{-1}) to faster agonist CMX-020 (0.63 ± 0.11 min^{-1}). The rate constant of the fall phase k_2 showed major differences with a maximal 32-fold difference between fastest agonist Tedalinab (0.063 ± 0.008 min^{-1}) and slowest detectable agonist Dronabinol (0.002 ± 0.001 min^{-1}).

The kinetic mathematical model allowed for a robust quantification of agonist-mediated inhibition of cAMP production and ß-arrestin-2 recruitment. The two potency values from the semi-kinetic and kinetic analyses, i.e., pEC_{50} and pIR_{50}, respectively, correlated for both the inhibition of cAMP production (R^2 0.73, $p < 0.0001$) and ß-arrestin-2 recruitment (R^2 0.90, $p < 0.0001$) (**Figure S3.13a,i**). Furthermore, efficacy E_{max} and kinetic efficacy IR_{max} values were well correlated for both pathways (R^2 0.44, p 0.0006 and R^2 0.80, $p < 0.0001$) (**Figure S3.13b,j**). The signaling rate constants, k_1 and k_2, of the agonists were not predictive for the kinetic potencies for either inhibition of cAMP production or ß-arrestin recruitment (**Figure S3.13c,d,k,l**). However, k_1 values from the inhibition of cAMP production were significantly correlated with ΔE_{max} values from the time-dependent analysis, i.e., agonists with fast k_1 values tended to gain efficacy over time (**Figure S3.13g**). For ß-arrestin-2 recruitment signaling parameters, only a fast k_2 value positively correlated with ΔE_{max} values, whereas no statistically significant correlation was found between k_1 values and ΔE_{max} values (**Figure S3.13o,p**). Interestingly, superagonists relative to CP55,940 in ß-arrestin-2 recruitment were characterized by a decrease in efficacy over time, i.e., negative ΔE_{max} values, and all displayed fast k_1 values (**Figure S3.13o**). Lastly, the interplay between inhibition of cAMP production and ß-arrestin-2 recruitment was investigated in terms of the kinetic parameters. Kinetic potency values for all agonists in inhibition of cAMP production and ß-arrestin-2 recruitment were significantly correlated (R^2 0.93, $p < 0.0001$) and only differed maximally 10-fold, indicating no overall pathway bias in the diverse agonist set (**Figure S3.13q**). Similarly, kinetic efficacy (IR_{max}) values were significantly correlated (R^2 0.53, p 0.0002) (**Figure S3.13r**). On the contrary, signaling rate constants k_1 and k_2 values were not correlated between the two readouts (p 0.7044, p 0.4600) (**Figure S3.13s,t**).

Altogether, investigation of benchmark agonists, endocannabinoids and clinical agonists in the multiplex assay highlighted the diversity of signaling potencies and efficacies at CB_2R within this large set of agonists. Furthermore, it emphasized the possibility and importance of kinetic evaluation, including kinetic mathematical analysis, of receptor signaling. The kinetic mathematical equations allowed quantification of common pharmacological

parameters, although with a kinetic context, i.e., kinetic potency (pIR_{50}) and kinetic efficacy (IR_{max}). Moreover, signaling rate constants k_1 and k_2 could be determined, which were not correlated between inhibition of cAMP production and ß-arrestin-2 recruitment suggesting these parameters may play a role in biased signaling.

3.2.7 Exploration of the kinetic context of CB_2R agonists

To investigate whether kinetic binding parameters of CB_2R agonists could be predictive for signaling parameters various correlation plots were generated (**Figure S3.14**). A fast association with CB_2R was significantly correlated with kinetic potencies pIR_{50} in both inhibition of cAMP production (R^2 0.66, $p < 0.0001$) and ß-arrestin-2 recruitment (R^2 0.73, $p < 0.0001$) (**Figure S3.14a**,**i**). In other words, the faster engaging agonists displayed higher kinetic functional potencies than the slowly engaging agonists. In contrast, no correlation was found between association rate constants and kinetic efficacy IR_{max} or the time-dependent increase in efficacy in either readout (**Figure S3.14b**,**d**,**j**,**l**). Unexpectedly, a quick engagement did not correlate with a quick activation, evident by the lack of statistically significant correlations between association rate constant k_{on} and signaling constant k_1 for either inhibition of cAMP production (R^2 <0.01, p 0.8045) or ß-arrestin-2 recruitment (R^2 0.03, p 0.5064) (**Figure S3.14c**,**k**).

Dissociation rate constants k_{off} were not correlated with pIR_{50} nor IR_{max} in both inhibition of cAMP production (R^2 0.02, p 0.5736; R^2 0.12, p 0.1512) or ß-arrestin-2 recruitment (R^2 0.04, p 0.4569; R^2 0.06, p 0.3127) (**Figure S3.14e**,**f**,**m**,**n**). On the contrary, a statistically significant correlation was observed for k_{off} values and time-dependent differences in efficacy for inhibition cAMP production (R^2 0.34, p 0.0139), but not ß-arrestin-2 recruitment (R^2 <0.01, p 0.9673) (**Figure S3.14h**,**p**). Specifically, fast dissociating agonists displayed an increase in cAMP efficacy over time (**Figure S3.14h**). Furthermore, no statistically significant correlations were found between dissociation rate constants and signaling (deactivation) rate constants k_2 in cAMP production ($R^2 < 0.01$, p 0.8798) or ß-arrestin-2 recruitment (R^2 0.19, p0.0705) (**Figure S3.14g**,**o**). Although, a small trend was displayed for slow dissociating agonists and slow deactivation in ß-arrestin-2 recruitment (**Figure S3.14o**).

Altogether, these correlations highlight that optimization of association rate constants rather than dissociation rate constants may contribute to high kinetic potencies but does not affect kinetic efficacy. Nevertheless, agonists with a fast dissociation rate constant might gain efficacy over time in inhibition of cAMP production and a fast k_{off} may play a role in deactivation of ß-arrestin-2 recruitment. This emphasizes the importance of providing a full kinetic overview of agonist-mediated CB_2R signaling.

3.2.8 Determination of ligand bias at CB_2R

Ultimately, biased signaling at CB_2R was investigated by using the different methods of analysis, i.e., an endpoint, a semi-kinetic and a kinetic analysis. The operational model was used to derive transduction coefficients LogR from the inhibition of cAMP production and

ß-arrestin-2 recruitment dose-response curves. To investigate the time-dependency of bias and the impact of different analysis strategies, the model was applied to the dose-response curves generated after 7.5 and 60 min of agonist activation (endpoint), AUC (semi-kinetic) and IR (kinetic) determination. In all cases, the LogR values were normalized to most balanced agonist HU308 resulting in ΔLogR for each agonist per pathway. Subsequently, these ratios were compared per agonist between the cAMP and ß-arrestin-2 pathways, which presented the relative bias ΔΔLogR (**Figure 3.6**, **Table S3.6**). As mentioned earlier, CBD, GW-842166X and EHP-101 failed to activate (or bind to) CB_2R, and consequently no LogR values were calculated for these agonists.

No clear preference for either pathway was observed for Olorinab, S-777469, ART-27.13, NTRX-07 and Tedalinab relative to HU308 using any of the methods of analysis. HU910 displayed a slight preference for inhibition of cAMP production over ß-arrestin-2 recruitment in the endpoint analysis after 7.5 and 60 min of activation, whereas in the semi-kinetic determination the preference flipped to ß-arrestin-2 recruitment and no clear

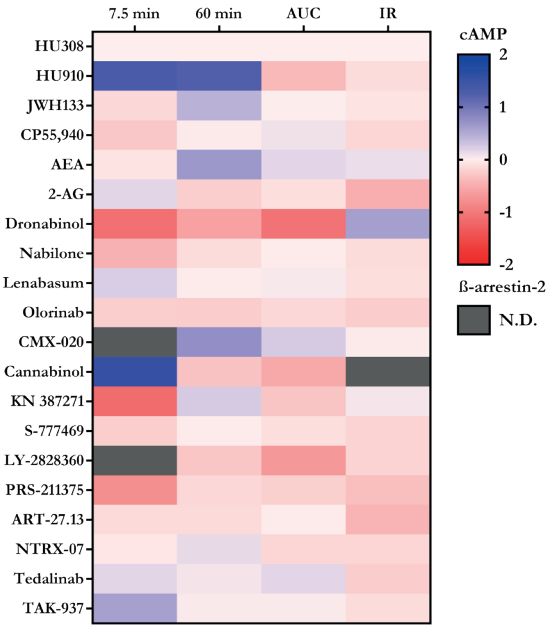

Figure 3.6 Quantification of biased agonism between inhibition of cAMP production and ß-arrestin-2 recruitment by benchmarks agonists, endocannabinoids and clinical agonists determined in the multiplex assay on CB_2R using an endpoint, semi-kinetic or kinetic analysis.
The dose response curves of all agonists based on endpoint (i.e., 7.5 and 60 min after agonist addition), semi-kinetic (AUC) or kinetic (IR) analysis were analyzed using the operational model of agonism to obtain transduction coefficients LogR, which were normalized to the balanced agonist HU308 per pathway (ΔLogR ratios). The bias between the two pathways was reported as ΔΔLogR and is shown in the heatmap. Blue indicates bias towards cAMP production, whereas red indicates bias towards ß-arrestin-2 recruitment. Agonists for which bias could not be determined (N.D.) due to absence of a dose response curve are presented in grey. CBD, GW-842166X and EHP-101 are omitted from the heatmap due to lack of receptor affinity and activation. One-way ANOVA was performed to analyze differences in ΔΔLogR values of agonists compared to HU308 (* $p<0.05$). Data are mean from at least three independent experiments performed in duplicate. Bias factors can be found in Table 3.S6.

bias was observed when analyzing the kinetic dose-response curves. On the other hand, after 7.5 min of activation, Nabilone and PRS-211375 demonstrated a small bias towards ß-arrestin-2 recruitment over inhibition of cAMP production relative to HU308, but the preference for ß-arrestin-2 recruitment was attenuated after 60 min of activation, as well as in the semi-kinetic and kinetic analysis. Time-dependent bias was observed for JWH133, AEA, 2-AG, CBN, KN 387271 evident by switched preferences after either 7.5 or 60 min of activation. A bias towards ß-arrestin-2 recruitment over inhibition of cAMP production was observed for Dronabinol in the endpoint and semi-kinetic analysis, whereas the bias was flipped towards inhibition of cAMP production in the kinetic analysis. No bias factor could be calculated for LY-2828360 after 7.5 min of activation due to the absence of a complete dose-response curve in the inhibition of cAMP production, while potency could be determined in ß-arrestin-2 recruitment. This may suggest that at the early time point LY-2828360 is strongly biased towards ß-arrestin-2 recruitment over inhibition of cAMP production, which is also observed in the semi-kinetic and kinetic analysis although slightly less pronounced. Although trends in biased signaling were observed for all other agonists, no statistically significant bias between inhibition of cAMP production and ß-arrestin-2 recruitment was found relative to HU308 in our system independent of the method of analysis used. However, in general a small trend towards ß-arrestin bias may be observed for several agonists (**Figure 3.6**).

Ultimately, we explored whether CB_2R binding kinetics could be predictive for the degree of bias. To maintain the kinetic context, correlation plots were generated for association and dissociation rate constants and the ΔΔLogR values obtained from kinetic analysis. No statistically significant correlation was found between k_{on} or k_{off} values and ΔΔLogR values of the agonists (R^2 <0.01, p 0.9865; R^2 0.15, p 0.1296) (**Figure S3.14q,r**).

Altogether, no statistically significant bias was observed for any of the agonists between the inhibition of cAMP production and ß-arrestin-2 recruitment determined in our multiplex assay. Small differences were observed in trends for biased signaling, which were in some cases dependent on the method of analysis (**Figure 3.6**, **Table S3.6**).

3.3 Discussion

Ligand bias is an emerging concept that holds great promise to advance drug discovery by selectively targeting therapeutic relevant signaling pathways[1–3]. However, examination of ligand bias *in vitro* is rather challenging, and experiments need to be designed with great caution to reduce system or observation bias[1]. To this end, we developed a novel multiplex assay that simultaneously detects cAMP production and ß-arrestin-2 recruitment in a kinetic manner in the same cells. We demonstrated the applicability of this kinetic multiplex assay on CB_2R by screening a large panel of diverse agonists (**Figure 3.1**, **Table 3.1**).

Multiplex assays have been designed to better capture the complexity of biological measurements as opposed to results obtained from a single screening unit. Most multiplex applications rely on fluorescent labeling, but multiplex luciferase reporters have also emerged for detection of genes as indicator of downstream signaling[39,40]. Nevertheless, these

technologies often rely on sequential analysis of two (or more) luciferases by quenching the light of the first enzyme before addition of the second substrate. On top of this, cells often need to be lysed, which removes the dynamic context of signaling events[40,41]. In the multiplex assay presented in this study, we successfully combined the GloSensor technology for capturing differences in cAMP production and NanoBiT for ß-arrestin-2 recruitment to CB_2R (**Figure 3.3**, **Table S3.3**), which generated similar potency values for reference agonist CP55,940 as previously seen in literature[28,35,42].

To investigate the time-dependency of activation and the impact of data analysis approaches, we analyzed the multiplex data using three methods: 1) as endpoint, i.e., after 7.5 and 60 min, 2) semi-kinetic AUC analysis, both methods provide the traditional potency and efficacy values, and 3) kinetic analysis using mathematical models that provided kinetic potency and kinetic efficacy based on initial rates (pIR_{50}, IR_{max}) and signaling rate constants k_1 and k_2[20]. Since the recent introduction of these novel curve fitting models, they are carefully being incorporated in pharmacological studies to aid more accurate characterization of ligand-receptor interactions for a variety of receptors and pathways[5,43–47]. Importantly, the impact of the chosen method of data analysis became clear in ligand bias analyses (**Figure 3.6**, **Table S3.6**). A trend in increased bias towards cAMP over time was observed for HU910, while the slight cAMP bias of TAK-937 was attenuated and 2-AG switched from cAMP preference at 7.5 min to ß-arrestin-2 preference after 60 min. These results are in line with results on the dopamine D_2 receptor, where it was demonstrated that ligand bias could change over time[13]. Biased signaling at CB_2R has never been investigated in a kinetic context and, to our knowledge, experiments have always been conducted in different functional (endpoint) assays with different cellular backgrounds, which could potentially introduce system bias[31,33–35,37]. Furthermore, incubation times with agonists spanned a wide range from 5 min to 90 min and sometimes even differed between assays within the same study. However, our results clearly demonstrate that time-dependence should be considered when studying biased signaling to reduce the effect of system and observation bias and thus draw proper conclusions on ligand bias.

To this end, the semi-kinetic and kinetic analyses were employed to reduce the influence of time and use the obtained signaling time traces to their fullest extent. In general, the observed potency values for inhibition of cAMP production and ß-arrestin-2 recruitment were slightly lower compared to literature[28,35,48–50]. On the other hand, Lin *et al.* observed no ß-arrestin-2 recruitment to CB_2R after activation by LY-2828360, whereas in our multiplex assay we found a low potency for LY-2828360 although with low efficacy (**Table 3.4**)[50]. Not only were previously reported pharmacological parameters determined at specific time points, but the performed assays also relied on lysis of cells or measurement of cAMP accumulation and/or irreversible ß-arrestin-2 recruitment and thus removing the dynamic context. Noteworthy, we observed strong correlations between the potency and efficacy values from the semi-kinetic (AUC) compared to the kinetic analysis for both inhibition of cAMP production and ß-arrestin-2 recruitment (**Figure S3.13**), which indicates that the novel kinetic analyses are fit to rapport 'classical' pharmacological parameters, such as potency and efficacy. Moreover, the observed statistically significant correlations between the pIR_{50} and IR_{max} values from inhibition of cAMP production and ß-arrestin-2 recruitment suggest a lack of bias in the overall agonist set. However, the signaling rate

constants k_1 and k_2 were not correlated and as such may contribute to the small trends in bias that were observed for Dronabinol and 2-AG. We envision that kinetic analysis, or early time point analysis, in *in vitro* assays generates parameters that better predict the *in vivo* pharmacological effects, i.e., starting GPCR activation and signal transduction without interference of artificial regulation mechanisms[20]. As such, kinetic potency (pIR_{50}) and efficacy (IR_{max}) as well as signaling rate constant k_1 require more attention. Interestingly, a faster engagement (k_{on}) of agonists with CB_2R correlated with both a higher affinity as well as a higher potency in both inhibition of cAMP production and ß-arrestin-2 recruitment (**Figure S3.1b**, **S3.14a**,**i**), and as such is a driving force for CB_2R binding and activation. While a quick engagement with CB_2R did not result in a quick activation (k_1), we found that superagonists Olorinab, PRS-211375, ART-27.13 and Tedalinab in ß-arrestin-2 recruitment were characterized by fast signaling rate constants k_1 in the kinetic analysis. However, not all agonists with fast k_1 values behaved as superagonists. Although no correlation was found for k_{off} and affinity or potency (**Figure S3.1c**, **S3.14e**,**m**), we observed that slowly dissociating agonists exhibited slow deactivation of ß-arrestin-2 recruitment, which may suggest that extended agonist binding results in a longer receptor interaction with ß-arrestin-2. Since the introduction of the target binding kinetics concept, the primary focus has been on optimization of RT, rather than on association rate constants[51]. However, this study clearly indicates that optimization of the association rate constants for CB_2R agonists is equally valuable to improvement of the dissociation rate constants.

The applied kinetic signaling models do not only allow for quantification of signaling parameters, but the shape of the traces may also be indicative of regulation mechanisms. Our inhibition of cAMP production data, after corrections and inversion, was best fit by the 'Baseline then rise-and-fall to baseline' model, which was also previously reported for cAMP production after activation of the adenosine A_1 receptor and $ß_2$-adrenoceptor[44,46]. This shape is generally described for second messenger signaling when there is no additional regulation of signaling by inhibitors, such as phosphodiesterase (PDE) inhibitors[43]. Agonist-dependent differences were observed in the time traces. Some agonists, such as Tedalinab, displayed a steep decrease of the inhibition of cAMP production, which was also reflected by higher signaling rate k_2 values (**Figure 3.4f**, **Table 3.3**). Yet the exact mechanism behind these differences requires more experimental validation, which could benefit from the use of PDE inhibitors to simplify the system[44]. On the other hand, the ß-arrestin-2 recruitment time traces were analyzed using the 'Baseline then rise-and-fall to steady state' model (**Figure 3.4**, **Table 3.4**), which has been previously used for ß-arrestin-2 recruitment time traces to other GPCRs[5,43,46]. As a general model, the 'rise-and-fall to steady state' equation was generated to capture complex regulation mechanisms, which in the case of ß-arrestin-2 recruitment has been hypothesized to refer to receptor desensitization, internalization, recycling to the cell membrane or degradation[43]. Several studies have reported that agonist-stimulated CB_2R also undergoes these processes[52–59]. Grimsey *et al.* described that HU308-induced internalization of CB_2R did not result in degradation of the receptor, but rather recycling of the receptor to the cell membrane. However, a remaining proportion of the receptors was not recycled nor degraded but remained in the cytoplasm[54]. The remaining luminescence above baseline in our assays, as a measure for complementation of CB_2R and ß-arrestin-2, may reflect the proportion of receptors that have been internalized,

but not (yet) recycled or degraded (**Figure 3.4**, **S3.6**, **S3.7**). Furthermore, since signaling rate constants k_1 and k_2 are not assigned to particular regulation mechanisms, the exact mechanisms, i.e., internalization, recycling or degradation, upon CB_2R activation by the different agonists cannot be deciphered. This would require additional investigation to reveal differential agonist-dependency for initiation of ß-arrestin-mediated internalization, recycling, or degradation at CB_2R, alike results found at the $ß_2$-adrenergic receptor[60]. Altogether, this study advocates the use of the kinetic multiplex assay with novel analyses to determine potency and efficacy in a kinetic context with the advantage of additional signaling rate constants k_1 and k_2, which can reveal differences between agonists that are otherwise overlooked.

For proper use of the Black-Leff operational model for bias analysis the maximal response of the system needs to be accurately estimated[61,62]. Several agonists displayed superagonism in ß-arrestin-2 recruitment compared to full agonist CP55,940, which was most prominent for Tedalinab (**Table 3.3**, **3.4**). Therefore, Tedalinab was used as full agonist, which also improved the fits on all other agonists (data not shown). Similar to previous work, benchmark agonists HU308, HU910 and JWH133 remained balanced between the two studied pathways (**Figure 3.6**, **Table S3.6**)[35]. Although some trends towards biased signaling were observed, none of the calculated ΔΔLogR values were significantly different from balanced agonist HU308 (**Figure 3.6**, **Table S3.6**). Previously reported biased signaling of CB_2R agonists (bias factors ranging between 0.0015 and 90) may have been influenced by system and observational bias due to the use of a biased reference agonist, different cellular backgrounds, time points and measurements used to report bias amongst pathways[31,33–35,37]. FDA approved μ-opioid receptor biased agonist oliceridine only displayed a bias factor of 3 for G protein activation over ß-arrestin-2 recruitment, while bias factors up until 85 have been reported on the same receptor[63,64]. Nevertheless, more recent studies have hypothesized that the partial agonism of oliceridine may be responsible for the beneficial therapeutic effect rather than its biased profile[65]. It is important to note that bias factors only provide a ratio compared to a selected reference agonist in a specific system, which aids in prioritizing or selecting agonists for further testing in therapeutically relevant systems or *in vivo* models[11]. In this study, we did not observe significant degrees of bias signaling for the clinically relevant CB_2R agonists, which may be the reason for failure of several of these agonists in clinical trails. However to date, the mechanism of therapeutic effects at CB_2R and the potential importance of biased signaling is largely unknown. To prove whether signaling bias on CB_2R has therapeutic relevance, the mechanism should be further explored. This may be done by *in vitro* in relevant native cell background and/or *in vivo* by knockout studies of ß-arrestin-2 or $G\alpha_i$ proteins to specify which signaling pathway is therapeutically relevant[1,11].

In conclusion, this study describes the development and application of a novel multiplex assay that simultaneously detects cAMP production and ß-arrestin-2 recruitment in a time-dependent manner in the same cells. We demonstrate that agonist-mediated CB_2R activation and biased signaling is time sensitive dependent on the specific agonist used. Similar potency and efficacy parameters can be obtained from semi-kinetic and kinetic methods of analysis, while the latter additionally provides signaling rate constants that may accentuate differences between agonist-dependent signaling and bias. Moreover, this study demonstrates the

importance of fast agonist engagement (k_{on}) with CB_2R for increased affinity and potency, while slowly dissociating agonists extended the interaction between CB_2R and ß-arrestin-2. We envision that kinetic parameters that capture the early response, such as pIR_{50}, IR_{max} and signaling rate constant k_1, could be applied to *in vitro* studies as better predictors of their pharmacological effects *in vivo*. Ultimately, combining these parameters with binding kinetics results in more extensively profiled GPCR agonists to advance future drug discovery efforts.

3.4 Materials and methods

3.4.1 Chemical and reagents

RO6957022 and [^{3}H]RO6957022 (specific activity 82.83 Ci mmol^{-1}) were synthesized in-house as previously published [66]. [^{3}H]CP55,940 (specific activity 108.5 Ci mmol^{-1} #NET1051250UC), [^{35}S]GTPγS (specific activity 1250 Ci mmol^{-1} #NEG030H250UC), and GF/C filter plates (#6055690) were purchased from Revvity (Waltham, MA, USA). Bicinchoninic acid (BCA) and BCA protein assay reagent were obtained from Pierce Chemical Company (Rockford, IL, USA). CP55,940 (#C1112), AM630 (#SML0327), and DL-dithiothreitol (DTT, #646563) were obtained from Sigma-Aldrich (Saint Louis, MO, USA). Tedalinab (#T013730) and forskolin (FSK, #F701800) were from Toronto Research Chemicals. Δ^9-THC (#12068) and LY-2828360 (#26791) from Cayman Chemical (Ann Arbor, MI, USA). Anandamide (AEA, #1339), 2-Arachidonylglycerol (2-AG, #1298), JWH-133 (#1343), cannabidiol (CBD, #1570), cannabinol (CBN, #3130) and phenylmethylsulfonyl fluoride (PMSF, #4486) were purchased from Tocris Bioscience (Bristol, UK). GDP (#J61646) was from Thermo Fisher Scientific (Waltham, MA, USA), EHP-101 (#HY-128872) from MedChemExpress (Monmouth Junction, NJ, USA) and HU308 (#H800010) was obtained from LKT Laboratories (St. Paul, MN, USA). Nabilone, Lenabasum, Olorinab, CMX-020, KN 387271, GW-842166X, S-777469, PRS-211375, ART-27.13, NTRX-07 and TAK-937 were provided by F. Hoffmann-La Roche Ltd (Basel, Switzerland) and HU910 was a kind gift from Pal Pacher (NIH, MD, USA). FuGENE® 6 Transfection Reagent (#E2692), Nano-Glo® Vivazine™ Substrate (#N2581), GloSensor™ cAMP reagent (#E1291) and pGloSensor™-22F cAMP Plasmid (#E2301) were from Promega (Madison, WI, USA) and 96-well solid white flat bottom microplates (#3917) were obtained from Corning (Corning, NY, USA). All buffers and solutions were prepared using Millipore water (deionized using a MilliQ A10 Biocel™ with a 0.22 µm filter) and analytical grade reagents and solvents. Buffers were prepared at room temperature (rt) and stored at 4 °C, unless stated otherwise.

3.4.2 Physicochemical properties and pharmacokinetic properties determination

3.4.2.1 Lipophilicity

For the determination of the octanol/water distribution coefficient (LogD), the Carrier-Mediated Distribution System (CAMDIS)-assay was used as described previously[67].

3.4.2.2 Kinetic aqueous solubility (Lysa)

The compounds' solubility was assessed in a phosphate buffer with a pH of 6.5, originating from a 10 mM stock solution in DMSO that had been evaporated. For each compound, two samples were desiccated and reconstituted in the pH 6.5 phosphate buffer. Post-dissolution, the solutions underwent filtration and were subsequently diluted to three distinct concentrations. RapidFire mass spectrometry analysis was conducted on these dilutions. Quantification of each compound was achieved using a calibration curve comprising six points, which was established using the initial DMSO solution.

3.4.2.3 Lipid membrane binding assay (Limba LogDbrain)

The Lipid Membrane Binding Assay (LIMBA LogDbrain) was conducted consistent with previously published methods, allowing for high to medium throughput analysis[68].

3.4.2.4 Passive membrane permeability assay (PAMPA)

The PAMPA assay was carried out as a high-throughput experiment as previously described[68].

3.4.2.5 Human plasma protein binding (free fraction %)

Human plasma with EDTA as an anticoagulant was sourced from BioreclamationIVT (New York, USA)[69,70]. To determine the free fraction of a agonist, a 96-well equilibrium dialysis device with a Teflon build and a 150 µL half-cell volume was used. This device featured a membrane with a molecular weight cut-off between 12 and 14 kDa, chosen to reduce non-specific binding. Both the test compound and a known reference, diazepam, were assessed in groups ranging from 2 to 5 wells, starting at a concentration of 1000 nM. Each well was filled with equal amounts of a plasma sample containing the test compound or diazepam and a blank dialysis buffer, specifically Soerensen's buffer. The pH of the plasma and buffer was adjusted to 7.4 on the day of the experiment. The dialysis unit was then incubated at 37 °C with 5% CO_2 for 5 hours, which is generally sufficient for equilibrium to be reached for most small molecules under 600 Da. Following incubation, the samples were prepared for LC-MS/MS analysis. Each protein binding assessment was conducted in triplicate to ensure accuracy. The integrity of the dialysis membrane was verified by measuring the unbound fraction of diazepam in each well. At equilibrium, the concentration of the unbound drug in the plasma should equal that in the buffer, allowing for the calculation of the unbound fraction as the buffer concentration post-dialysis divided by the plasma concentration post-dialysis, multiplied by 100. Additionally, the recovery of the device was evaluated by comparing the concentration of the compound in the plasma before and after dialysis, with acceptable recovery rates ranging from 80% to 120% for the data to be considered valid.

3.4.2.6 P-glycoprotein-mediated efflux ratio

The generation of human P-gp efflux ratio values was conducted as previously reported[68].

3.4.3 Cell culture and membrane preparation

For functional assays, human embryonic kidney 293T cells (HEK293T, ATCC #CRL-3216) and HEK293T cells stably expressing full-length hCB_2R-SmBiT and LgBiT-ß-arrestin-2 constructs (HEK293T CB_2R-SmBiT LgBiT-ß-arrestin-2, a kind gift by Christophe Stove, Ghent University, Belgium [71]) were grown in monolayers. Both cell lines were cultured in Dulbecco's Modified Eagle's Medium supplemented with 10% FCS, 2 mM Glutamax, 100 IU/mL penicillin and 100 µ/mL streptomycin in a humidified atmosphere at 37 °C and 5% CO_2. For binding assays, Chinese Hamster Ovary (CHO) cells stably expressing hCB_2R or hCB_1R (CHOK1_hCB_2bgal, #93-0706C2 and CHOK1_hCB_1bgal, #93-0959C2, PathHunter EA Parental cell line, female, DiscoverX) were cultured in Ham's F12 Nutrient Mixture supplemented with 10% (v/v) fetal calf serum (FCS), 2 mM Glutamax, 100 IU/mL penicillin, 100 µg/mL streptomycin, 300 µg/mL hygromycin and 800 µg/mL G418 in a humidified atmosphere at 37 °C and 5% CO_2. All cells were subcultured twice weekly when reaching 80-90% confluence on 10 or 15 cm ø plates by trypsinization and used for further experiments within 20 passages.

3.4.4 Membrane preparation

HEK293T CB_2R-SmBiT LgBiT-ß-arrestin-2, CHOK1_hCB_2bgal and CHOK1_hCB_1bgal cells were harvested when reaching 80-90% confluence in 15 cm ø plates after one week subculture at a 1:15, 1:6 or 1:6 ratio, respectively. The cells were detached by scraping into 5 mL phosphate-buffered saline (PBS) and subsequently centrifuged at 2,000 × g for 5 min. Pellets were resuspended in ice-cold Tris buffer (50 mM Tris-HCl, pH 7.4) and homogenized with an Ultra Turrax homogenizer (IKA-Werke GmbH & Co. KG, Staufen, Germany). Cytosolic and membrane fractions were separated using an Optima LE-80 K ultracentrifuge (Beckman Coulter, Inc., Fullerton, CA) at 100,000 × g for 20 min at 4 °C. The membrane fractions were subjected to another round of homogenization and centrifugation. The final pellets were resuspended and homogenized in ice-cold Tris buffer and subsequently aliquoted and stored in 100 µL aliquots at -80 °C. Membrane protein concentrations were determined using a BCA protein determination assay, as described by the manufacturer (Pierce BCA protein assay kit)[72].

3.4.5 [^{3}H]RO6957022 binding assays

[^{3}H]RO6957022 displacement and competition association assays have previously been described with the main difference that the incubation temperature was changed to 10 °C for improved separation of kinetic differences[66]. In short, CHOK1_hCB_2bgal or HEK293T CB_2R-SmBiT LgBiT-ß-arrestin-2 membranes were thawed and subsequently homogenized using the Ultra Turrax homogenizer. For experiments with endocannabinoids and CMX-020, membranes were preincubated for 30 min with 50 µM PMSF. The reactions were carried out in 100 µL assay buffer (50 mM Tris-HCl (pH 7.4), 0.1% (w/v) bovine serum albumin (BSA)) containing 1 µg (CHOK1_hCB_2bgal) or 10 µg (HEK293T CB_2R-SmBiT LgBiT-ß-

arrestin-2) of membrane protein and 1.5 nM [^{3}H]RO6957022. Incubations were performed at 10 °C. Therefore, assay buffer, (radio)ligands and membranes were precooled to 10 °C prior to the experiment. Nonspecific binding (NSB) was determined using 10 μM AM630 and vehicle (i.e., acetonitrile for endocannabinoids and CMX-020, and DMSO for all other compounds) concentrations were constant and kept < 1% in all samples. Total radioligand binding (TB) did not exceed 10% of the amount added to prevent ligand depletion. For all assays, incubations were terminated by rapid vacuum filtration with ice-cold 50 mM Tris-HCl (pH 7.4), 0.1% (w/v) BSA buffer through Whatman GF/C filters using a Filtermate 96-well harvester (Revvity, Waltham, MA, USA). Filters were dried for at least 30 min at 55 °C and subsequently 25 μL MicroScint scintillation cocktail was added per well. Filter-bound radioactivity was measured by scintillation spectrometry using a Microbeta^2 2450 counter (Revvity, Waltham, MA, USA).

3.4.5.1 Displacement assays

Binding affinity of all clinical agonists for CB_2R was determined in displacement assays using radioligand and six increasing concentrations of competing compound (ranging from 0.01 nM to 10 μM) on CHOK1_hCB_2bgal membranes. Homologous displacement assays were performed on HEK293T CB_2R-SmBiT LgBiT-ß-arrestin-2 membranes with three concentrations of [^{3}H]RO6957022 of ~0.5 nM, ~1.5 nM and ~5.0 nM in the presence of competing RO6957022 (ranging from 0.01 nM to 1 μM) in assay buffer. The reaction mixture was incubated for 2 h at 10 °C, after which incubations were terminated and receptor-bound radioactivity was determined as described in section **3.4.5 [^{3}H]RO6957022 binding assays**.

3.4.5.2 Competition association assays

Binding kinetics were assessed in competition association experiments using radioligand and competing compound at its IC_{50} concentration obtained from displacement assays. Competition was initiated by addition of CHOK1_hCB_2bgal membrane homogenates at different time points for 2 h, after which incubations were terminated and receptor-bound radioactivity was determined as described in section **3.4.5 [^{3}H]RO6957022 binding assays**.

3.4.6 [^{3}H]CP55,940 displacement assays

Binding affinity for CB_1R was determined in [^{3}H]CP55,940 displacement assays. CHOK1_hCB_1bgal membranes were homogenized and diluted to 2.5 μg protein per well in assay buffer (50 mM Tris-HCl (pH 7.4), 5 mM $MgCl_2$, 0.1% (w/v) BSA). Membranes were incubated with six increasing concentrations (ranging from 0.01 nM to 10 μM) of competing compound in the presence of 1.5 nM [^{3}H]CP55,940. Incubations were for 2 h at 25 °C. NSB was determined using 10 μM SR141716A and vehicle (i.e., acetonitrile for endocannabinoids and CMX-020, and DMSO for all other compounds) concentrations were constant and kept < 1% in all samples. TB did not exceed 10% of the amount added to prevent ligand depletion. Incubations were terminated as described in section **3.4.5 [^{3}H]RO6957022 binding assays** except using ice-cold wash buffer containing 50 mM Tris-HCl, 5 mM $MgCl_2$ and 0.1% BSA.

3.4.7 Multiplexed cAMP production and ß-arrestin-2 recruitment assay

Inhibition of cAMP production and ß-arrestin-2 recruitment after CB_2R activation were measured using the GloSensor™ and NanoBiT® technologies, respectively, in a multiplexed manner. To this end, HEK293T CB_2R-SmBiT LgBiT-ß-arrestin-2 cells were seeded as 2×10^6 cells on 10 cm ø plates to reach 60% confluence on the day of transfection. The next day, cells were transfected with 10 µg pGloSensor™-22F cAMP plasmid using FuGENE® 6 transfection in a 3:1 reagent:DNA ratio [73]. In short, a mix of 10 µg GloSensor plasmid and 30 µL FuGENE® 6 was incubated in 850 µL Opti-MEM™ at room temperature (rt) for 15 minutes. The mixture was added to the cells without replacing the medium. Cells were left to grow overnight at 37 °C with 5% CO_2 to reach ~90% confluence. The next day, transfected cells were seeded at a density of 50,000 cells/well in poly-D-lysine treated solid white, flat bottom 96-well plates in culture medium and incubated for another 22-24 h at 37 °C with 5% CO_2. On the assay day, the culture medium was replaced by 30 µL assay medium (CO_2 independent medium + 10% (v/v) FCS) and 50 µL equilibration reagent in assay medium. The equilibration reagent for the GloSensor™ only contained 4% (v/v) GloSensor™ cAMP reagent, NanoBiT® reagent contained 2% (v/v) Vivazine™ substrate and the "multiplex reagent" contained a combination of the two reagents, i.e., 2% (v/v) Vivazine™ substrate and 4% (v/v) GloSensor™ cAMP reagent. The plate was incubated at 25 °C for 2 h in the dark after which baseline cAMP levels and ß-arrestin recruitment were measured for 7.5 min in the plate reader using the protocol as described below.

To induce cAMP production, cells were prestimulated with 1 µM forskolin (FSK) until reaching a stable plateau of cAMP production. Specifically, induction of cAMP production was initiated by addition of 10 µL FSK mixture and luminescence was monitored for 52.5 min in the plate reader. For experiments with endocannabinoids or CMX-020, the FSK prestimulation mixture additionally contained 50 µM phenylmethylsulfonyl fluoride (PMSF). Immediately after, cells were stimulated with 10 µL increasing concentrations of compound of interest (ranging from 0.01 nM to 10 µM). Compounds were added using a MINI 96 portable electronic pipette to ensure no time delay (INTEGRA Biosciences, Tokyo, Japan). The maximal response was determined by 1 µM CP55,940 and vehicle (i.e., acetonitrile for endocannabinoids and CMX-020, and DMSO for all other compounds) concentrations were constant and kept < 1% in all samples. Luminescence was measured for another 90 min in the plate reader resulting in a total read time of 150 min.

The simultaneous luminescent signals were measured in a Wallac EnVision 2104 Multilabel reader (Revvity, Waltham, MA, USA). To this end, the individual signals were detected by two emission filters in a dual luminescent manner. Specifically, the Cy3 595 filter (595/60 nm, barcode 229) was used to detect the cAMP responses and emission filter NanoBRET Blue (460/80 nm, barcode 703) was used to detect ß-arrestin-2 recruitment to CB_2R. Each wavelength was measured for 250 ms/well and the total interval between plate repeats was 90 s.

To investigate cAMP responses independent of CB_2R, the same protocol was applied to parental HEK293T cells, but only using the GloSensor™ equilibration reagent containing 4% (v/v) GloSensor™ cAMP reagent.

3.4.8 Data analysis and statistics

All experimental data were analyzed using GraphPad Prism 9.0 (GraphPad Software Inc., San Diego, CA, USA). All values obtained are means ± standard error of the mean (SEM) of at least three independent experiments performed in duplicate, unless stated otherwise.

3.4.8.1 Displacement assays

[^{3}H]RO6957022 (CB_2R) and [^{3}H]CP55,940 (CB_1R) assays were baseline-corrected with NSB and normalized to this value (0%) and TB (100%). The equilibrium dissociation constant (K_D) of [^{3}H]RO6957022 and receptor expression level (B_{max}) were calculated from homologous displacements by non-linear regression analysis, using the "one-site homologous" model. The half-maximal inhibitory concentrations (pIC_{50}) of the compounds in [^{3}H]RO6957022 and [^{3}H]CP55,940 displacement assays were obtained by non-linear regression analysis of the displacement curves and further converted into inhibitory constant pK_i using the Cheng-Prusoff equation[74] with the experimentally determined K_D values 0.78 nM and 0.84 nM, respectively (data not shown). CB_2R selectivity of the compounds was determined when two pK_i values were obtained using **Equation 3.1**:

$$\text{Selectivity}=10^{(pK_i\ CB_2R-pK_i\ CB_1R)} \qquad \textbf{(Equation 3.1)}$$

3.4.8.2 Competition association assays

From [^{3}H]RO6957022 competition association assays, the k_{on} and k_{off} values of compounds of interest were determined by non-linear regression analysis, using the "kinetics of competitive binding" model as described by Motulsky and Mahan[75]:

$$K_a=k_1[L]\cdot10^{-9}+k_2$$

$$K_b=k_3[I]\cdot10^{-9}+k_4$$

$$S=\sqrt{(K_a-K_b)^2+4\cdot k_1\cdot k_3\cdot[L]\cdot[I]\cdot10^{-18}}$$

$$K_f=0.5(K_a+K_b+S)$$

$$K_s=0.5(K_a+K_b-S)$$

$$Q=\frac{B_{max}\cdot k_1\cdot[L]\cdot10^{-9}}{K_f-K_s}$$

$$[Y]=Q\left(\frac{k_4\cdot(K_f-K_s)}{K_f\cdot K_s}+\frac{k_4-K_f}{K_f}\cdot e^{(-K_f\cdot X)}-\frac{k_4-K_s}{K_s}\cdot e^{(-K_S\cdot X)}\right)$$

Where [L] is the radioligand concentration per experiment (~1.5 nM), I is the IC_{50} concentration of compound (nM), X is the time (s), and Y is the specific binding of the radioligand (dpm). K_a and K_b are the observed association rate constants (k_{obs}) of the radioligand and the compound of interest, respectively. k_1 and k_3 are the association rate constants (k_{on} in $M^{-1}s^{-1}$) of [^{3}H]RO6957022 (determined per experiment) and the compound of interest, respectively. Similarly, k_2 and k_4 are the dissociation rate constants

(k_{off} in s^{-1}) of [^{3}H]RO6957022 (experimentally determined at 4.3×10^{-4} s^{-1}, data not shown) and the compound of interest, respectively. The engagement time (ET in seconds) of the compounds of interest was determined at 1 μM of compound using **Equation 3.2**[76]:

$$ET = \frac{1}{k_{on} \cdot 10^{-6}} \quad \textbf{(Equation 3.2)}$$

The residence time (RT in min) was calculated using **Equation 3.3**[14]:

$$RT = \frac{1}{k_{off} \cdot 60} \quad \textbf{(Equation 3.3)}$$

The association and dissociation rate constants were used to calculate the kinetic K_D using **Equation 3.4**:

$$K_D = \frac{k_{off}}{k_{on}} \quad \textbf{(Equation 3.4)}$$

3.4.8.3 Inhibition of forskolin-induced cAMP production (multiplex signal 1)

Functional forskolin-induced cAMP data from the multiplex assay was analyzed based on an endpoint, semi-kinetic and kinetic approach. Forskolin-induced cAMP responses after 7.5, 15, 30 and 60 min of agonist addition were baseline-corrected with the vehicle response and normalized to 1 μM CP55,940. Dose-response curves were generated and pEC_{50} and E_{max} values were determined using non-linear regression curve fitting 'log(agonist) vs. response' (three parameters).

Forskolin-induced cAMP time traces from the multiplex assay was corrected for well-to-well variation by subtracting the mean of the baseline measurement and subsequently subtracting the mean of the final five FSK measurements. Next, vehicle response was subtracted, and the data was inverted to represent inhibition of cAMP production. The agonist-induced inhibition of cAMP production was quantified by taking the net area under the curve (AUC) from the final five FSK measurements until the end of agonist measurement (54 - 150 min). Dose-response curves were generated and pEC_{50} and E_{max} values were determined using non-linear regression curve fitting 'log(agonist) vs. response' (three parameters) after normalization to 1 μM CP55,940.

The agonist-induced inhibition of cAMP production was further kinetically analyzed by applying the 'Baseline then rise-and-fall to baseline time course' equation according to Hoare *et al.*[20]. This equation (**3.5**) was provided as a plug-in, which was downloaded into GraphPad Prism[77]:

$$Y = IF\left(X<X_0, \text{Baseline}, \text{Baseline} + \left(\frac{IR}{k_1 - k_2}\left(e^{-k_2(X-X_0)} - e^{-k_1(X-X_0)}\right)\right)\right) \quad \textbf{(Equation 3.5)}$$

Where 'IR' is a fitting constant (cps min^{-1}), which is equal to the initial rate of signaling and represented by the initial linear phase of signal generation after receptor activation, X is the time (min), X_0 is the time at which the signal starts, and Y is the luminescent signal (cps). k_1 and k_2 are the observed signaling rate constants (min^{-1}), where k_1 is constrained to be greater than k_2. When time traces did not fall back to baseline in the assay time, as was the case for lower agonist concentrations, the 'baseline then rise to steady state time course' was fitted

according to **Equation 3.6**:

$$Y=IF\left(X<X_0, Baseline, SSR \cdot \left(1-e^{-k(X-X_0)}\right)+Baseline\right) \quad \textbf{(Equation 3.6)}$$

Where SSR is the steady-state response representing the maximal activation as time reaches infinity (cps), X is the time (min), X_0 is the time at which the signal starts, and Y is the luminescent signal (cps). k is the observed signaling rate constant (min^{-1}).

Dose-response curves were generated from the Initial Rate data and pIR_{50} and IR_{max} values were determined using non-linear regression curve fitting 'log(agonist) vs. response' (three parameters) after normalization to 1 μM CP55,940. More detailed information on the use of these models and a step-by-step procedure can be found in **Supplementary methods 3.S1.2.1**.

3.4.8.4 ß-arrestin-2 recruitment (multiplex signal 2)

Functional ß-arrestin-2 recruitment data from the multiplex assay was analyzed based on an endpoint, semi-kinetic and kinetic approach. Recruitment of ß-arrestin-2 after 7.5, 15, 30 and 60 min of agonist addition were baseline-corrected with the vehicle response and normalized to 1 μM CP55,940. Dose-response curves were generated and pEC_{50} and E_{max} values were determined using non-linear regression curve fitting 'log(agonist) vs. response' (three parameters).

Functional ß-arrestin-2 recruitment time traces from the multiplex assay was corrected for well-to-well variation by subtracting the mean of the baseline (final five FSK measurements count as baseline) and subsequently vehicle response was subtracted. The ß-arrestin-2 recruitment to CB_2R was quantified by taking the net area under the curve (AUC) from the baseline measurements until the end of agonist measurement (54 - 150 min). Dose-response curves were generated and pEC_{50} and E_{max} values were determined using non-linear regression curve fitting 'log(agonist) vs. response' (three parameters) after normalization to 1 μM CP55,940.

The ß-arrestin-2 recruitment was further kinetically analyzed by applying the 'Baseline then rise-and-fall to steady state time course' equation according to Hoare *et al.*[20]. This equation (**3.7**) was provided as a plug-in, which was downloaded into GraphPad Prism[77]:

$$Y=IF\left(X<X_0, Baseline, Baseline+SSR\left(1-D \cdot e^{-k_1(X-X_0)}+(D-1)e^{-k_2(X-X_0)}\right)\right) \quad \textbf{(Equation 3.7)}$$

Where SSR is the steady-state response representing the maximal activation as time reaches infinity (cps), D is a unitless fitting constant, X is the time (min), X_0 is the time at which the signal starts, and Y is the luminescent signal (cps). k_1 and k_2 are the observed signaling rate constants (min^{-1}), where k_1 is constrained to be greater than k_2. Initial rate can be calculated using **Equation 3.8**:

$$IR=SSR(D \cdot k_1-(D-1)k_2) \quad \textbf{(Equation 3.8)}$$

When time traces did not fall back to baseline in the assay time, as was the case for lower agonist concentrations, the 'baseline then rise to steady state time course' was fitted as described for **3.4.8.3 Inhibition of forskolin-induced cAMP production.**

Dose-response curves were generated from the Initial Rate data and pIR_{50} and IR_{max} values were determined using non-linear regression curve fitting 'log(agonist) vs. response' (three parameters) after normalization to 1 μM CP55,940. More detailed information on the use of these models and a step-by-step procedure can be found in **Supplementary methods 3.S1.2.2**.

3.4.8.5 Bias calculation

Dose-response curves from the endpoint analysis (early and late time point), semi-kinetic AUC and kinetic initial rate analysis for all compounds and for each functional readout were analyzed using the Black and Leff operational model to calculate the transduction coefficient $Log(\tau/K_A)$ or LogR values as previously described[61,78]. In the model, the slope (n) was set to 1, basal to 0 as the data was baseline corrected and E_{max} was set to the maximal activation in the system (Tedalinab). For each functional readout, the LogR value of the agonists was compared to most balanced agonist HU308 generating transduction ratios ΔLogR using **Equation 3.9**:

$$\Delta LogR_{agonist} = LogR_{agonist} - LogR_{HU308} \quad \textbf{(Equation 3.9)}$$

The relative bias of each agonist between the cAMP and ß-arrestin-2 pathway, represented as ΔΔLogR, was calculated using **Equation 3.10**:

$$\Delta\Delta LogR_{agonist} = \Delta LogR_{agonist,\ cAMP} - \Delta LogR_{agonist,\ \beta\text{-arrestin}} \quad \textbf{(Equation 3.10)}$$

Ultimately, the bias factor was calculated as the inverse logarithm of the ΔΔLogR values using **Equation 3.11**:

$$\text{Bias factor} = 10^{\Delta\Delta LogR_{agonist}} \quad \textbf{(Equation 3.11)}$$

Statistical analysis was performed on ΔΔLogR values to test for significance of ligand bias relative to balanced agonist HU308. To this end, a one-way ANOVA with Dunnett's multiple comparisons test was performed. $p < 0.05$ was considered statistically significant.

3.5 Acknowledgements

We thank Christophe Stove (Ghent University) for sharing the cell line for NanoBiT assays, Isabelle Geron (Revvity) for the technical support on the Envision plate reader and Isabelle Kaufmann, Björn Wagner, Carina Cantrill, Janneke Keemink, Elisa Di Lenarda, Anne Christine Cascais and Marie-Elise Brun (all Roche) for their excellent support in sample handling and compound characterization.

References

1. Kolb, P. *et al.* Community guidelines for GPCR ligand bias: IUPHAR review 32. *Br J Pharmacol* **179**, 3651–3674 (2022).
2. Kenakin, T. & Christopoulos, A. Signalling bias in new drug discovery: detection, quantification and therapeutic impact. *Nat Rev Drug Discov* **12**, 205–216 (2012).
3. Kenakin, T. Biased Receptor Signaling in Drug Discovery. *Pharmacol Rev* **71**, 267–315 (2019).
4. Kenakin, T. P. Biased signalling and allosteric machines: new vistas and challenges for drug discovery. *Br J Pharmacol* **165**, 1669 (2012).
5. French, A. R., Meqbil, Y. J. & van Rijn, R. M. ClickArr: a novel, high-throughput assay for evaluating β-arrestin isoform recruitment. *Front Pharmacol* **14**, (2023).
6. Hauser, A. S. *et al.* Common coupling map advances GPCR-G protein selectivity. *Elife* **11**, (2022).
7. Caroli, J. *et al.* A community Biased Signaling Atlas. *Nat Chem Biol* **19**, 531–535 (2023).
8. Mullard, A. FDA approves first GPCR biased agonist. *Nat Rev Drug Discov* **19**, 659 (2020).
9. Stahl, E. L. & Bohn, L. M. Low Intrinsic Efficacy Alone Cannot Explain the Improved Side Effect Profiles of New Opioid Agonists. *Biochemistry* **61**, 1923–1935 (2022).
10. Nagi, K. How can we improve the measurement of receptor signaling bias? *Expert Opin Drug Discov* **18**, 575–578 (2023).
11. Kenakin, T. Bias translation: The final frontier? *Br J Pharmacol* 1–16 (2024).
12. Pineyro, G. & Nagi, K. Signaling diversity of mu- and delta- opioid receptor ligands: Re-evaluating the benefits of β-arrestin/G protein signaling bias. *Cell Signal* **80**, (2021).
13. Klein Herenbrink, C. *et al.* The role of kinetic context in apparent biased agonism at GPCRs. *Nat Commun* **7**, 10842 (2016).
14. Copeland, R. A., Pompliano, D. L. & Meek, T. D. Drug–target residence time and its implications for lead optimization. *Nat Rev Drug Discov* **5**, 730–739 (2006). Guo, D., Mulder-Krieger, T., IJzerman, A. P. & Heitman, L. H. Functional efficacy of adenosine A_{2A} receptor agonists is positively correlated to their receptor residence time. *Br J Pharmacol* **166**, 1846–1859 (2012).
15. Rosethorne, E. M. *et al.* Long receptor residence time of C26 contributes to super agonist activity at the human β2 adrenoceptor. *Mol Pharmacol* **89**, 467–475 (2016).
16. Olsen, R. H. J. *et al.* TRUPATH, an open-source biosensor platform for interrogating the GPCR transducerome. *Nat Chem Biol* **16**, 841–849 (2020).
17. Von Moo, E. *et al.* Ligand-directed bias of G protein signaling at the dopamine D2 receptor. *Cell Chem Biol* **29**, 226-238.e4 (2022).
18. Kise, R. & Inoue, A. GPCR signaling bias: an emerging framework for opioid drug development. *The Journal of Biochemistry* mvae013 (2024).
19. Hoare, S. R. J., Tewson, P. H., Quinn, A. M., Hughes, T. E. & Bridge, L. J. Analyzing kinetic signaling data for G-protein-coupled receptors. *Sci Rep* **10**, 12263 (2020).
20. Maccarrone, M. *et al.* Goods and Bads of the Endocannabinoid System as a Therapeutic Target: Lessons Learned after 30 Years. *Pharmacol Rev* **75**, 885–958 (2023).
21. Howlett, A. C. *et al.* International Union of Pharmacology. XXVII. Classification of cannabinoid receptors. *Pharmacol Rev* **54**, 161–202 (2002).
22. Pertwee, R. G. *et al.* International Union of Basic and Clinical Pharmacology. LXXIX. Cannabinoid Receptors and Their Ligands: Beyond CB_1 and CB_2. *Pharmacol Rev* **62**, 588–631 (2010).
23. Simard, M., Rakotoarivelo, V., Di Marzo, V. & Flamand, N. Expression and Functions of the CB_2 Receptor in Human Leukocytes. *Front Pharmacol* **13**, (2022).
24. Brennecke, B. *et al.* Cannabinoid receptor type 2 ligands: An analysis of granted patents since 2010. *Pharm Pat Anal* **10**, 111–163 (2021).
25. Whiting, Z. M., Yin, J., de la Harpe, S. M., Vernall, A. J. & Grimsey, N. L. Developing the Cannabinoid Receptor 2 (CB2) pharmacopoeia: past, present, and future. *Trends Pharmacol Sci* **43**, 754–771 (2022).
26. Jones, É. & Vlachou, S. A Critical Review of the Role of the Cannabinoid Compounds Δ^9-Tetrahydrocannabinol (Δ^9-THC) and Cannabidiol (CBD) and their Combination in Multiple Sclerosis Treatment. *Molecules* **25**, 4930 (2020).

27. Bouma, J. *et al.* Dual allosteric and orthosteric pharmacology of synthetic analog cannabidiol-dimethylheptyl, but not cannabidiol, on the cannabinoid CB_2 receptor. *Biochem Pharmacol* **218**, 115924 (2023). **(Chapter 5)**
28. Castillo-Arellano, J., Canseco-Alba, A., Cutler, S. J. & León, F. The Polypharmacological Effects of Cannabidiol. *Molecules* **28**, (2023).
29. Carruthers, E. R. & Grimsey, N. L. Cannabinoid CB_2 receptor orthologues; in vitro function and perspectives for preclinical to clinical translation. *Br J Pharmacol* (2023).
30. Dhopeshwarkar, A. & Mackie, K. Functional selectivity of CB_2 cannabinoid receptor ligands at a canonical and noncanonical pathways. *Journal of Pharmacology and Experimental Therapeutics* **358**, 342–351 (2016).
31. Ibsen, M. S., Connor, M. & Glass, M. Cannabinoid CB_1 and CB_2 Receptor Signaling and Bias. *Cannabis Cannabinoid Res* **2**, 48–60 (2017).
32. Zagzoog, A. *et al.* Assessment of select synthetic cannabinoid receptor agonist bias and selectivity between the type 1 and type 2 cannabinoid receptor. *Sci Rep* **11**, 10611 (2021).
33. Oyagawa, C. R. M. *et al.* Cannabinoid Receptor 2 Signalling Bias Elicited by 2,4,6-Trisubstituted 1,3,5-Triazines. *Front Pharmacol* **9**, 1202 (2018).
34. Soethoudt, M. *et al.* Cannabinoid CB_2 receptor ligand profiling reveals biased signalling and off-target activity. *Nat Commun* **8**, 1–14 (2017).
35. Atwood, B. K., Wager-Miller, J., Haskins, C., Straiker, A. & Mackie, K. Functional Selectivity in CB_2 Cannabinoid Receptor Signaling and Regulation: Implications for the Therapeutic Potential of CB_2 Ligands. *Mol Pharmacol* **81**, 250–263 (2012).
36. Sharma, R. *et al.* Novel Cannabinoid Receptor 2 (CB2) Low Lipophilicity Agonists Produce Distinct cAMP and Arrestin Signalling Kinetics without Bias. *Int J Mol Sci* **24**, 6406 (2023).
37. Patel, M., Grimsey, N. L., Banister, S. D., Finlay, D. B. & Glass, M. Evaluating signaling bias for synthetic cannabinoid receptor agonists at the cannabinoid CB_2 receptor. *Pharmacol Res Perspect* **11**, (2023).
38. Graham, H., Chandler, D. J. & Dunbar, S. A. The genesis and evolution of bead-based multiplexing. *Methods* **158**, 2–11 (2019).
39. Sarrion-Perdigones, A. *et al.* Examining multiple cellular pathways at once using multiplex hextuple luciferase assaying. *Nat Commun* **10**, 1–16 (2019).
40. Thorne, N., Inglese, J. & Auld, D. S. Illuminating Insights into Firefly Luciferase and Other Bioluminescent Reporters Used in Chemical Biology. *Chem Biol* **17**, 646–657 (2010).
41. Felder, C. C. *et al.* Comparison of the Pharmacology and Signal Transduction of the Human Cannabinoid CB_1 and CB_2 Receptors. *Mol Pharmacol* **48**, 443–450 (1995).
42. Hoare, S. R. J. *et al.* Quantifying the Kinetics of Signaling and Arrestin Recruitment by Nervous System G-Protein Coupled Receptors. *Front Cell Neurosci* **15**, 84457 (2022).
43. Cullum, S. A., Veprintsev, D. B. & Hill, S. J. Kinetic analysis of endogenous β_2-adrenoceptor-mediated cAMP GloSensor™ responses in HEK293 cells. *Br J Pharmacol* **180**, 1304–1315 (2022).
44. Manning, J. J., Rawcliffe, G., Finlay, D. B. & Glass, M. Cannabinoid 1 (CB_1) receptor arrestin subtype-selectivity and phosphorylation dependence. *Br J Pharmacol* **180**, 369–382 (2023).
45. Saecker, L., Häberlein, H. & Franken, S. Investigation of adenosine A1 receptor-mediated β-arrestin 2 recruitment using a split-luciferase assay. *Front Pharmacol* **14**, (2023).
46. Grätz, L. *et al.* NanoBiT- and NanoBiT/BRET-based assays allow the analysis of binding kinetics of Wnt-3a to endogenous Frizzled 7 in a colorectal cancer model. *Br J Pharmacol* (2023).
47. Bouma, J. *et al.* Cellular Assay to Study β-Arrestin Recruitment by the Cannabinoid Receptors 1 and 2. in *Endocannabinoid Signaling. Methods in Molecular Biology* (ed. Maccarrone, M.) vol. 2576 189–199 (Humana, New York, NY, 2022). **(Chapter 2)**
48. Han, S. *et al.* Discovery of APD371: Identification of a Highly Potent and Selective CB_2 Agonist for the Treatment of Chronic Pain. *ACS Med Chem Lett* **8**, 1309–1313 (2017).
49. Lin, X., Dhopeshwarkar, A. S., Huibregtse, M., MacKie, K. & Hohmann, A. G. Slowly signaling G protein-biased CB_2 cannabinoid receptor agonist LY2828360 suppresses neuropathic pain with sustained efficacy and attenuates morphine tolerance and dependence. *Mol Pharmacol* **93**, 49–62 (2018).
50. IJzerman, A. P. & Guo, D. Drug–Target Association Kinetics in Drug Discovery. *Trends Biochem Sci* **44**, 861–871 (2019).

51. Chen, X. *et al.* Involvement of ß-arrestin-2 and Clathrin in Agonist-Mediated Internalization of the Human Cannabinoid CB2 Receptor. *Curr Mol Pharmacol* **7**, 67–80 (2014).

52. Derocq, J. M. *et al.* Genomic and functional changes induced by the activation of the peripheral cannabinoid receptor CB2 in the promyelocytic cells HL-60. Possible involvement of the CB2 receptor in cell differentiation. *Journal of Biological Chemistry* **275**, 15621–15628 (2000).

53. Grimsey, N. L., Goodfellow, C. E., Dragunow, M. & Glass, M. Cannabinoid receptor 2 undergoes Rab5-mediated internalization and recycles via a Rab11-dependent pathway. *Biochim Biophys Acta* **1813**, 1554–1560 (2011).

54. Carrier, E. J. *et al.* Cultured Rat Microglial Cells Synthesize the Endocannabinoid 2-Arachidonylglycerol, Which Increases Proliferation via a CB_2 Receptor-Dependent Mechanism. *Mol Pharmacol* **65**, 999–1007 (2004).

55. Bouaboula, M., Dussossoy, D. & Casellas, P. Regulation of peripheral cannabinoid receptor CB_2 phosphorylation by the inverse agonist SR 144528. Implications for receptor biological responses. *Journal of Biological Chemistry* **274**, 20397–20405 (1999).

56. Patel, M. *et al.* Delineating the interactions between the cannabinoid CB_2 receptor and its regulatory effectors; β-arrestins and GPCR kinases. *Br J Pharmacol* **179**, 2223–2239 (2022).

57. Ibsen, M. S. *et al.* Cannabinoid CB1 and CB2 Receptor-Mediated Arrestin Translocation: Species, Subtype, and Agonist-Dependence. *Front Pharmacol* **10**, (2019).

58. Moo, E. Von, van Senten, J. R., Bräuner-Osborne, H. & Møller, T. C. Arrestin-dependent and -independent internalization of G protein–coupled receptors: Methods, mechanisms, and implications on cell signaling. *Mol Pharmacol* **99**, 242–255 (2021).

59. Nobles, K. N. *et al.* Distinct Phosphorylation Sites on the $ß_2$-Adrenergic Receptor Establish a Barcode That Encodes Differential Functions of ß-Arrestin. *Sci Signal* **185**, ra51 (2011).

60. van der Westhuizen, E. T., Breton, B., Christopoulos, A. & Bouvier, M. Quantification of ligand bias for clinically relevant b2-adrenergic receptor ligands: Implications for drug taxonomy s. *Mol Pharmacol* **85**, 492–509 (2014).

61. Kenakin, T., Watson, C., Muniz-Medina, V., Christopoulos, A. & Novick, S. A simple method for quantifying functional selectivity and agonist bias. *ACS Chem Neurosci* **3**, 193–203 (2012).

62. DeWire, S. M. *et al.* A G protein-biased ligand at the μ-opioid receptor is potently analgesic with reduced gastrointestinal and respiratory dysfunction compared with morphines. *Journal of Pharmacology and Experimental Therapeutics* **344**, 708–717 (2013).

63. Schmid, C. L. *et al.* Bias Factor and Therapeutic Window Correlate to Predict Safer Opioid Analgesics. *Cell* **171**, 1165–1175 (2017).

64. Kelly, E., Conibear, A. & Henderson, G. Biased Agonism: Lessons from Studies of Opioid Receptor Agonists. *Annu. Rev. Pharmacol. Toxicol.* **63**, 491–515 (2023).

65. Martella, A. *et al.* A Novel Selective Inverse Agonist of the CB_2 Receptor as a Radiolabeled Tool Compound for Kinetic Binding Studies. *Mol Pharmacol* **92**, 389–400 (2017).

66. Wagner, B., Fischer, H., Kansy, M., Seelig, A. & Assmus, F. Carrier Mediated Distribution System (CAMDIS): A new approach for the measurement of octanol/water distribution coefficients. *European Journal of Pharmaceutical Sciences* **68**, 68–77 (2015).

67. He, Y. *et al.* Discovery, synthesis and evaluation of novel reversible monoacylglycerol lipase radioligands bearing a morpholine-3-one scaffold. *Nucl Med Biol* **108–109**, 24–32 (2022).

68. Banker, M. J., Clark, T. H. & Williams, J. A. Development and Validation of a 96-Well Equilibrium Dialysis Apparatus for Measuring Plasma Protein Binding. *J Pharm Sci* **92**, 967–974 (2003).

69. Zamek-Gliszczynski, M. J. *et al.* Validation of 96-well equilibrium dialysis with non-radiolabeled drug for definitive measurement of protein binding and application to clinical development of highly-bound drugs. *J Pharm Sci* **100**, 2498–2507 (2011).

70. Cannaert, A., Franz, F., Auwärter, V. & Stove, C. P. Activity-Based Detection of Consumption of Synthetic Cannabinoids in Authentic Urine Samples Using a Stable Cannabinoid Reporter System. *Anal Chem* **89**, 9527–9536 (2017).

71. Smith, P. K. *et al.* Measurement of protein using bicinchoninic acid. *Anal Biochem* **150**, 76–85 (1985).

72. Jacobsen, L. B., Calvin, S. A., Colvin, K. E. & Wright, M. J. FuGENE 6 Transfection Reagent: The gentle power. *Methods* **33**, 104–112 (2004).

73. Cheng, Y.-C. & Prusoff, W. H. Relationship between the inhibition constant (K1) and the concentration of inhibitor which causes 50 per cent inhibition (I50) of an enzymatic reaction. *Biochem Pharmacol* **22**, 3099–3108 (1973).

74. Motulsky, H. J. & Mahan, L. C. The kinetics of competitive radioligand binding predicted by the law of mass action. *Mol Pharmacol* **25**, 1–9 (1984).

75. Li, X. *et al.* Structural basis of selective cannabinoid CB_2 receptor activation. *Nat Commun* **14**, 1447 (2023). **(Chapter 4)**

76. Hoare, S. R. J. Pharmechanics time course equations in GraphPad Prism. https://www.pharmechanics.com/time-course-tool-pack (2023).

77. Black, J. W. & Leff, P. Operational models of pharmacological agonism. *Proc. R. Soc. Lond. B* **220**, 141–162 (1983).

3.S1 Supplementary methods

3.S1.1 [^{35}S]GTPγS assays

G protein activation of CB_2R was measured by binding of [^{35}S]GTPγS as previously described[39]. In short, HEK293T CB_2R-SmBiT LgBiT-ß-arrestin-2 membrane homogenates (5 µg) were diluted in assay buffer (50 mM Tris-HCl, 5 mM $MgCl_2$, 150 mM NaCl, 1 mM EDTA, 0.05% BSA (w/v) and 1 mM DTT, freshly prepared each day) and supplemented with 5 µg saponin and 1 µM GDP to a total volume of 100 µL. For endocannabinoid and CMX-020 samples, the membranes were additionally preincubated for 30 min with 50 µM PMSF. To determine pEC_{50} and E_{max} values, increasing concentrations of compound of interest (ranging from 0.01 nM to 10 µM) were incubated with [^{35}S]GTPγS (0.3 nM) for 90 minutes at 25 °C while shaking at 400 rpm. The basal activity was measured in the presence of vehicle and the maximal response was determined by 10 µM CP55,940. Vehicle (i.e., acetonitrile for endocannabinoids and CMX-020, and DMSO for all other compounds) concentrations were constant and kept < 1% in all samples. Incubations were terminated by rapid vacuum filtration with ice-cold 50 mM Tris-HCl (pH 7.4) and 5 mM $MgCl_2$ buffer through Whatman GF/C filters using a Filtermate 96-well harvester (PerkinElmer). Filters were dried for at least 30 min at 55 °C and subsequently 25 µL MicroScint scintillation cocktail was added per well. Filter-bound radioactivity was measured by scintillation spectrometry using a Microbeta^2 2450 counter (Revvity, Waltham, MA, USA).

3.S1.2 Data analysis

3.S1.2.1 Inhibition of forskolin-induced cAMP production (step-by-step)

The inhibition of cAMP production can be kinetically analyzed for each agonist concentration by applying time course equations according to Hoare *et al.*[20]. The equations can be downloaded from https://www.pharmechanics.com/time-course-tool-pack. The following directions are for GraphPad Prism v9.0, which requires some manual calculations. In newer versions more parameters are already calculated by the software.

1. Insert all time trace data per concentration in Prism and add vehicle in column A.
   i. The model requires X values to be greater than 0. Enter the time values as they are in reality, with baseline starting at 0 min. This allows X_0, the signal rise start time, to be a fitted parameter in the analysis resulting in better fits.
   ii. Insert average of the five baseline measurements in the top row for ease of correction, without an X value.
   iii. For the same reason, add the average of the final five FSK measurements in the bottom row, without an X value.
2. Correct for well-to-well variation by first subtracting the average of the baseline measurement and subsequently average of the FSK measurement.
   i. Select 'Repeated measures' in the baseline correction in GraphPad Prism, which will use the values from the specific well when you have duplicates.

3. Correct for vehicle and invert the data by transforming the Y values using Y= 0 -Y.
4. Allow Prism to compare between two non-linear fits based on the time trace using the F-test:
   i. Use simplest model first 'Baseline then rise to steady state' and compare to the more complex model 'Baseline then rise-and-fall to baseline'.
   ii. Constrain the following parameters for better fitting results:
      a. Baseline then rise to steady state:
         1. X_0 must be greater than 0
         2. Baseline no constraint
         3. SteadyState must be greater than 0
         4. k must be greater than 0
      b. Baseline then rise-and-fall to baseline
         1. X_0 must be greater than 0
         2. Baseline no constraint
         3. Initial Rate must be greater than 0
         4. k_1 no constraint
         5. k_2 must be greater than 0
         6. k_1 must be greater than 1 times k_2
      c. Don't constrain X_0 to the time of agonist addition as there might be a delay in the response, which will now be captured by the model.
      d. Don't constrain Baseline to allow some more flexibility of the model.
   iii. For all curves manually change the Initial Value (in the corresponding tab) for X_0 to the time of agonist addition or slightly before.
      a. This helps the model to better guess when your baseline run-in period turns into a response.
   iv. Only analyze the data from the final five FSK measurements (baseline) to the end of the assay.
   v. In the 'Confidence' tab change the Confidence Intervals (CI) of the parameters to the 'Symmetrical (asymptotic) approximate CI' if you do not need the CI.
      a. This mainly allows for a quicker fitting of the curves and does not influence the calculation of the fitted parameter but will only not report the CI.
   vi. From these analyses, the Initial Rate, Peak Response (given as SteadyState), and k_1 and k_2 values are determined.
5. The inactive concentrations, i.e., concentrations at which no inhibition of cAMP production is detected anymore, can also be analyzed to determine the slope. This will be (close to) 0.
   i. Use the 'Straight line time course' equation as described by Hoare *et al.*[20] with default parameters. The reported slope is the same as initial rate.

3.S1.2.2 ß-arrestin-2 recruitment (step-by-step)

The ß-arrestin-2 recruitment data can be kinetically analyzed for each agonist concentration by applying time course equations according to Hoare *et al.*[20]. The equations can be downloaded from https://www.pharmechanics.com/time-course-tool-pack. The following directions are for GraphPad Prism v9.0, which requires some manual calculations. In newer versions more parameters are already calculated by the software.

1. Insert all time trace data per concentration in Prism and add vehicle in column A.
   i. The model requires X values to be greater than 0. Enter the time values as they are in reality, with baseline starting at 0 min. This allows X_0, the signal rise start, to be a fitted parameter in the analysis resulting in better fits.
   ii. Insert the average of the final five FSK measurements (to represent baseline) in the bottom row for ease of correction, without an X value.
2. Correct for well-to-well variation by subtracting the FSK measurement.
   i. Select 'Repeated measures' in the baseline correction in GraphPad Prism, which will use the values from the specific well when you have duplicates.
3. Correct for vehicle.
4. Allow Prism to compare between two non-linear fits based on the time trace using the F-test:
   i. Use simplest model first 'Baseline then rise to steady state' and compare to the more complex model 'Baseline then rise-and-fall to steady state'.
   ii. Constrain the following parameters for better fitting results:
      a. Baseline then rise to steady state:
         1. X_0 must be greater than 0
         2. Baseline no constraint
         3. SteadyState must be greater than 0
         4. k must be greater than 0
      b. Baseline then rise-and-fall to baseline
         1. X_0 must be greater than 0
         2. Baseline no constraint
         3. SteadyState must be greater than 0
         4. D must be greater than 0
         5. k_1 no constraint
         6. k_2 must be greater than 0
         7. k_1 must be greater than 1 times k_2
      c. Don't constrain X_0 to the time of agonist addition as there might be a delay in the response, which will now be captured by the model.
      d. Don't constrain Baseline to allow some more flexibility of the model.
   iii. For all curves manually change the Initial Value (in the corresponding tab) for X_0

to the time of agonist addition or slightly before.

a. This helps the model to better guess when your baseline run-in period turns into a response.

iv. Only analyze the data from the final five FSK measurements (baseline) to the end of the assay.

v. In the 'Confidence' tab change the Confidence Intervals (CI) of the parameters to the 'Symmetrical (asymptotic) approximate CI' if you do not need the CI.

a. This mainly allows for a quicker fitting of the curves and does not influence the calculation of the fitted parameter but will only not report the CI.

vi. From these analyses, the k_1 and k_2 values are determined, but Initial Rate and Peak Response need to be calculated[77]:

$$IR=SSR(D \cdot k_1-(D-1)k_2)$$

$$\text{Peak time}=\frac{1}{k_2-k_1}\ln\left(\frac{(D-1)k_2}{Dk_1}\right)$$

$$\text{Peak response}=SSR(1-De^{-k_1 \cdot \text{Peak time}}+(D-1)e^{-k_2 \cdot \text{Peak time}}$$

5. The inactive concentrations, i.e., concentrations at which no inhibition of ß-arrestin-2 recruitment is detected anymore, can also be analyzed to determine the slope. This will be (close to) 0.

i. Use the 'Straight line time course' equation as described by Hoare *et al.*[20] with default parameters. The reported slope is the same as initial rate.

3.S1.2.3 [^{35}S]GTPγS assays

Functional agonist responses from the [^{35}S]GTPγS binding assays were baseline-corrected with the basal activity and normalized to 10 μM of CP55,940. pEC_{50} and E_{max} values were determined using non-linear regression curve fitting 'log(agonist) vs. response' (three parameters).

3.S2 Supplementary figures

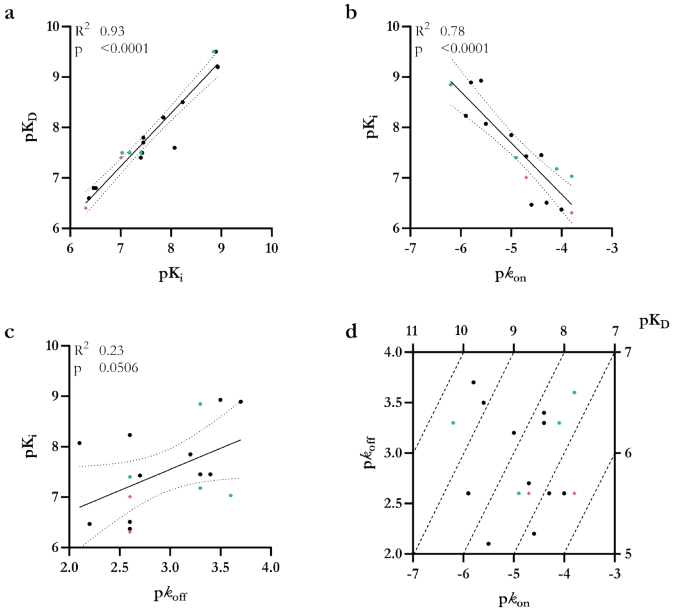

Figure 3.S1 Correlation plots between affinity and binding kinetic parameters of benchmark agonists, endocannabinoids and clinical agonists from [^{3}H]RO6957022 binding assays on CB_2R.
Correlation plots with parameters from [^{3}H]RO6957022 binding assays on CB_2R comparing (a) equilibrium affinity pK_i and kinetic affinity pK_D, (b) pk_{on} and pK_i, and (c) pk_{off} and pK_i. (d) Kinetic map representing the relationship between pk_{on}, pk_{off} and pK_D. Benchmark agonists are turquoise hexagons (⬢), endocannabinoids coral diamonds (◆) and clinical agonists black circles (●). Data are mean from at least three independent experiments performed in duplicate. The solid line represents a linear correlation between the parameters and the dotted lines indicate the 95% confidence interval. R^2 values represent a measure of goodness-of-fit of the simple linear regression and $p < 0.05$ indicate a slope statistically significant different from 0.

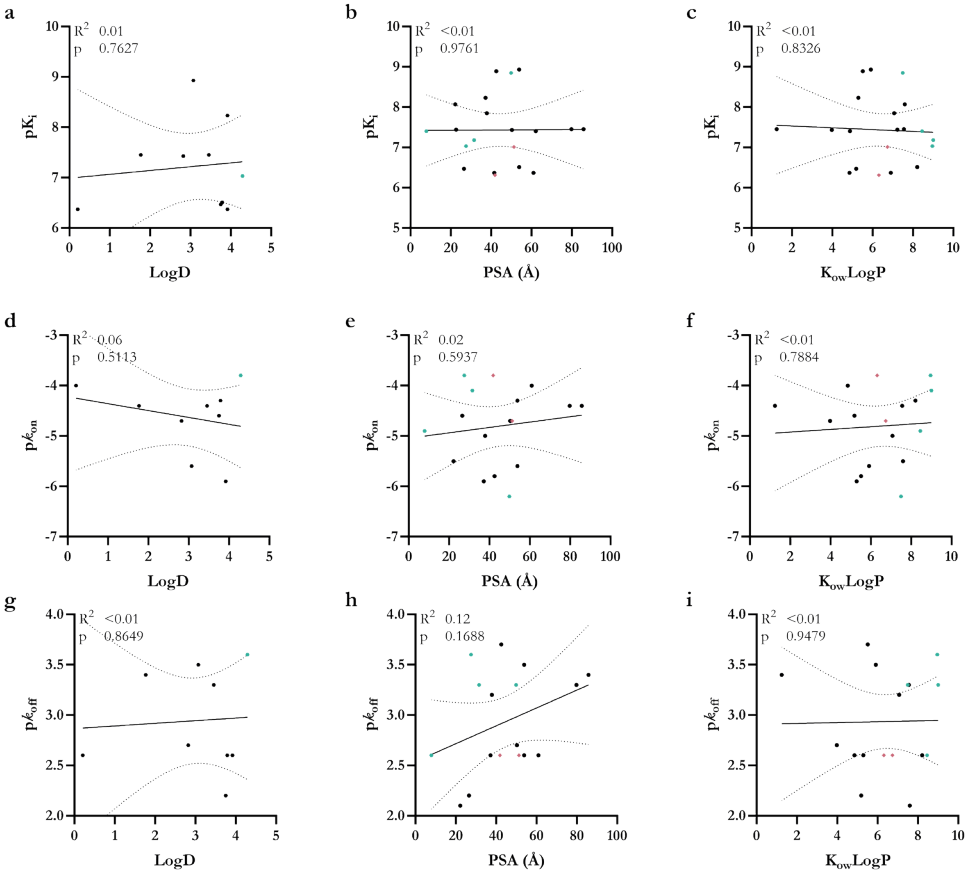

Figure 3.S2 Correlation plots between physicochemical parameters and binding affinity and binding kinetic parameters for benchmark agonists, endocannabinoids and clinical agonists on CB_2R.
Correlation plots comparing (a) distribution coefficient LogD, (b) polar surface area PSA and (c) calculated partition coefficient K_{ow}LogP with equilibrium affinity pK_i. Correlation plots comparing (d) LogD, (e) PSA and (f) K_{ow}LogP with association rate constant pk_{on}. Correlation plots comparing (g) LogD, (h) PSA and (i) K_{ow}LogP with dissociation rate constant pk_{off}. Benchmark agonists are turquoise hexagons (⬢), endocannabinoids coral diamonds (◆) and clinical agonists black circles (●). Data are mean from at least three independent experiments performed in duplicate. The solid line represents a linear correlation between the parameters and the dotted lines indicate the 95% confidence interval. R^2 values represent a measure of goodness-of-fit of the simple linear regression and $p < 0.05$ indicate a slope statistically significant different from 0.

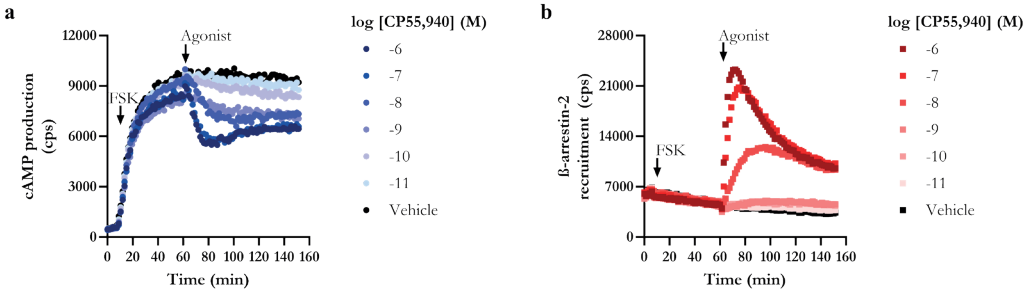

Figure 3.S3 Raw time traces from the multiplexed cAMP production and ß-arrestin-2 recruitment assay on HEK293T CB_2R-SmBiT LgBiT-ß-arrestin-2 cells with full agonist CP55,940.

Representative luminescent time traces indicative of (a) cAMP production and (b) ß-arrestin-2 recruitment simultaneously recorded in the multiplex assay on HEK293T CB_2R-SmBiT LgBiT-ß-arrestin-2 cells. Baseline luminesce was measured for 7.5 min prior to forskolin (FSK) addition to induce cAMP production. After 1 h, cells were stimulated with increasing concentrations of agonist CP55,940 and luminescence was recorded for 90 min. Data are shown as mean from a representative experiment performed in duplicate.

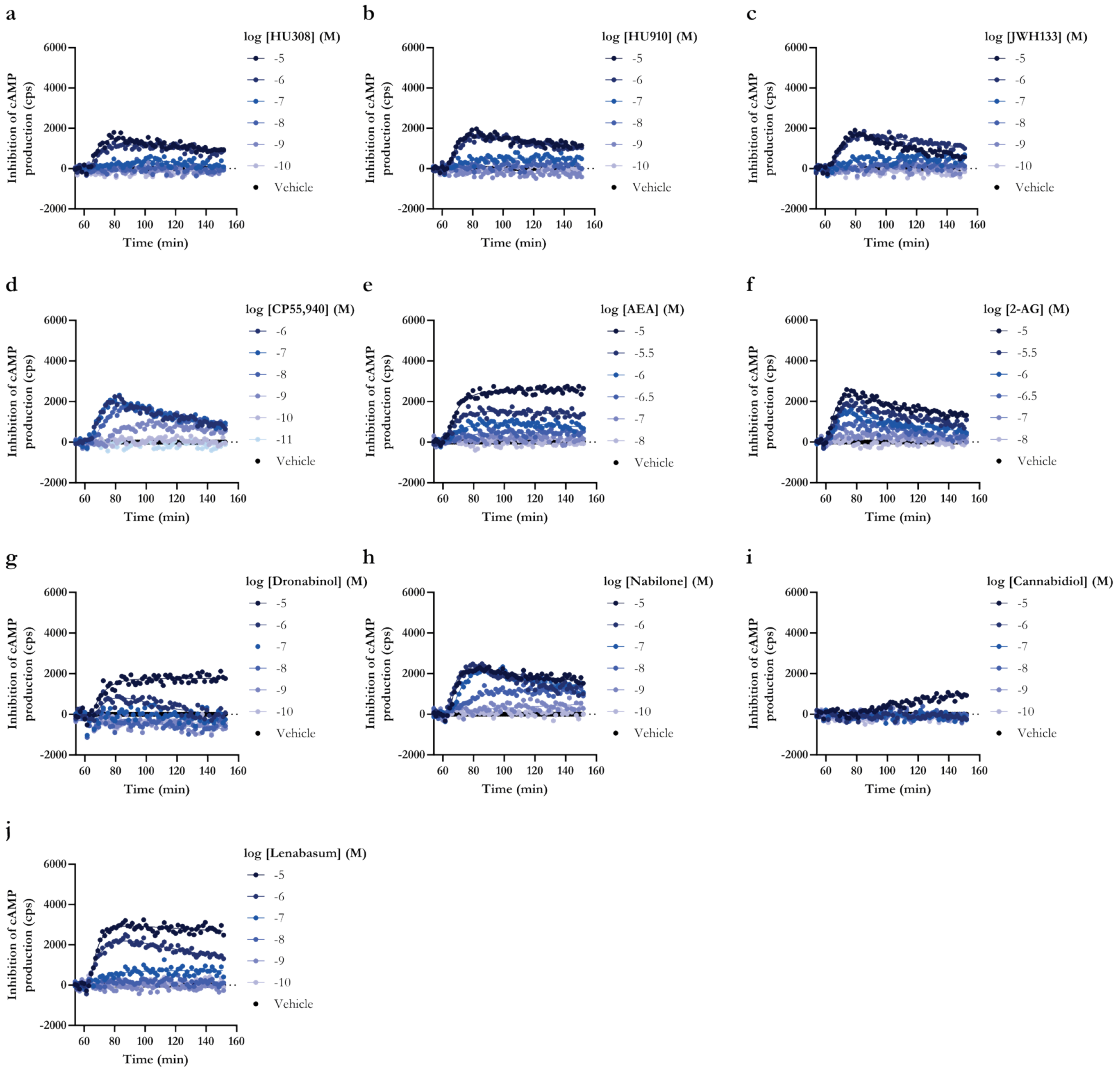

Figure 3.S4 Time traces of inhibition of cAMP production by benchmark agonists, endocannabinoids, launched and clinical agonists from the multiplex assay on HEK293T CB_2R-SmBiT LgBiT-ß-arrestin-2 cells. Representative forskolin- and vehicle-corrected time traces for inhibition of cAMP production by increasing concentrations of (a-d) benchmark agonists, (e, f) endocannabinoids, clinical agonists that (g-i) are on the market or (j) reached phase 3. Data are shown as mean from a representative experiment performed in duplicate.

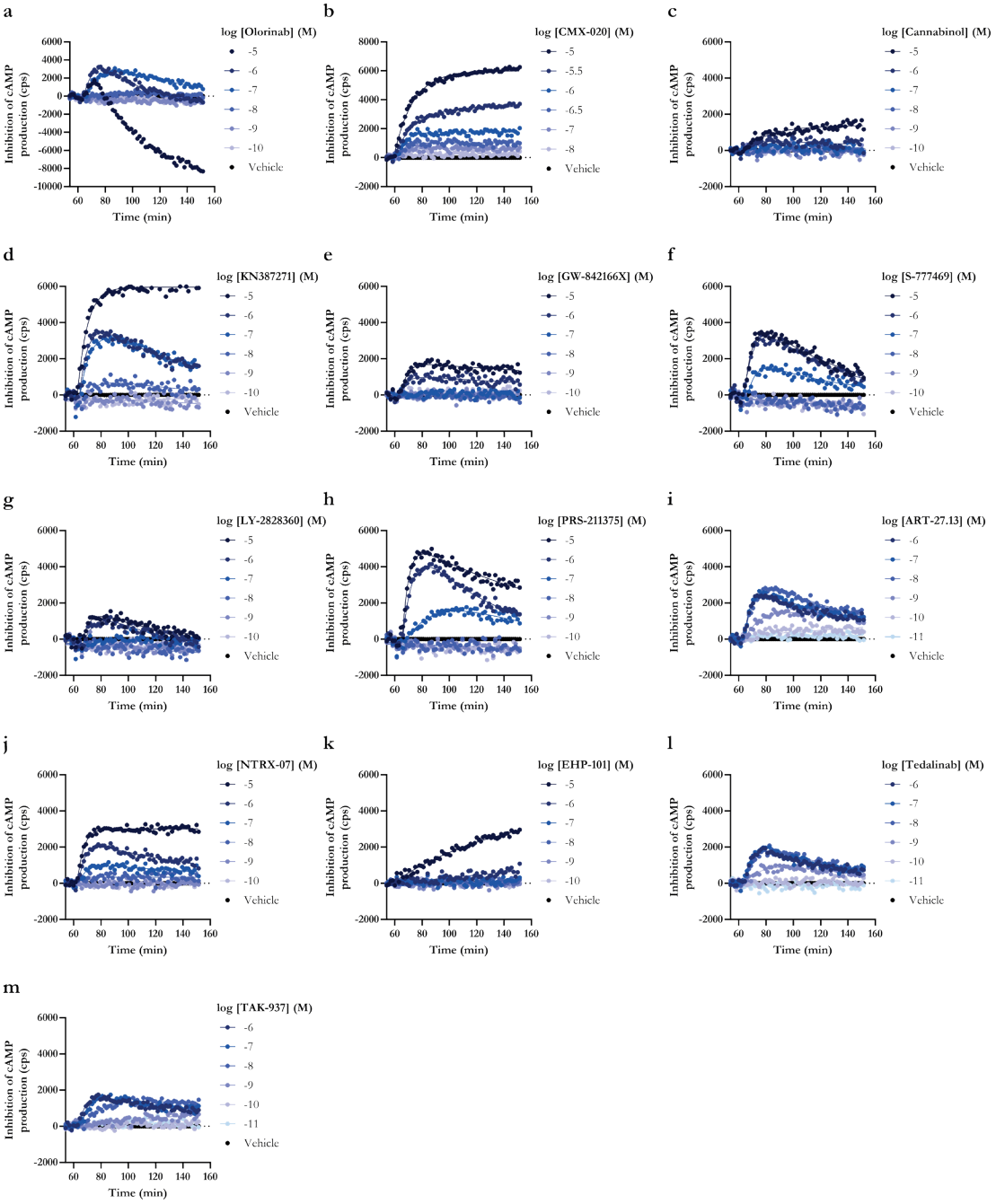

Figure 3.S5 Time traces of inhibition of cAMP production by benchmark agonists, endocannabinoids, launched and clinical agonists from the multiplex assay on HEK293T CB_2R-SmBiT LgBiT-ß-arrestin-2 cells. Representative forskolin- and vehicle-corrected time traces for inhibition of cAMP production by increasing concentrations of clinical agonists that (a-h) reached phase 2 or (i-m) phase 1. Data are shown as mean from a representative experiment performed in duplicate.

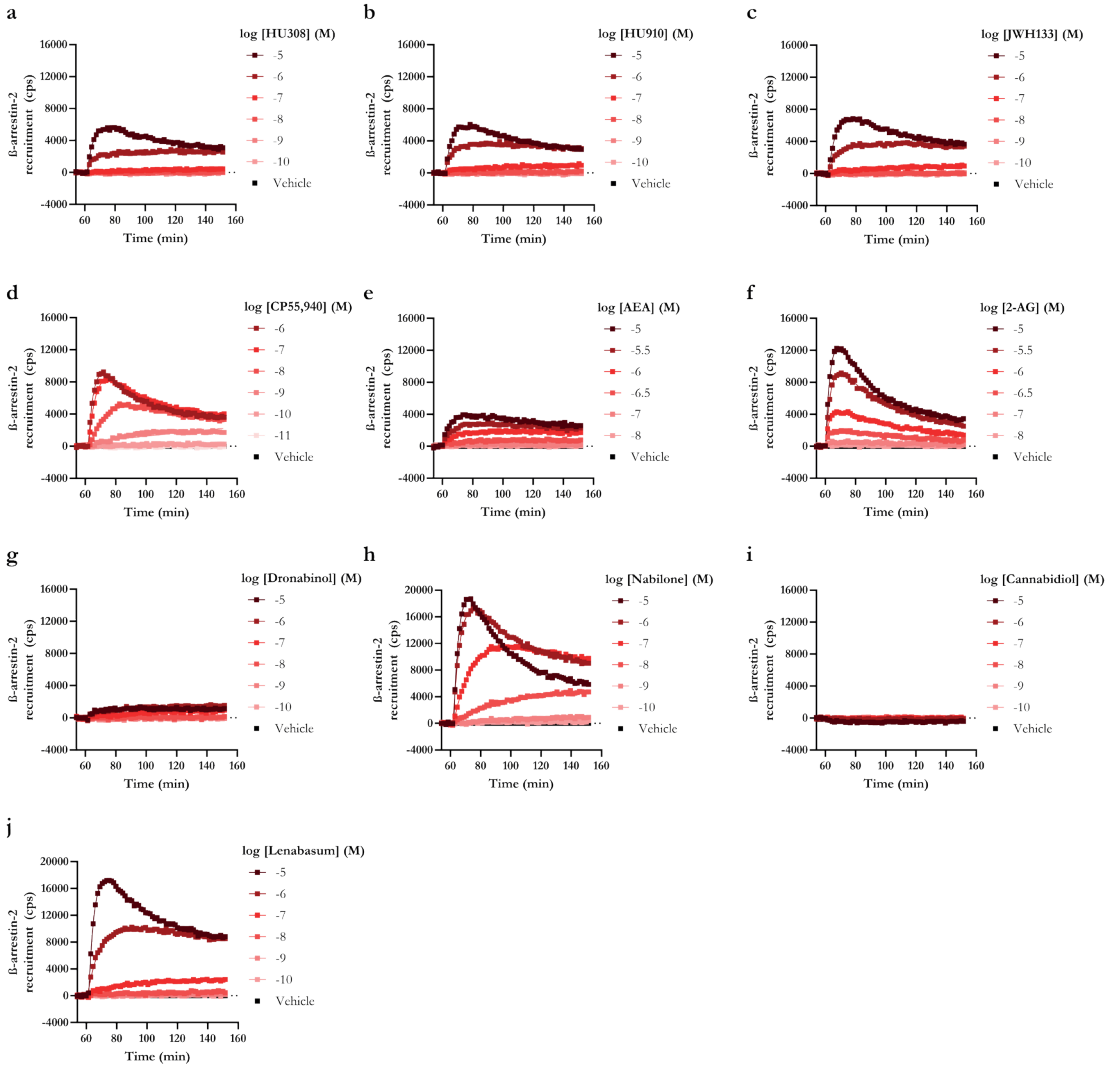

Figure 3.S6 Time traces of ß-arrestin-2 recruitment by benchmark agonists, endocannabinoids, launched and clinical agonists from the multiplex assay on HEK293T CB_2R-SmBiT LgBiT-ß-arrestin-2 cells. Representative vehicle-corrected time traces for ß-arrestin-2 recruitment to CB_2R by increasing concentrations of (a-d) benchmark agonists, (e, f) endocannabinoids, clinical agonists that (g-i) are on the market or (j) reached phase 3. Data are shown as mean from a representative experiment performed in duplicate.

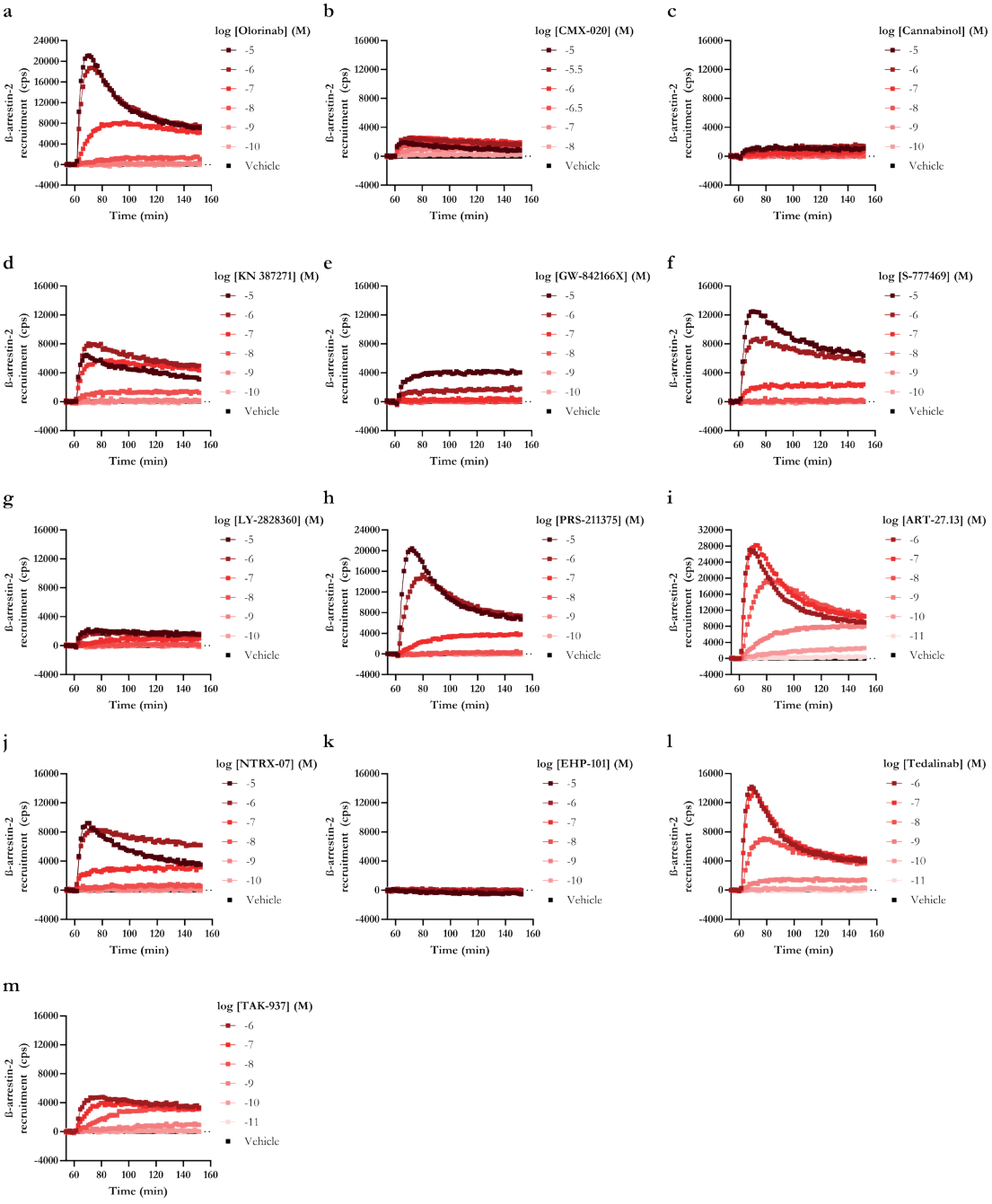

Figure 3.S7 Time traces of ß-arrestin-2 recruitment by clinical agonists from the multiplex assay on HEK293T CB_2R-SmBiT LgBiT-ß-arrestin-2 cells.

Representative vehicle-corrected time traces for ß-arrestin-2 recruitment to CB_2R by increasing concentrations of clinical agonists that (a-h) reached phase 2 or (i-m) phase 1. Data are shown as mean from a representative experiment performed in duplicate.

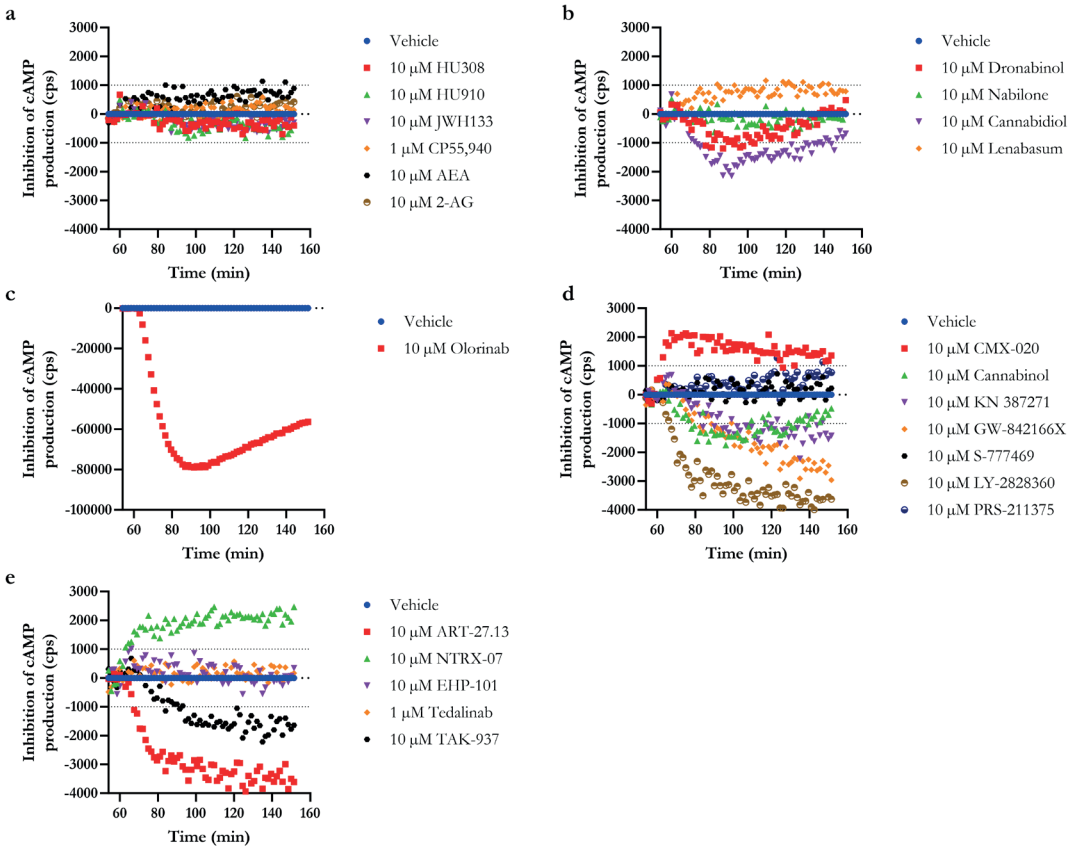

Figure 3.S8 CB_2R-independent modulation of cAMP production by benchmark agonists, endocannabinoids and clinical agonists in a forskolin-induced cAMP assay on HEK293T cells.
Representative time traces of 10 or 1 µM (a) benchmark agonists and endocannabinoids, agonists that are (b) launched or clinically investigated in phase 3, (c, d) phase 2, (e) phase 1. Data are shown as mean from a representative experiment performed in duplicate.

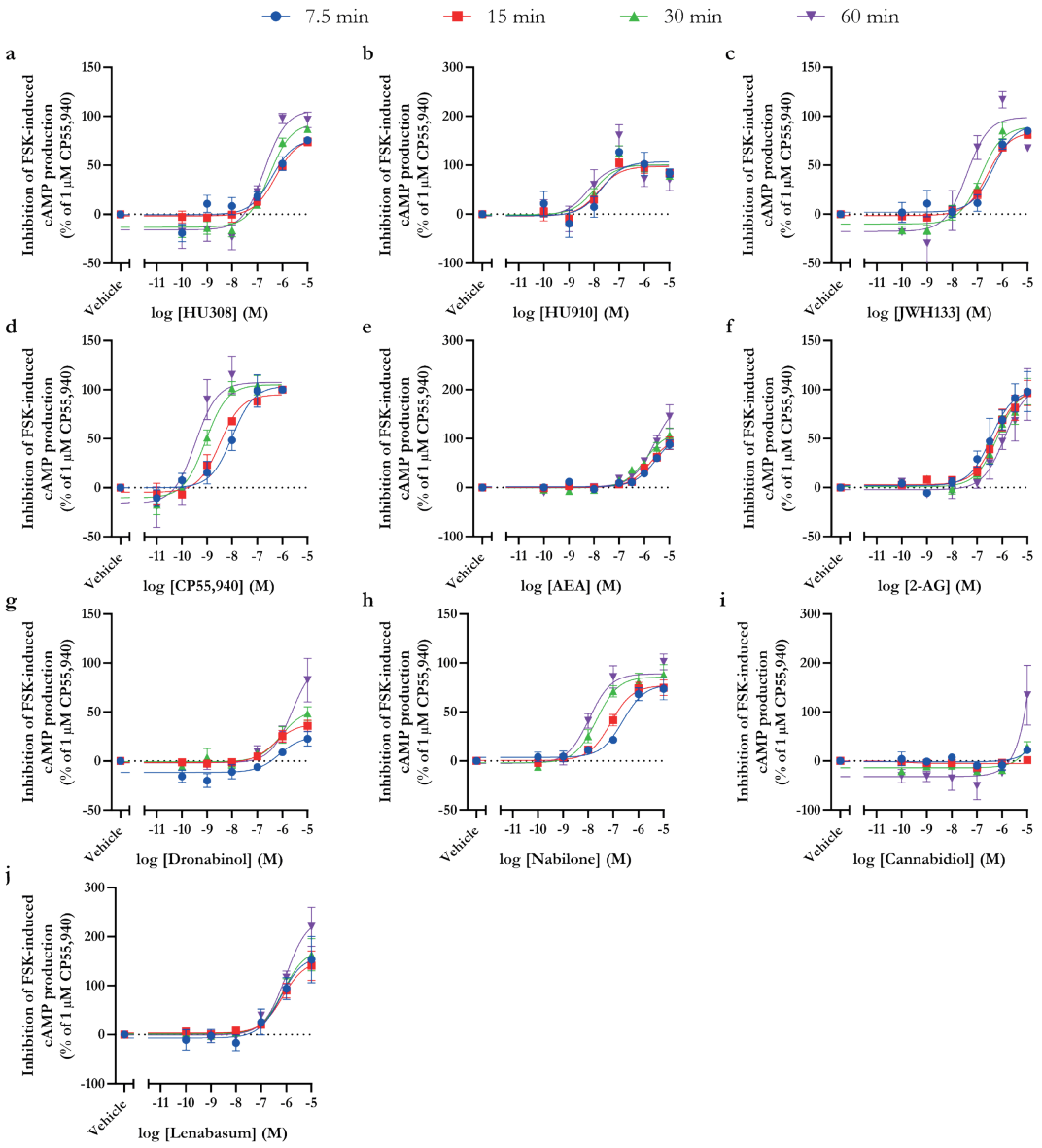

Figure 3.S9 Time-dependent inhibition of cAMP production by benchmark agonists, endocannabinoids, launched and clinical agonists from the multiplex assay on HEK293T CB_2R-SmBiT LgBiT-ß-arrestin-2 cells.

Inhibition of cAMP production at 7.5, 15, 30 or 60 min after addition of increasing concentrations of (a-d) benchmark agonists, (e, f) endocannabinoids, clinical agonists that (g-i) are on the market or (j) reached phase 3. Efficacy was calculated as percentage of the maximum effect induced by 1 µM CP55,940 at the specific time point. Data are shown as mean ± SEM from at least three independent experiments performed in duplicate.

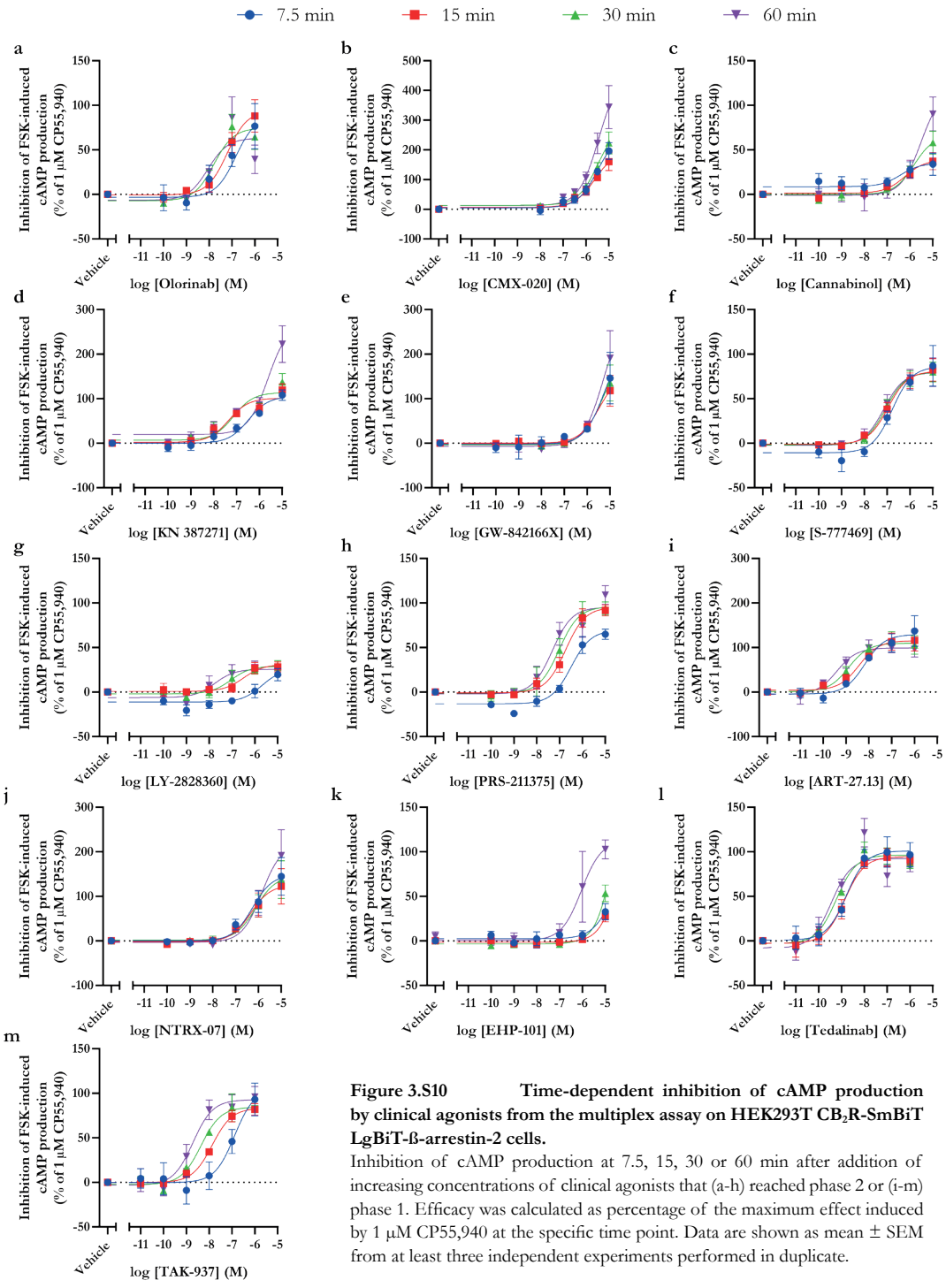

Figure 3.S10 Time-dependent inhibition of cAMP production by clinical agonists from the multiplex assay on HEK293T CB_2R-SmBiT LgBiT-ß-arrestin-2 cells.

Inhibition of cAMP production at 7.5, 15, 30 or 60 min after addition of increasing concentrations of clinical agonists that (a-h) reached phase 2 or (i-m) phase 1. Efficacy was calculated as percentage of the maximum effect induced by 1 µM CP55,940 at the specific time point. Data are shown as mean ± SEM from at least three independent experiments performed in duplicate.

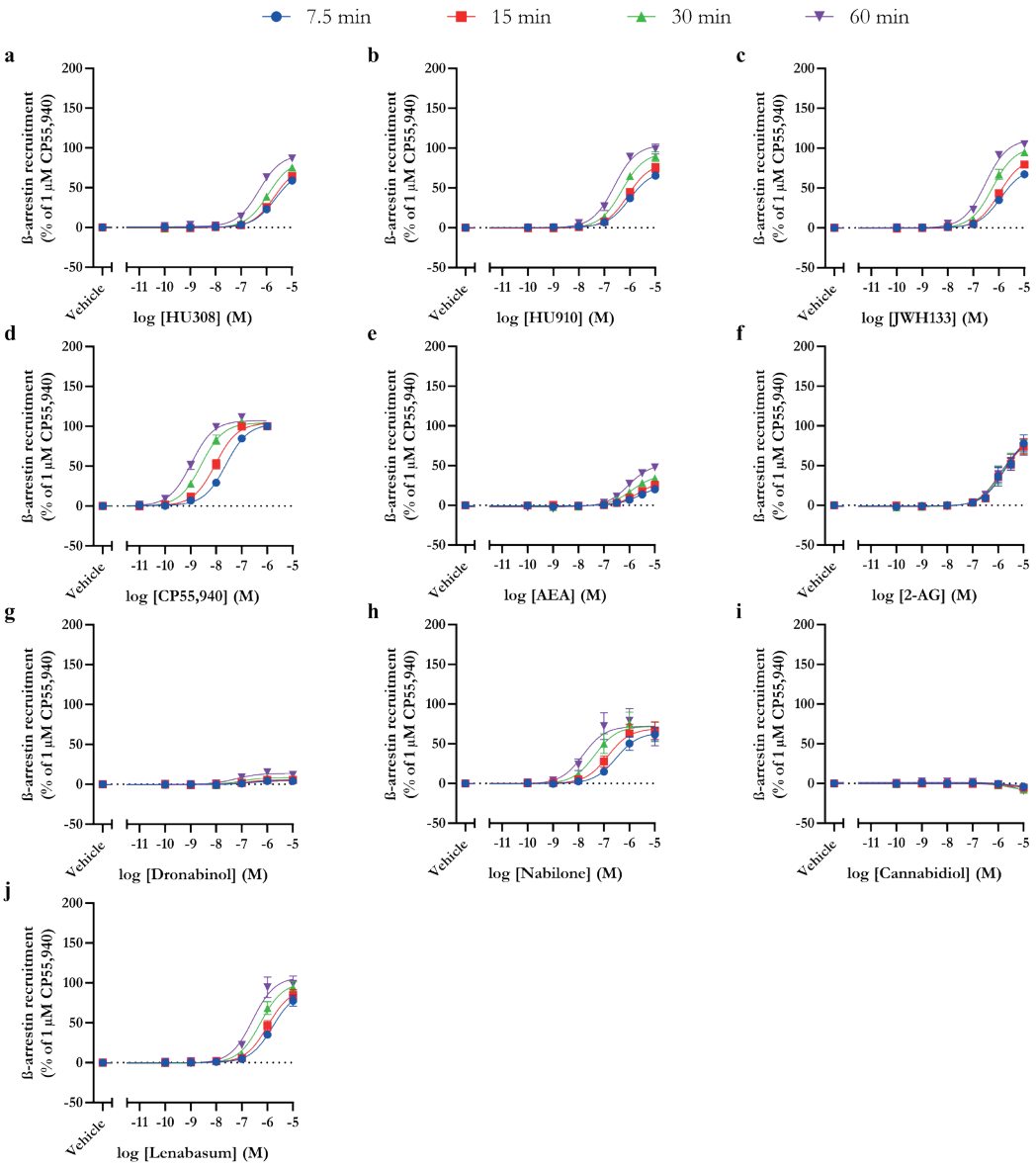

Figure 3.S11 Time-dependent ß-arrestin-2 recruitment to CB_2R by benchmark agonists, endocannabinoids, launched and clinical agonists from the multiplex assay on HEK293T CB_2R-SmBiT LgBiT-ß-arrestin-2 cells.

Recruitment of ß-arrestin-2 at 7.5, 15, 30 or 60 min after addition of increasing concentrations of (a-d) benchmark agonists, (e, f) endocannabinoids, clinical agonists that (g-i) are on the market or (j) reached phase 3. Efficacy was calculated as percentage of the maximum effect induced by 1 µM CP55,940 at the specific time point. Data are shown as mean ± SEM from at least three independent experiments performed in duplicate.

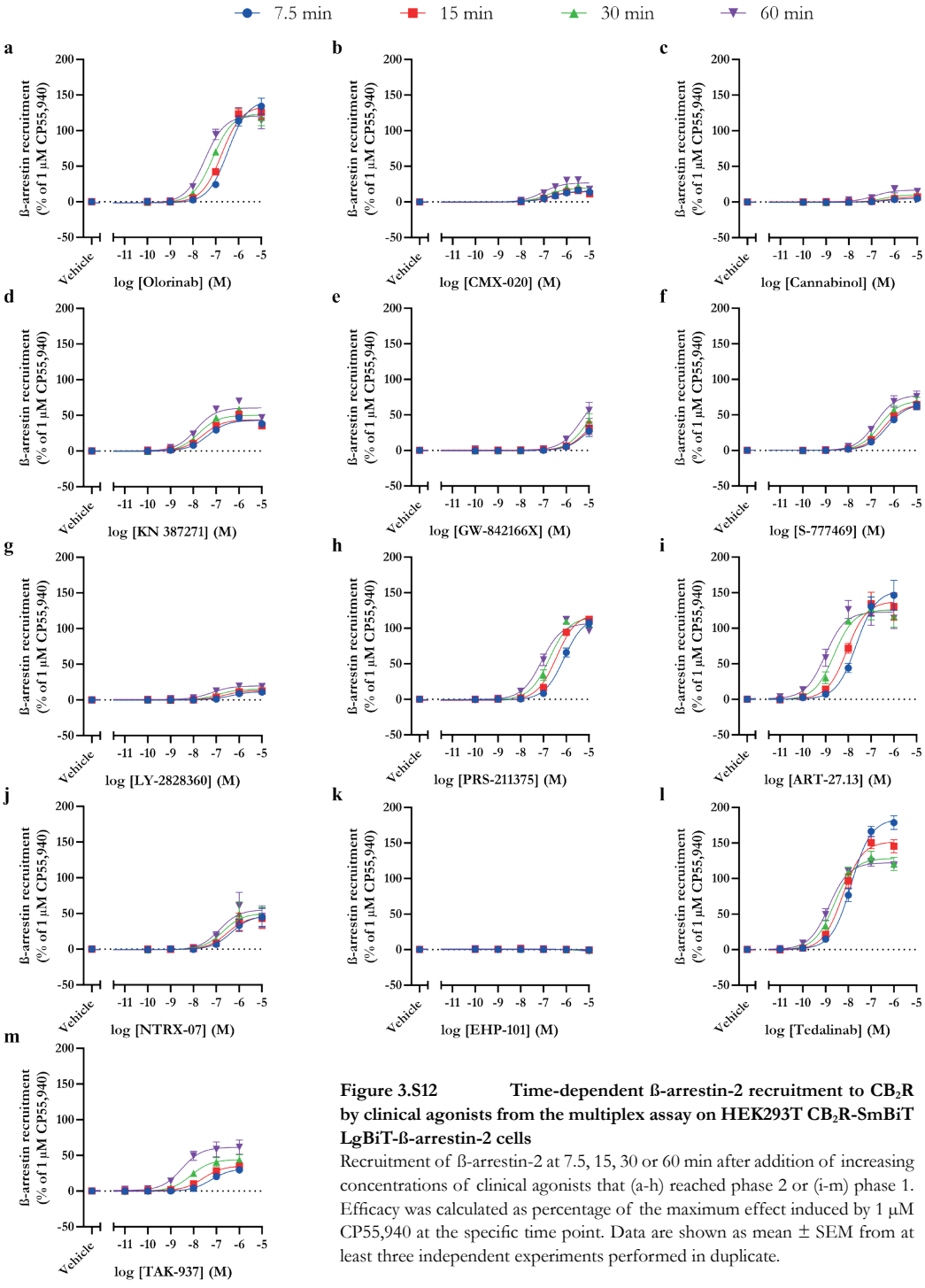

Figure 3.S12 Time-dependent ß-arrestin-2 recruitment to CB_2R by clinical agonists from the multiplex assay on HEK293T CB_2R-SmBiT LgBiT-ß-arrestin-2 cells

Recruitment of ß-arrestin-2 at 7.5, 15, 30 or 60 min after addition of increasing concentrations of clinical agonists that (a-h) reached phase 2 or (i-m) phase 1. Efficacy was calculated as percentage of the maximum effect induced by 1 µM CP55,940 at the specific time point. Data are shown as mean ± SEM from at least three independent experiments performed in duplicate.

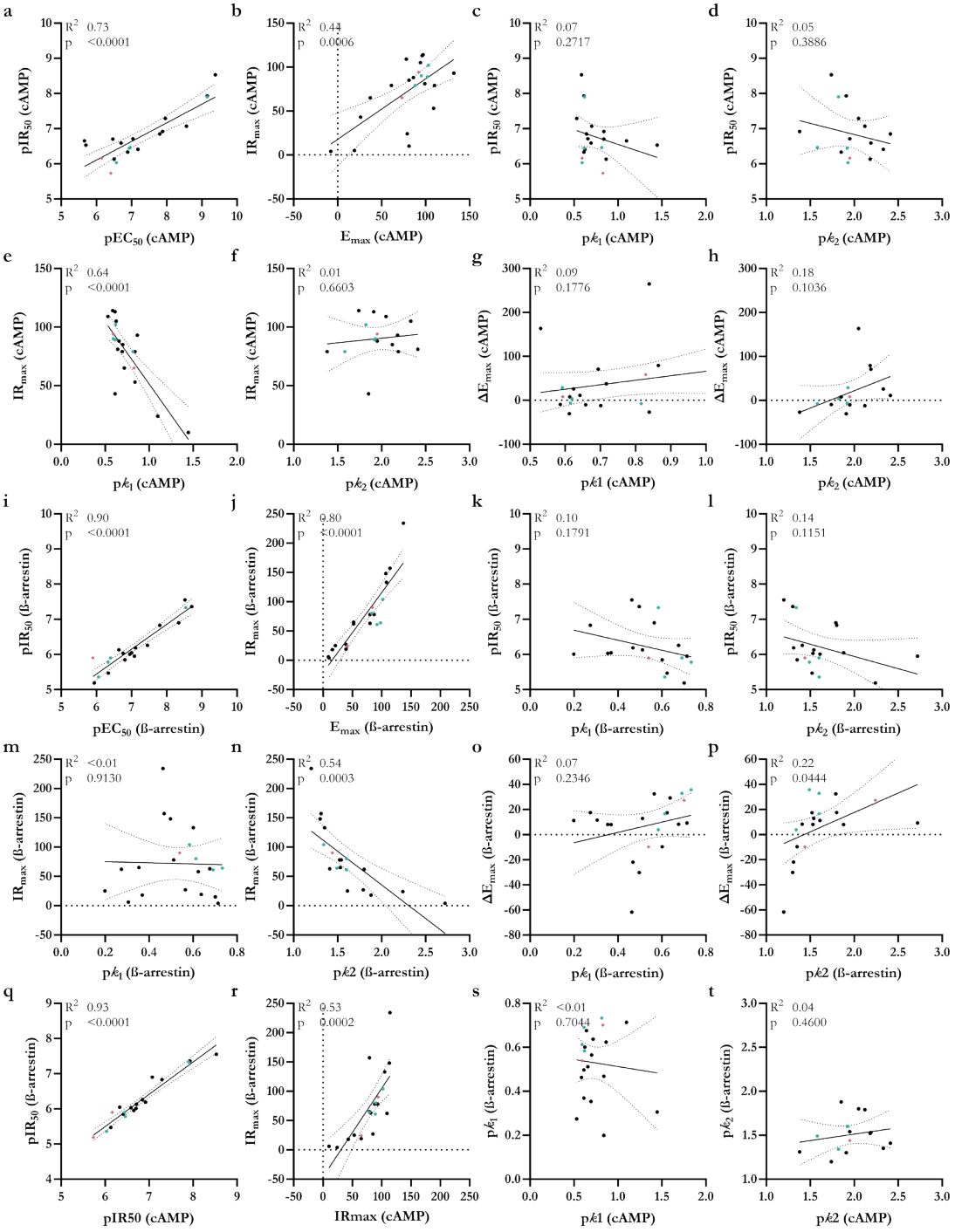
a
R² 0.73
p <0.0001
pIR50 (cAMP)
pEC50 (cAMP)
b
R² 0.44
p 0.0006
IRmax (cAMP)
Emax (cAMP)
c
R² 0.07
p 0.2717
pIR50 (cAMP)
pk1 (cAMP)
d
R² 0.05
p 0.3886
pIR50 (cAMP)
pk2 (cAMP)
e
R² 0.64
p <0.0001
IRmax (cAMP)
pk1 (cAMP)
f
R² 0.01
p 0.6603
IRmax (cAMP)
pk2 (cAMP)
g
R² 0.09
p 0.1776
ΔEmax (cAMP)
pk1 (cAMP)
h
R² 0.18
p 0.1036
ΔEmax (cAMP)
pk2 (cAMP)
i
R² 0.90
p <0.0001
pIR50 (ß-arrestin)
pEC50 (ß-arrestin)
j
R² 0.80
p <0.0001
IRmax (ß-arrestin)
Emax (ß-arrestin)
k
R² 0.10
p 0.1791
pIR50 (ß-arrestin)
pk1 (ß-arrestin)
l
R² 0.14
p 0.1151
pIR50 (ß-arrestin)
pk2 (ß-arrestin)
m
R² <0.01
p 0.9130
IRmax (ß-arrestin)
pk1 (ß-arrestin)
n
R² 0.54
p 0.0003
IRmax (ß-arrestin)
pk2 (ß-arrestin)
o
R² 0.07
p 0.2346
ΔEmax (ß-arrestin)
pk1 (ß-arrestin)
p
R² 0.22
p 0.0444
ΔEmax (ß-arrestin)
pk2 (ß-arrestin)
q
R² 0.93
p <0.0001
pIR50 (ß-arrestin)
pIR50 (cAMP)
r
R² 0.53
p 0.0002
IRmax (ß-arrestin)
IRmax (cAMP)
s
R² <0.01
p 0.7044
pk1 (ß-arrestin)
pk1 (cAMP)
t
R² 0.04
p 0.4600
pk2 (ß-arrestin)
pk2 (cAMP)

← Figure 3.S13 Correlation plots between parameters from the multiplex cAMP production and ß-arrestin-2 recruitment assay on CB_2R for benchmark agonists, endocannabinoids and clinical agonists. Correlation plots with forskolin-induced cAMP production parameters from the multiplex assay comparing (a) potency pEC_{50} and kinetic potency pIR_{50}, (b) efficacy E_{max} and kinetic efficacy IR_{max} (c) signaling rate constant pk_1 and pIR_{50}, (d) signaling rate constant pk_2 and pIR_{50}, (e) pk_1 and IR_{max}, (f) pk_2 and IR_{max}, (g) pk_1 and ΔE_{max} from the time-dependent analysis and (h) pk_2 and ΔE_{max}. Correlation plots with ß-arrestin-2 recruitment parameters from the multiplex assay comparing (i) pEC_{50} and pIR_{50}, (j) E_{max} and IR_{max} (k) pk_1 and pIR_{50}, (l) pk_2 and pIR_{50}, (m) pk_1 and IR_{max}, (n) pk_2 and IR_{max}, (o) pk_1 and ΔE_{max} from time-dependent analysis and (p) pk_2 and ΔE_{max}. Correlation plots comparing cAMP production and ß-arrestin recruitment in terms of kinetic parameters from the two readouts (q) IR_{50}, (r) IR_{max}, signaling rate constants (s) pk_1 and (t) pk_2. Benchmark agonists are turquoise hexagons (⬢), endocannabinoids coral diamonds (◆) and clinical agonists black circles (●). Data are mean from at least three independent experiments performed in duplicate. The solid line represents a linear correlation between the parameters and the dotted lines indicate the 95% confidence interval. R^2 values represent a measure of goodness-of-fit of the simple linear regression and $p < 0.05$ indicate a slope statistically significant different from 0.

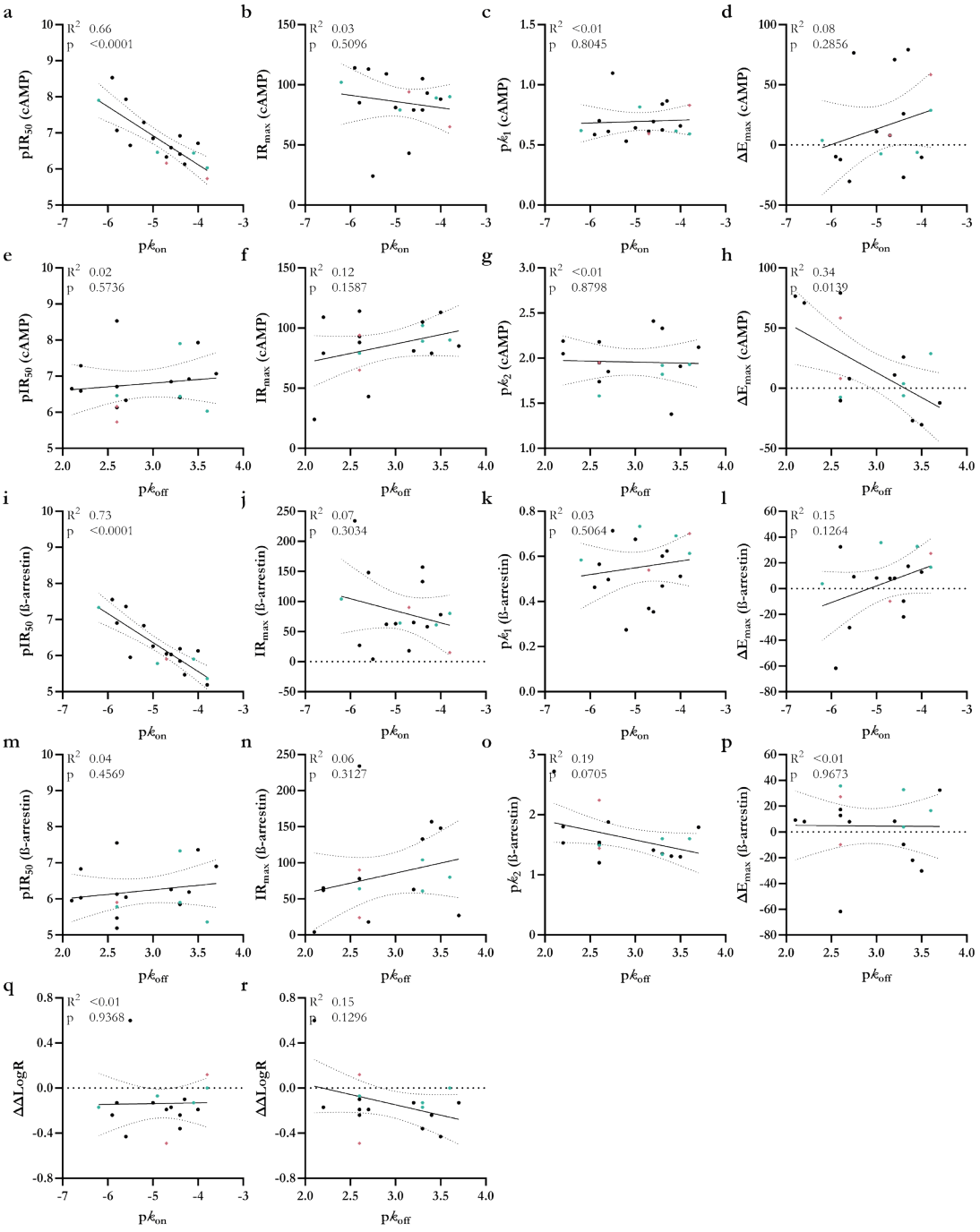
a
R² 0.66
p <0.0001
pIR50 (cAMP)
pkon
b
R² 0.03
p 0.5096
IRmax (cAMP)
pkon
c
R² <0.01
p 0.8045
pKi (cAMP)
pkon
d
R² 0.08
p 0.2856
ΔEmax (cAMP)
pkon
e
R² 0.02
p 0.5736
pIR50 (cAMP)
pkoff
f
R² 0.12
p 0.1587
IRmax (cAMP)
pkoff
g
R² <0.01
p 0.8798
pKi (cAMP)
pkoff
h
R² 0.34
p 0.0139
ΔEmax (cAMP)
pkoff
i
R² 0.73
p <0.0001
pIR50 (β-arrestin)
pkon
j
R² 0.07
p 0.3034
IRmax (β-arrestin)
pkon
k
R² 0.03
p 0.5064
pKi (β-arrestin)
pkon
l
R² 0.15
p 0.1264
ΔEmax (β-arrestin)
pkon
m
R² 0.04
p 0.4569
pIR50 (β-arrestin)
pkoff
n
R² 0.06
p 0.3127
IRmax (β-arrestin)
pkoff
o
R² 0.19
p 0.0705
pKi (β-arrestin)
pkoff
p
R² <0.01
p 0.9673
ΔEmax (β-arrestin)
pkoff
q
R² <0.01
p 0.9368
ΔΔLogR
pkon
r
R² 0.15
p 0.1296
ΔΔLogR
pkoff

← Figure 3.S14 Correlation plots between binding affinity, binding kinetic parameters and parameters from the multiplex assay on CB_2R for benchmark agonists, endocannabinoids and clinical agonists.
Correlation plots comparing association rate constant pk_{on} with cAMP production parameters from the multiplex assay (a) kinetic potency pIR_{50}, (b) kinetic efficacy IR_{max}, (c) signaling rate constant pk_1, (d) ΔE_{max} from the time-dependent analysis and dissociation rate constant pk_{off} with cAMP production parameters from the multiplex assay (e) pIR_{50}, (f) IR_{max}, (g) signaling rate constant pk_2 and (h) ΔE_{max}. Correlation plots comparing association rate constant pk_{on} with ß-arrestin-2 recruitment parameters from the multiplex assay (i) pIR_{50}, (j) IR_{max}, (k) signaling rate constant pk_1, (l) ΔE_{max} from the time-dependent analysis and dissociation rate constant pk_{off} with cAMP production parameters from the multiplex assay (m) pIR_{50}, (n) IR_{max}, (o) signaling rate constant pk_2 and (p) ΔE_{max}. Correlation plots between target binding kinetic parameters and bias parameters comparing (q) pk_{on} and $\Delta\Delta LogR$, and (r) pk_{off} and $\Delta\Delta LogR$. Benchmark agonists are turquoise hexagons (⬢), endocannabinoids coral diamonds (◆) and clinical agonists black circles (●). Data are mean from at least three independent experiments performed in duplicate. The solid line represents a linear correlation between the parameters and the dotted lines indicate the 95% confidence interval. R^2 values represent a measure of goodness-of-fit of the simple linear regression and $p < 0.05$ indicate a slope statistically significant different from 0.

Table 3.S1 Physicochemical properties and pharmacokinetic properties of benchmark agonists, endocannabinoids (eCB) and clinical agonists.

	Agonist	MW[a] (g/mol)	PSA[b] (Å)	LogD[c]	K_{ow}LogP[d]	Kinetic solubility[e] (µg/mL)	LIMBA LogDbrain[f]	PAMPA P_{eff}[g] ($\times 10^{-6}$ cm/s)	Human plasma protein binding (free fraction %)	hP-gp Efflux ratio
Benchmark	**HU308**	414.6	27.580	4.29	8.965	<0.5	N.D.	2.530 ± 1.460#	N.D.	1.266
	HU910	414.6	31.540	N.D.	9.001	<0.5	N.D.	0.315 ± 0.420#	<1.790	1.182
	JWH133	312.5	7.910	>3.00	8.458	<0.4	N.D.	0.930 ± 0.810#	0.070 ± 0.010	N.D.
	CP55,940	376.6	49.860	N.D.	7.498	1.4	0.7	N.D.	<1	0.950
eCB	**AEA**	347.5	41.910	N.D.	6.310	N.D.	N.D.	0.26 ± 0.16	N.D.	N.D.
	2-AG	378.5	51.250	N.D.	6.738	N.D.	N.D.	N.D.	N.D.	N.D.
Clinical	**Dronabinol**	314.5	22.240	N.A.	7.598	N.A.	N.A.	N.A.	N.A.	N.A.
	Nabilone	372.5	37.850	N.D.	7.069	<0.7	N.D.	N.D.	<0.1	N.D.
	Cannabidiol	314.5	31.120	N.D.	8.013	<0.2	N.D.	N.D.	N.D.	1.390
	Lenabasum	400.6	53.860	3.79	8.241	22.0	2.73	N.D.	<0.1	0.877
	Olorinab	357.4	85.780	1.77	1.244	368.0	-0.08	2.860 ± 0.298#	23.660 ± 0.428	1.220
	CMX-020	416.6	41.540	3.92	6.904	5.1	2.07	6.220 ± 2.250	<0.1	1.240
	Cannabinol	310.4	22.630	N.D.	7.232	<0.6	N.D.	N.D.	<1	1.18
	KN 387271	430.4	62.100	N.D.	4.881	<0.8	2.28	N.D.	<0.1	1.010
	GW-842166X	449.3	57.500	3.84	4.321	<0.2	2.40	3.540	0.620	0.980
	S-777469	414.5	60.940	0.21	4.857	45.0	0.27	3.520 ± 0.180	3.980 ± 0.078	1.310
	LY-2828360	426.9	50.310	2.82	3.979	>427.0	1.52	4.100 ± 0.220	5.810 ± 0.838	1.080
	PRS-211375	470.6	79.800	3.46	7.556	332.0	1.85	N.D.	N.D.	N.D.
	ART-27.13	413.5	53.860	3.07	5.913	4.6	1.56	4.390 ± 1.110	12.370 ± 0.270	2.150
	NTRX-07	335.4	26.520	3.75	5.184	N.D.	2.18	12.900	1.710 ± 0.134	1.220
	EHP-101	433.6	52.650	N.D.	7.862	N.D.	N.D.	N.D.	1.00 ± 0.095	N.D.
	Tedalinab	345.4	37.480	3.92	5.293	4.0	2.42	7.460 ± 1.640	1.240 ± 0.031	0.990
	TAK-937	423.6	42.520	N.D.	5.514	5.9	2.15	3.570 ± 0.070	1.230 ± 0.016	1.220

Table 3.S2 Assay characteristics of functional assays used in this study for investigation of agonist-mediated activation of CB_2R.

Assay	GloSensor™	NanoBiT®	[^{35}S]GTPγS binding
Transducer/Effector	cAMP	ß-arrestin-2	G protein
Endpoint or kinetic	Kinetic	Kinetic	Endpoint
Time point or span for data collection	54 – 150 min	54 – 150 min	90 min
System	Live cells	Live cells	Membrane fractions
Cell line	HEK293T CB_2R-SmBiT LgBiT-ß-arrestin-2		
Receptor expression levels[a]	11 ± 2 pmol/mg		
Measured process	Production	Recruitment	Binding
Measured molecule	cAMP	CB_2R-SmBiT	[^{35}S]GTPγS
Measured molecule 2 (if any)	N.A.	LgBiT-ß-arrestin-2	N.A.
Temperature	25 °C	25 °C	25 °C
Signal detection	Luminescence (Fluc)	Luminescence (NLuc)	Radioactivity
Reference ligand for bias	HU308		
Reference ligand for E_{max} per assay	CP55,940		
Multiplex possibilities	With NanoBiT	With GloSensor	N.A.

[a] Determined in [^{3}H]RO6957022 homologous displacement assays on HEK293T CB_2R-SmBiT LgBiT-ß-arrestin-2 membrane fractions. N.A. is not applicable.

Table 3.S3 Validation and characterization of the multiplexed cAMP production and ß-arrestin-2 recruitment assay on HEK293T CB_2R-SmBiT LgBiT-ß-arrestin-2 cells with full agonist CP55,940.

	cAMP channel	ß-arrestin channel
Reagent	**pEC_{50}**	**pEC_{50}**
cAMP reagent	8.86 (8.85; 8.86)	N.A.
Vivazine	N.A.	8.20 (8.28; 8.12)
Multiplex reagent	8.55 (8.58; 8.53)	8.16 (8.13; 8.20)

Potency values (pEC_{50} and pIR_{50}) of CP55,940 on inhibition of forskolin-induced cAMP production and ß-arrestin-2 recruitment obtained from the multiplex assay by quantification of AUC. Data are mean from two independent experiments performed in duplicate with individual values between brackets. N.A is not applicable.

← **Table 3.S1** *(continued legend)*

[a] Molecular weight (MW). [b] Polar surface area (PSA) calculated as surface sum of all polar atoms in the molecule. [c] Distribution coefficient (LogD) experimentally determined in 0.025 M phosphate/1-octanol buffer at pH 7.4. [d] Calculated partition coefficient value (cLogP) from experimentally determined octanol-water partition coefficient (K_{ow}). [e] Solubility of agonist in aqueous (0.05 M phosphate) buffer at pH 6.5 after lyophilization from DMSO stock. [f] Lipid Membrane Binding Assay (LIMBA) LogD to determine non-specific binding of agonists to brain lipids at pH 7.4. [g] Parallel artificial membrane permeability assay (PAMPA) for determination of membrane permeation coefficient values (P_{eff}) at pH 7.4 or 6.4 (#). [h] P-glycoprotein (P-gp) transport efflux ratio. Values represent the mean of a single experiment or the mean ± SD of at least two independent experiments. N.A. is not applicable due to restrictions. N.D. is not detectable due to intrinsic properties of agonists.

Table 3.S4 Inhibition of forskolin-induced cAMP production by benchmark agonists, endocannabinoids (eCB) and clinical agonists determined in the multiplex assay on CB_2R after 7.5 or 60 min.

		7.5 min		60 min	
	Agonist	**pEC_{50}**	**E_{max} or activation at 10 μM (%)**	**pEC_{50}**	**E_{max} or activation at 10 μM (%)**
Benchmark	**HU308**	6.75 ± 0.46	78 ± 4	7.03 ± 0.35	106 ± 7*
	HU910	8.19 ± 0.37	108 ± 11	8.59 ± 0.40	102 ± 8
	JWH133	6.76 ± 0.44	91 ± 6	7.96 ± 0.18	84 ± 4
	CP55,940	8.04 ± 0.22	104 ± 6	9.41 ± 0.08*	108 ± 8
eCB	**AEA**	5.37 ± 0.17	127 ±10	5.59 ± 0.13	185 ± 46
	2-AG	6.57 ± 0.38	101 ± 17	5.86 ± 0.19	109 ± 29
Clinical	**Dronabinol**	6.03 ± 0.15	27 ± 9	5.62 ± 0.04	103 ± 29
	Nabilone	6.64 ± 0.10	78 ± 11	7.95 ± 0.17*	90 ± 8
	Cannabidiol	N.D.	23 ± 4	N.D.	134 ± 61#
	Lenabasum	6.39 ± 0.24	160 ± 54	6.07 ± 0.11	240 ± 48
	Olorinab	6.83 ± 0.08	90 ± 31	8.05 ± 0.08*	63 ± 20
	CMX-020	N.D.	196 ± 28	5.49 ± 0.07	461 ± 114
	Cannabinol	6.35 ± 0.35	38 ± 13	5.49 ± 0.23	132 ± 35
	KN 387271	6.53 ± 0.37	109 ± 18	5.70 ± 0.17	272 ± 66
	GW-842166X	N.D.	146 ± 58	N.D.	183 ± 59#
	S-777469	6.75 ± 0.17	90 ± 22	7.14 ± 0.13	80 ± 13
	LY-2828360	N.D.	20 ± 7	7.45 ± 0.38	28 ± 6
	PRS-211375	6.44 ± 0.11	70 ± 7	7.33 ± 0.28*	96 ± 10
	ART-27.13	8.20 ± 0.17	131 ± 29	9.44 ± 0.26*	101 ± 16
	NTRX-07	6.31 ± 0.13	148 ± 45	5.84 ± 0.02*	219 ± 66
	EHP-101	N.D.	33 ± 9	N.D.	123 ± 22#*
	Tedalinab	9.01 ± 0.42	103 ± 10	9.53 ± 0.16	93 ± 7
	TAK-937	6.89 ± 0.12	105 ± 18	8.79 ± 0.19*	93 ± 11

Potency (pEC_{50}) and efficacy (E_{max}) values were determined from dose-response curves derived from the cAMP time traces in the multiplex assay analyzed at 7.5 and 60 min after agonist addition, respectively. #In the absence of a DRC, maximal activation (%) was determined at 10 μM of agonist. Multiple unpaired t-tests were performed to analyze differences in potency and efficacy at 60 min compared to 7.5 (* $p<0.05$). Data are mean from at least three independent experiments performed in duplicate. N.A is not applicable, N.D. is not detectable.

Table 3.S5 ß-arrestin-2 recruitment by benchmark agonists, endocannabinoids (eCB) and clinical agonists determined in the multiplex assay on CB_2R after 7.5 or 60 min.

		7.5 min		60 min	
	Agonist	pEC_{50}	E_{max} or activation at 10 µM (%)	pEC_{50}	E_{max} or activation at 10 µM (%)
Benchmark	**HU308**	5.66 ± 0.02	72 ± 4	6.08 ± 0.19	88 ± 8
	HU910	6.02 ± 0.02	72 ± 3	6.61 ± 0.04*	104 ± 6*
	JWH133	5.92 ± 0.07	76 ± 2	6.53 ± 0.06*	111 ± 3*
	CP55,940	7.62 ± 0.06	103 ± 0	8.97 ± 0.09*	107 ± 0*
eCB	**AEA**	5.57 ± 0.02	26 ± 0	6.02 ± 0.05	53 ± 3*
	2-AG	5.78 ± 0.16	93 ± 10	5.95 ± 0.11	83 ± 10
Clinical	**Dronabinol**	6.66 ± 0.08	5 ± 0	7.25 ± 0.08*	14 ± 2*
	Nabilone	6.51 ± 0.06	64 ± 9	7.80 ± 0.09*	72 ± 14
	Cannabidiol	N.A.	N.A.	N.A.	N.A.
	Lenabasum	5.79 ± 0.04	90 ± 7	6.57 ± 0.02*	107 ± 12
	Olorinab	6.47 ± 0.03	143 ± 12	7.47 ± 0.03*	121 ± 11
	CMX-020	6.59 ± 0.10	16 ± 0	7.06 ± 0.05*	27 ± 1*
	Cannabinol	6.28 ± 0.14	5 ± 1	6.99 ± 0.18*	17 ± 5
	KN 387271	7.38 ± 0.06	43 ± 1	7.90 ± 0.08*	61 ± 2*
	GW-842166X	N.D.	27 ± 8	N.D.	56 ± 11[#]
	S-777469	6.31 ± 0.06	65 ± 5	6.76 ± 0.08*	78 ± 8
	LY-2828360	6.37 ± 0.07	12 ± 0	7.22 ± 0.07*	20 ± 1*
	PRS-211375	6.09 ± 0.11	117 ± 7	7.11 ± 0.15*	107 ± 3
	ART-27.13	7.70 ± 0.13	154 ± 24	9.10 ± 0.22*	123 ± 16
	NTRX-07	6.35 ± 0.10	48 ± 14	6.88 ± 0.14*	56 ± 18
	EHP-101	N.A.	N.A.	N.A.	N.A.
	Tedalinab	7.87 ± 0.06	184 ± 8	8.85 ± 0.09*	122 ± 5*
	TAK-937	7.21 ± 0.12	32 ± 3	8.55 ± 0.09*	64 ± 10*

Potency (pEC_{50}) and efficacy (E_{max}) values were determined from dose-response curves derived from the ß-arrestin-2 time traces in the multiplex assay analyzed at 7.5 and 60 min after agonist addition, respectively. [#]In the absence of a DRC, maximal activation (%) was determined at 10 µM of agonist. Multiple unpaired t-tests were performed to analyze differences in potency and efficacy at 60 min compared to 7.5 (* $p<0.05$). Data are mean from at least three independent experiments performed in duplicate. N.A is not applicable, N.D. is not detectable.

Table 3.S6 **ΔΔLogR ratios and bias factors for benchmark agonists, endocannabinoids (eCB) and clinical agonists between forskolin-induced cAMP production and ß-arrestin-2 recruitment in the multiplex assay on CB_2R using an endpoint, semi-kinetic (AUC) or kinetic (IR) analysis.**

		7.5 min		60 min		AUC		IR	
	Agonist	ΔΔLogR[a]	Bias factor[b]	ΔΔLogR	Bias factor	ΔΔLogR	Bias factor	ΔΔLogR	Bias factor
Benchmark	**HU308**	0.00 ± 0.20	1.00	0.00 ± 0.13	1.00	0.00 ± 0.07	1.00	0.00 ± 0.21	1.00
	HU910	1.32 ± 0.40	20.78	1.24 ± 0.42	17.34	-0.40 ± 0.08	0.40	-0.13 ± 0.20	0.73
	JWH133	-0.16 ± 0.18	0.69	0.44 ± 0.22	2.78	-0.01 ± 0.09	0.98	-0.07 ± 0.19	0.86
	CP55,940	-0.28 ± 0.37	0.52	0.02 ± 0.21	1.05	0.09 ± 0.21	1.23	-0.17 ± 0.28	0.67
eCB	**AEA**	-0.07 ± 0.21	0.85	0.66 ± 0.17	4.55	0.16 ± 0.13	1.44	0.12 ± 0.25	1.33
	2-AG	0.17 ± 0.39	1.47	-0.23 ± 0.27	0.58	-0.10 ± 0.20	0.79	-0.49 ± 0.32	0.32
Clinical	**Dronabinol**	-1.10 ± 0.37	0.08	-0.61 ± 0.34	0.25	-1.07 ± 0.27	0.09	0.60 ± 0.29	3.95
	Nabilone	-0.46 ± 0.22	0.35	-0.12 ± 0.26	0.76	0.01 ± 0.14	1.03	-0.13 ± 0.21	0.74
	Cannabidiol	N.A.	N.A.	N.A.	N.A.	N.A.	N.A.	N.A.	N.A.
	Lenabasum	0.23 ± 0.38	1.68	0.01 ± 0.15	1.02	0.04 ± 0.13	1.10	-0.10 ± 0.20	0.80
	Olorinab	-0.23 ± 0.43	0.59	-0.24 ± 0.24	0.57	-0.15 ± 0.21	0.71	-0.24 ± 0.21	0.57
	CMX-020	N.D.	N.D.	0.74 ± 0.19	5.46	0.25 ± 0.44	1.76	0.02 ± 0.42	1.06
	Cannabinol	1.56 ± 1.05	36.48	-0.32 ± 0.37	0.48	-0.53 ± 0.21	0.30	N.D.	N.D.
	KN 387271	-1.15 ± 0.31	0.07	0.25 ± 0.42	1.77	-0.31 ± 0.38	0.49	0.06 ± 0.29	1.15
	GW-842166X	N.A.	N.A.	N.A.	N.A.	N.A.	N.A.	N.A.	N.A.
	S-777469	-0.23 ± 0.22	0.59	-0.02 ± 0.26	0.95	-0.10 ± 0.18	0.80	-0.19 ± 0.23	0.65
	LY-2828360	N.D.	N.D.	-0.29 ± 0.58	0.51	-0.69 ± 0.50	0.21	-0.19 ± 0.30	0.64
	PRS-211375	-0.79 ± 0.23	0.16	-0.16 ± 0.37	0.69	-0.21 ± 0.41	0.61	-0.36 ± 0.24	0.43
	ART-27.13	-0.14 ± 0.17	0.73	-0.14 ± 0.24	0.73	-0.02 ± 0.30	0.96	-0.43 ± 0.19	0.37
	NTRX-07	-0.05 ± 0.34	0.89	0.14 ± 0.32	1.39	-0.17 ± 0.15	0.68	-0.17 ± 0.29	0.67
	EHP-101	N.A.	N.A.	N.A.	N.A.	N.A.	N.A.	N.A.	N.A.
	Tedalinab	0.17 ± 0.40	1.48	0.07 ± 0.25	1.17	0.16 ± 0.26	1.43	-0.24 ± 0.23	0.57
	TAK-937	0.59 ± 0.42	3.88	0.03 ± 0.17	1.07	0.03 ± 0.14	1.08	-0.13 ± 0.20	0.75

[a] ΔΔLogR ratios were calculated to determine ligand bias between the cAMP and ß-arrestin-2 pathway using **Equation 3.10**. [b] The ligand bias factor for each ligand, relative to HU308, was determined following **Equation 3.11**. One-way ANOVA was performed to analyze differences in ΔΔLogR values of agonists compared to HU308 (* $p<0.05$). Values are presented as mean (± SEM) from at least three independent experiments performed in duplicate. N.D. is not determined. N.A. is not applicable.

Table 3.S7 G protein activation by benchmark agonists, endocannabinoids (eCB) and clinical agonists determined in [^{35}S]GTPγS assays on CB_2R.

	Agonist	pEC_{50}	E_{max} (%)
Benchmark	**HU308**	6.79 ± 0.10	72 ± 1
	HU910	7.01 ± 0.25	65 ± 1
	JWH133	7.02 ± 0.11	85 ± 6
	CP55,940	8.54 ± 0.11	91 ± 2
eCB	**AEA**	6.67 ± 0.17	25 ± 1
	2-AG	6.54 ± 0.15	67 ± 6
Clinical	**Dronabinol**	N.D.	-5 ± 7#
	Nabilone	7.31 ± 0.10	97 ± 8
	Cannabidiol	N.D.	-36 ± 5#
	Lenabasum	7.04 ± 0.08	71 ± 2
	Olorinab	7.87 ± 0.13	88 ± 2
	CMX-020	N.D.	3 ± 4#
	Cannabinol	N.D.	16 ± 5#
	KN 387271	7.46 ± 0.12	50 ± 3
	GW-842166X	N.D.	21 ± 3#
	S-777469	6.92 ± 0.06	83 ± 5
	LY-2828360	N.D.	9 ± 4#
	PRS-211375	7.50 ± 0.09	94 ± 2
	ART-27.13	9.06 ± 0.10	106 ± 3
	NTRX-07	6.66 ± 0.03	71 ± 5
	EHP-101	N.D.	-4 ± 15#
	Tedalinab	8.33 ± 0.20	105 ± 5
	TAK-937	8.73 ± 0.34	21 ± 2

Potency (pEC_{50}), efficacy (E_{max}) values were determined from dose-response curves. #In the absence of a DRC, maximal activation (%) was determined at 10 μM agonist. Data are mean from at least three independent experiments performed in duplicate. N.D. is not detectable